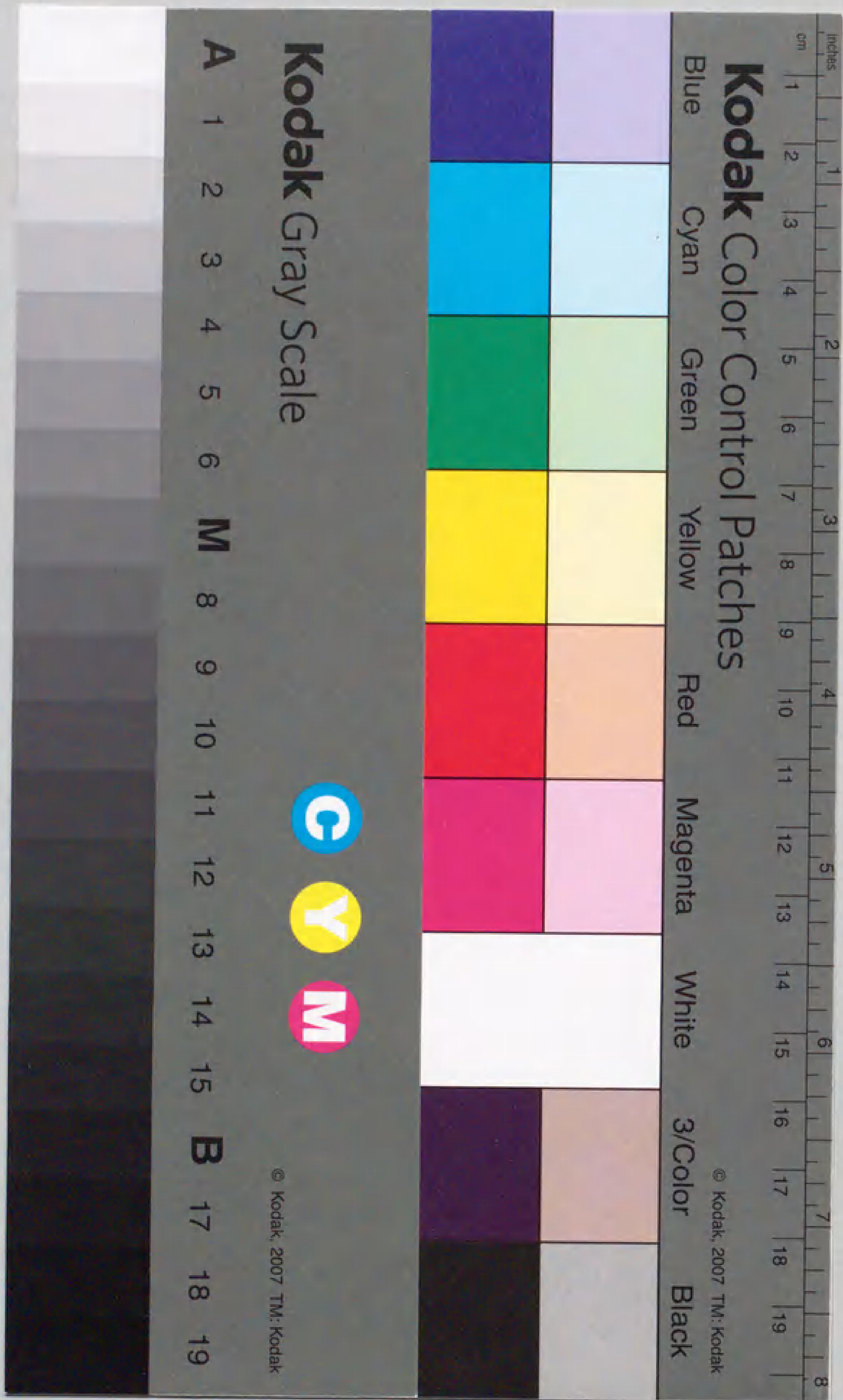

報告番号 甲第 2965 号

Force and Position Measurements of Micromachines by Atomic Force Microscopy

Akihiro Torii

Force and Position Measurements of Micromachines by Atomic Force Microscopy

Akihiro Torii

Department of Electronic-Mechanical Engineering
Nagoya University

1994

Contents

1 Introduction 1
1.1 History of Micromachines 1
1.2 Surface Micromachining 3
1.3 Problems in Surface Micromachining 6
1.4 Atomic Force Microscopy 10
1.5 Purpose and Outline of the Thesis 13
1.5.1 Purpose of This Thesis 13
1.5.2 Outline of This Thesis 13

2 Principle of Atomic Force Microscopy 15
2.1 AFM Using Optical Beam Deflection Method 15
2.2 AFM Using Interferometry 18
2.3 AFM Probes 20

3 Atomic Force Microscope Used in This Thesis 23
3.1 AFM Using Heterodyne Interferometry 23

4 Elastic Force Measurement 29
4.1 Introduction 29
4.2 Measurement Technique 32
4.3 Experiments 40
4.4 Results and Discussions 43
4.4.1 Elasticity Measurement of Microcantilever 43
4.4.2 Measurement of the Young's Modulus of PVD Thin Film 46
4.5 Conclusions 46

5 Adhesive Force Measurement 49
5.1 Introduction 50

5.2 Experiments 51
5.3 Results and Discussions 54
5.4 Conclusions 67

6 Adhesive Force Distribution Measurement 71
6.1 Introduction 72
6.2 Experiments 73
6.3 Results and Discussions 75
6.4 Conclusions 84

7 Position Measurement 87
7.1 Introduction 88
7.2 Principle and Experiments 89
7.3 Results and Discussions 96
7.3.1 Single Probe Experiments 96
7.3.2 Double Probe Experiments 102
7.4 Conclusions 109

8 Summary 113
8.1 General Summary 113
8.1.1 Elastic Force Measurements in Microcantilever 114
8.1.2 Adhesive Force Measurements in Nanometer Region 114
8.1.3 Adhesive Force Distribution Measurements on Microstructures 115
8.1.4 Position Measurements Using Multiple Probe AFM 116
8.2 Future Prospects 116

Chapter 1

Introduction

1.1 History of Micromachines

During the past few years, there has been an explosion of interest in micromachines. Study of micromachines covers the emerging fields of microelectronics, micromechanics and micromachining, and includes physics, chemistry and system control. Fabrications of several new devices in science and engineering have been proposed. First micromechanical system appeared in the last 1960s. It was called integrated sensors, which were fabricated by combing the techniques for sensors and integrated circuits (ICs). Using silicon micromachining techniques, micromechanical temperature and pressure sensors were fabricated[1]. In the silicon micromachining techniques, which were basic fabrication processes for ICs, film formation, lithography and etching have been used. Silicon micromachining techniques have become a fundamental tool for the fabrication of the ICs. Not only two-dimensional but also three-dimensional structures have been fabricated by the techniques. By the sacrificial layer etching and bonding processes[2], three-dimensional microstructures can be produced. The LIGA (Lithograph Galvanoformung Abformung) process[3] is

another technique to fabricate three-dimensional high aspect ratio microstructures. These technologies developed during the 1980s have provided new micromechanical systems. Gears[4], cranks[5], levers[6] and other micron-dimensional mechanical components[7] which are capable of rotating, sliding and performing complex motions have been fabricated. Furthermore, combining the electronic system, the micromechanical systems such as micromotors[8], microvalves[9], micropumps[10] and micropositioners[11] were fabricated. Coupling with the integrated sensors, these components will open up new fields of application. These systems are now called microelectromechanical systems (MEMSs) or micromachines. In the last 1980s, micromachines attracted the world-wide attentions.

Since microactuators, microsensors and interface circuits can be fabricated by the IC fabrication techniques, all the elements of MEMSs are formed on the same silicon substrate[12]. Accordingly, there have been many proposals for the advanced MEMS. Microrobots for security, medical micromachines for surgical operation, micromachines for precise assembly have been proposed. Today, we have reached only entrance of the large application area of the MEMS. If these proposals are feasible, we can see the MEMS consisting of mechanical, electrical and other technical components in everyday life. Such devices will have potentials to revolutionize instrumentation of machines. However, it is also true that those newly proposed devices require much time to be realized. Many applications proposed about ten years ago have not been practically available. Therefore, when we discuss a prospect of the MEMS, it is important to consider not only their potentials but also their practical problems which must be overcome technically.

1.2 Surface Micromachining

Although many techniques, for example, LIGA process[3], conventional machining[13], etc., are used to fabricate the MEMS, silicon based surface micromachining has become a fundamental tool for MEMS's fabrication[12]. Techniques such as thin film formation, lithography and etching have been developed to fabricate the IC. These techniques are also useful to construct micromachines. Thin film materials such as silicon (Si), silicon dioxide (SiO_2), silicon nitride (Si_3N_4) and polycrystalline silicon (poly-Si) are often used in micromachines. Oxidation and film deposition on a silicon wafer are main techniques to form the films. These films are shaped into micromechanical parts by the lithographic process. Both conductive and non-conductive thin films are used in the MEMS. Especially, thermal oxides, dielectric layers, poly-Si and metal films are generally used in the surface micromachining. A deposited SiO_2 film is used for insulation or sacrificial layers. A dielectric layer such as Si_3N_4 film is used not only for insulation but also for mechanical materials. A poly-Si film is mainly used for materials of mechanical structures.

The lithography is a process of transferring patterns of geometric shapes on a mask to a thin layer of radiation-sensitive material (called resist) covering the surface of a semiconductor wafer. These patterns specify various regions in the MEMS such as contact windows and bonding areas. The resist patterns formed by the lithographic process are not permanent elements of the final device but only replicas of MEMS's features. To produce the MEMS, these resist patterns must be transferred into the underlying layers. The pattern is transferred by the etching process which removes unmasked portions of a layer selectively. There are various

lithographic methods. Both the wet etching and the dry etching techniques are used to remove unmasked portions of the layer. The anisotropic wet etching is one of key technologies to fabricate three-dimensional micromachines.

Figure 1.1 illustrates the processing steps for fabricating free-standing microcantilevers by the anisotropic etching[14, 15, 16]. The microcantilever is fabricated by using one photomask and a positive resist. The silicon dioxide film is formed by the thermal oxidation of a silicon substrate. (1) In this case, the positive photoresist is used. The wafer is held on a vacuum spindle and the liquid resist is applied to the center of the wafer. The wafer is then rotated at a constant speed, which is maintained for approximately 30 s. After the spinning step, the wafer is baked to remove the solvent from the photoresist film and to improve resist adhesion to the wafer. (2) The wafer is aligned with respect to the mask in an optical lithographic system, then the resist is exposed to light. (3) The exposed resist is dissolved in the developer. The photoresist is usually developed by spraying the wafer with the developer solution. The wafer is then rinsed and dried. After development, post baking is required to increase adhesion of the resist to the substrate. The wafer is then put in the etchant, which etches the exposed layer but does not attack the resist. For the etching of the silicon dioxide, buffered hydrofluoric acid (Buffered HF) is commonly used. (5) Some etchants dissolve anisotropically a certain crystal plane of the semiconductor material faster than other planes. This results in orientation-dependent etching. For silicon, a typical etchant is potassium hydroxide (KOH). After the etching process, the wafer is rinsed and self-standing microcantilevers are fabricated as shown in Fig.1.1.

Another key technique to fabricate three-dimensional micromechanical structures

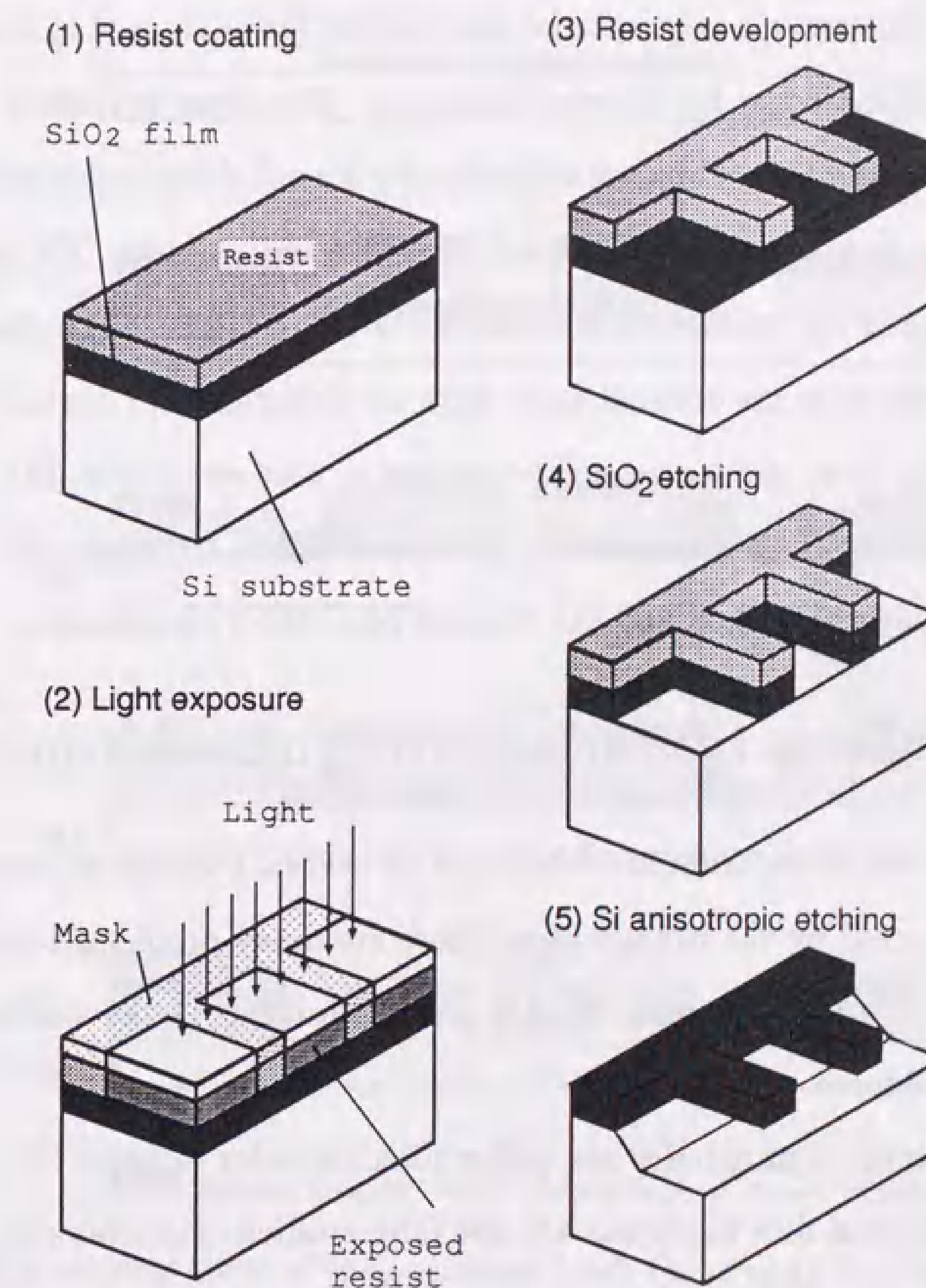

Figure 1.1: Schematic sequence of microstructure fabrication.

is the sacrificial layer etching[4]. The sacrificial layer is deposited on a substrate to make a small gap between layered films. The sacrificial layer is finally etched completely. The fundamental procedure of the sacrificial layer etching is shown in Fig.1.2, which illustrates a sequence of micromotor fabrication. (1) An SiO_2 layer is grown on a silicon wafer by thermal oxidation. This layer is used as a sacrificial layer. (2) Poly-Si and SiO_2 films are deposited by chemical vapor deposition (CVD). The poly-Si film is used as the material for a rotor and a stator. The poly-Si layer and the SiO_2 layer are etched by reactive ion etching (RIE). (3) After forming a rotor and a stator, they are covered again with an SiO_2 thin film deposited by CVD. This second SiO_2 layer also makes a gap between a rotor and a axle. (4) The poly-Si layer is deposited again, which is etched to form a axle with a cap. (5) Finally, the SiO_2 sacrificial layer is etched and the moving part (rotor) is released.

1.3 Problems in Surface Micromachining

Although many micromachines are fabricated by several techniques, most micromachines are fabricated by the lithography. There are many problems to be solved for the fabrication of micromachines. In this thesis, problems in the surface micromachining are considered.

Although electrical properties are well studied in order to make ICs, mechanical properties of the thin film materials are not fully studied. For example, a elasticity of the microstructure is not measured directly. It has been difficult to apply a small force (in the nanonewton region) and to measure a little deflection of the structure (in the submicron meter region) in a very small area. A distortional force generated in the fabricated structures can be calculated by using the finite elements method.

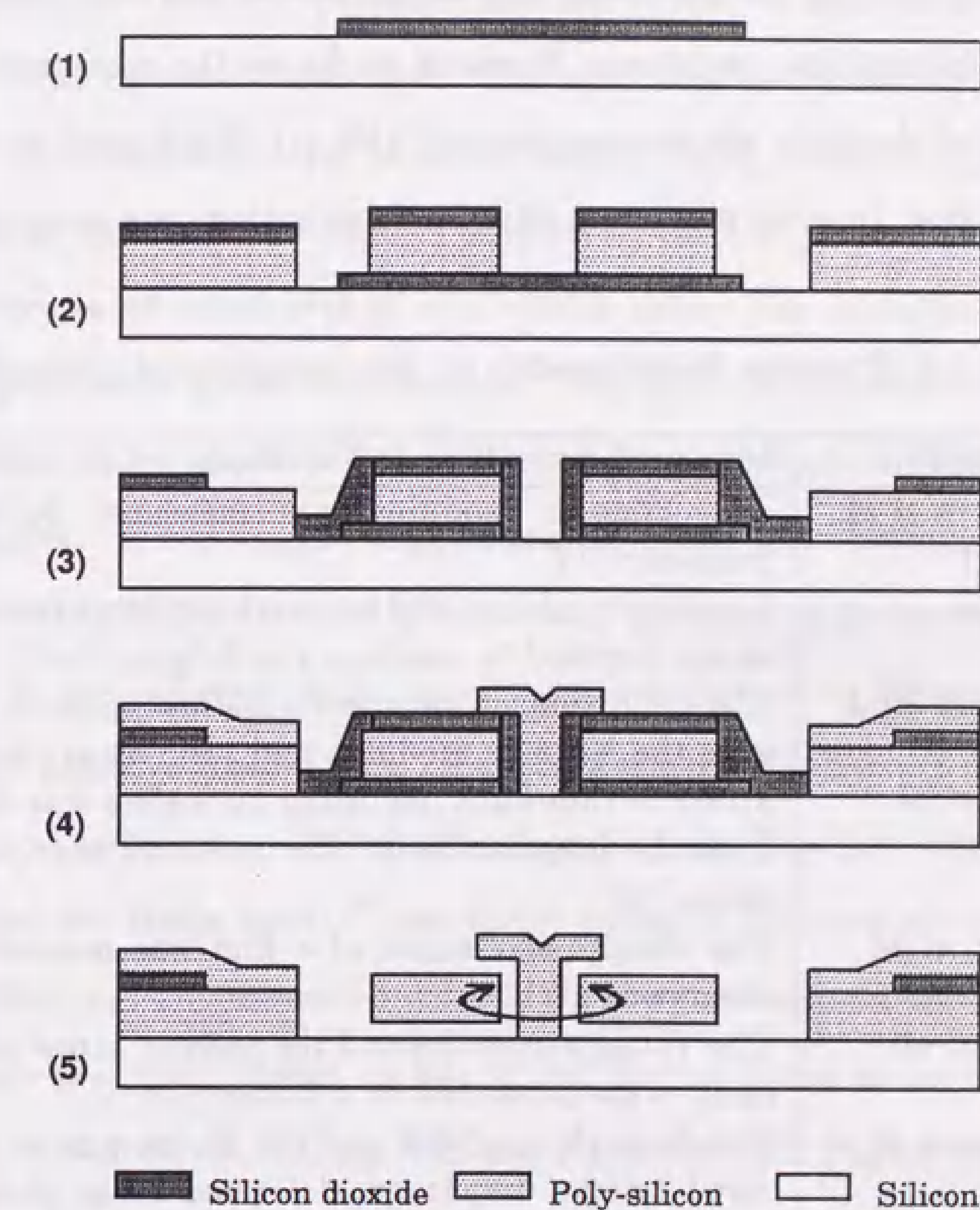

Figure 1.2: Processing steps of the sacrificial layer technology for the fabrication of a micromotor.

However, the elastic constant of the film has not been measured. In addition, the elasticity of the film depends strongly on fabrication conditions. The distortional force has not been investigated experimentally in detail. The Young's modulus, the poison ratio, etc. of the materials used in the MEMS have not been measured under several fabrication conditions. Previous works on the measurements of the micromechanical elasticity are summarized in Table 1.1. Each work is described in detail in chapter 4. In most measurements, the force acting on a sample is indirect.

Table 1.1: Previous measurements on micromechanical properties

Year	Author(s)	Measured properties and methods
1979	Petersen et al.	The Young's modulus was measured by resonance frequency.[17]
1980	Borden	A periodic shape of the overhang structure gave the strain required to conform the SiO_2 to the Si.[18]
1983	Bromley et al.	The deflection of the membrane by pressure difference gave the Young's modulus and yield strength.[19]
1983	Howe et al.	Stress in thin films deposited on wafers was determined from the lengthening of the undercut edge of a silicon stripe.[20]
1985	Guckel et al.	The compressive stress of a film was measured by the observation.[21]
1987	Allen et al.	The Young's modulus and the residual stress of the polyimide were measured by a bridge.[22]
1989	Sugiyama et al.	The Young's modulus and the Poisson ratio were measured using a diaphragm deformed by air pressure.[23]
1990	Zhang et al.	The Young's modulus and internal stress in microresonators were measured by the resonant frequencies.[24]
1991	Hane et al.	Resonance frequencies were measured by the photothermal technique.[25]
1992	Griffin et al.	The stress-strain curves were used to determine the Young's modulus of aluminum films.[26]

Thus, it is difficult to investigate the elasticity of a small portion of micromachines by applying a localized force.

Suspended surface microstructures are commonly used in microsensors, for example, acceleration sensors, pressure sensors[27], etc. These structures typically consist of a layer on a sacrificial layer. The layer is etched to form plates, beams or cantilevers. The sacrificial layer is finally etched. Many kinds of liquid are used in the wet etching and rinse processes. The adhesive force is generated in the rinse and the dry processes after removal of a sacrificial layer. The adhesive force is strong enough to generate a plastic deformation. The microstructures often collapse and adhere to their underlying substrate. This is a fundamental problem in the surface micromachining. However, the phenomena have not been investigated in detail. The adhesion of microstructures is important problem to be solved. Magnitude and nature of the adhesive force have to be investigated to design the micromachines. The adhesive force acting on the micromachines has not been measured directly up to the present. The adhesive force includes capillary force, electrostatic force and van der Waals force. These forces acting in the nanometer region are so small that they are not measured directly by the conventional measurement techniques. There are many papers on lateral and normal forces in the scanning probe microscopy[28, 29, 30, 31, 32, 33, 34] and there are some papers on the adhesive force. Previous works on the adhesive force measurement are summarized in Table 1.2. Each work is described in detail in chapters 5 and 6.

In addition, it is also basically important to measure accurately dimensions of microstructures. The precise positioning technique and the calibration method for the displacement in nanometer region have to be developed for the study of micro-

Table 1.2: Previous works of the adhesion

Year	Author(s)	Topic(s)
1990	Linder et al.	Sticking of poli-Si beam was caused by electrostatic force.[35]
1991	Butt	Force versus distance curves were obtained at different solutions with charged tips.[36]
1992	Hartmann	Van der Waals forces, capillary forces and ionic forces which may be present in the force microscopy were theoretically analyzed.[37]
1992	Cohen	Adhesion between two materials were concluded by a contaminant layer.[32]
1992	Alley et al.	Peel-off force was measured using specially designed butterfly structure.[38]
1992	Scheeper	Sticking of beam was due to the water molecules.[39]
1992	Israelachvili	Adhesion and friction properties of liquids in ultrathin films were discussed on ideal surfaces and interfaces.[40]
1993	Mastrangelo et al.	Adhesive force was measured using microcantilevers different in length and thickness.[41, 42]

machines.

1.4 Atomic Force Microscopy

The atomic force microscopy (AFM) is one version of the scanning tunneling microscopy (STM). The principle of the STM consists essentially in scanning a metal tip over a conductive surface at constant tunnel current[43, 44]. From the displacements of the STM tip, a topographic picture of the surface is obtained. The very high resolution of the STM is caused by the strong dependence of the tunnel current between the STM tip and the sample surface.

The principle of the AFM is similar to that of the STM as shown in Fig.1.3. Atomic images of the conductive and non-conductive materials are reported[44]. There are two types of the AFM, a dynamic AFM and a static AFM. In the dynamic AFM, the gradient of the attractive force acting between an AFM tip and a sample is measured. The force gradient is measured by detecting the vibrational frequency of the AFM probe. Small change in the resonant frequency is monitored by the change in the phase or amplitude of the vibration. Although the dynamic AFM offers a non-contact sensing, the measured value is not the force. In the static AFM, the repulsive force acting between an AFM tip and a sample is measured and controlled by detecting the instantaneous deflection of an AFM probe. Since the force as small as 1 nN can be detected by the static AFM, the static AFM is useful to investigate the elastic and inelastic properties of microstructure. The static AFM is used in this study.

Recently, the AFM is used for the evaluation of surface mechanical properties in the nanometer region[45]. However, the AFM has not been used for the evaluation of the micromachines up to the present. In addition, some research groups used the STM/AFM for precise positioning. Their works on the precise positioning are summarized in Table 1.3. Each work is described in detail in chapter 7.

Table 1.3: Previous works of precise position measurement

Year	Author(s)	Topic(s)
1991	Kawakatsu et al.	An STM image is calibrated with graphite. [46]
1991	Li et al.	An AFM is calibrated with latex particles.[47]
1992	Mamin et al.	An AFM is applied to data storage.[48]

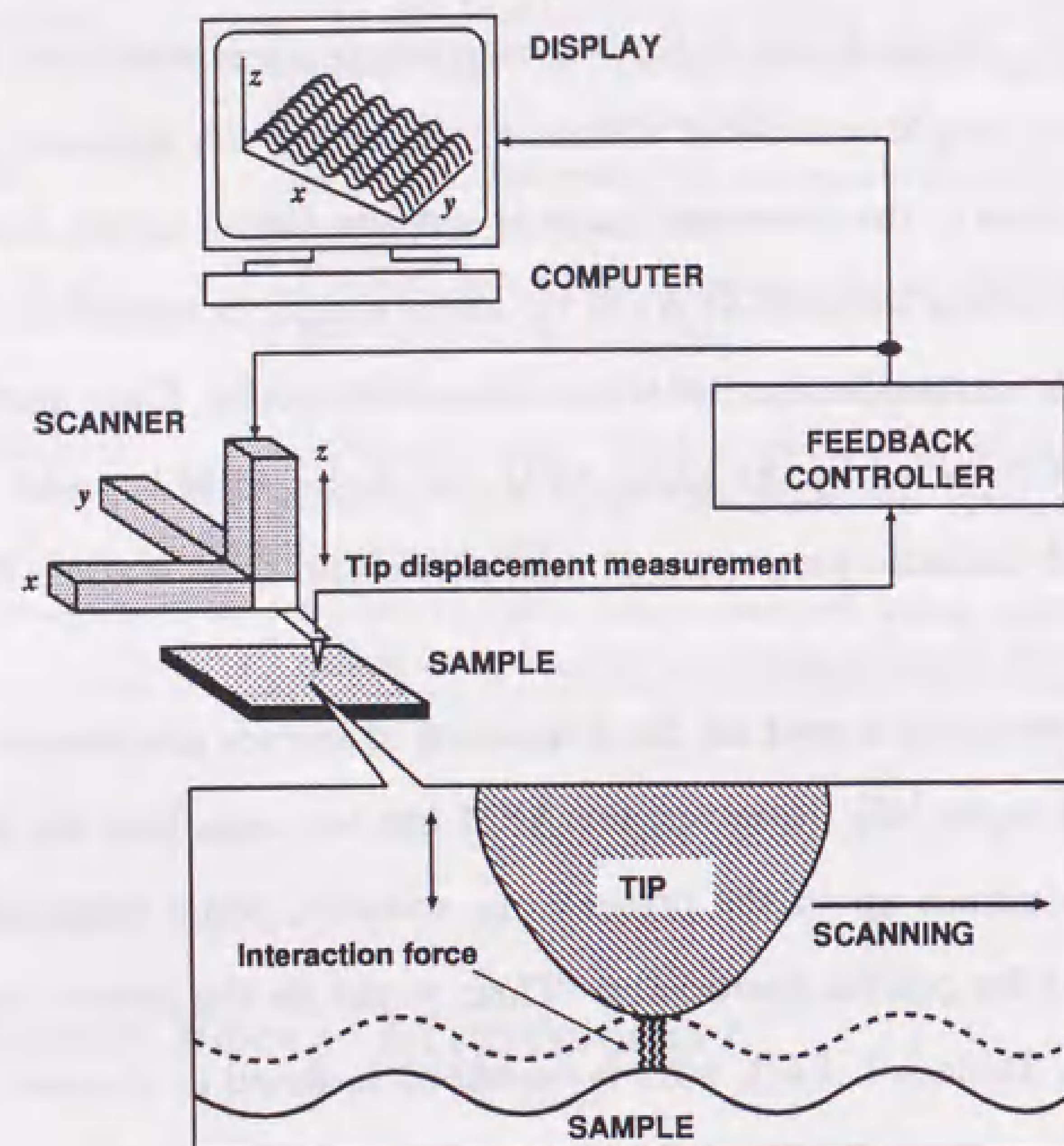

Figure 1.3: Schematic principle of AFM.

1.5 Purpose and Outline of the Thesis

1.5.1 Purpose of This Thesis

It is necessary to investigate the basic mechanical properties of microstructures in order to fabricate the reliable and practical micromachines. Especially, to fabricate the MEMS by the surface micromachining, the following problems should be solved as described in section 1.3. (1) Mechanical strength of micromechanical parts has to be measured precisely. (2) Adhesive forces generated in the etching process should be investigated quantitatively. (3) Accurate dimensions of micromechanical parts should be measured.

In this study, the AFM is used to solve the problems described above. New techniques for the respective measurements are proposed in this thesis.

1.5.2 Outline of This Thesis

In chapter 2, a principle of the AFM is described. The AFM using an interferometer and the AFM using an optical beam deflection method are described.

In chapter 3, the developed AFM using a heterodyne interferometer is described. The developed AFM is used in most of the measurements in this thesis.

In chapter 4, an application of the AFM to the elasticity evaluation of micromechanical cantilever beams is described. A force curve (force as a function of a tip-sample distance) is used to evaluate a small force generated by a distorted microstructure. Gradient of the force curve changes by the surface elasticity. From the force curve measurements, the elasticity of the microfabricated cantilever and the Young's modulus of the thin film are obtained.

In chapter 5, the adhesive forces generated by solutions are measured using the AFM. In the wet etching process, several kinds of solution are used to etch and rinse the substrate. The adhesive force is investigated theoretically by considering electrostatic force, capillary force, etc. Using the capillary force theory, the adhesive force is explained.

In chapter 6, adhesive force distributions on microstructures are measured. The Adhesive forces acting on grating structure and ordered latex particles are investigated by using an AFM tip. Relation between the topography and the adhesive force distribution is discussed.

In chapter 7, position sensing using a multiple probe AFM is proposed. Samples having periodic structure are measured by the AFM. Periodic signals are obtained by the developed AFM. The relation between the surface topography and the AFM signal is investigated, and the influence of the probe shape is discussed. The encoding signals are obtained by the proposed AFM.

Finally, chapter 8 gives summary of this dissertation. The scope of future works concerning the application of the force microscopy to the microelectromechanical systems is discussed.

Chapter 2

Principle of Atomic Force Microscopy

2.1 AFM Using Optical Beam Deflection Method

The principle of the AFM is based on sensing of forces acting between a sharp stylus and a surface. The interaction forces cause the displacement of the AFM tip. In its original implementation, a tunneling junction is used to detect the motion of a tip (a diamond stylus) attached to an electrically conductive cantilever as shown in Fig.2.1. The force is measured from the elastic deformation of the cantilever with the STM.

Since the displacement of the order of 10^{-4} Å can be detected with a simple optical technique in the photothermal spectroscopy, it is convenient to apply the technique to the AFM. The cantilever displacement is measured by detecting the deflection of a laser beam which is reflected from the rear surface of the cantilever. The deflection is sensed with a photodetector.

Figure 2.2 show an optical beam deflection method to detect a deflection of an AFM probe. A laser beam is focused on the free end of the cantilever. In the static

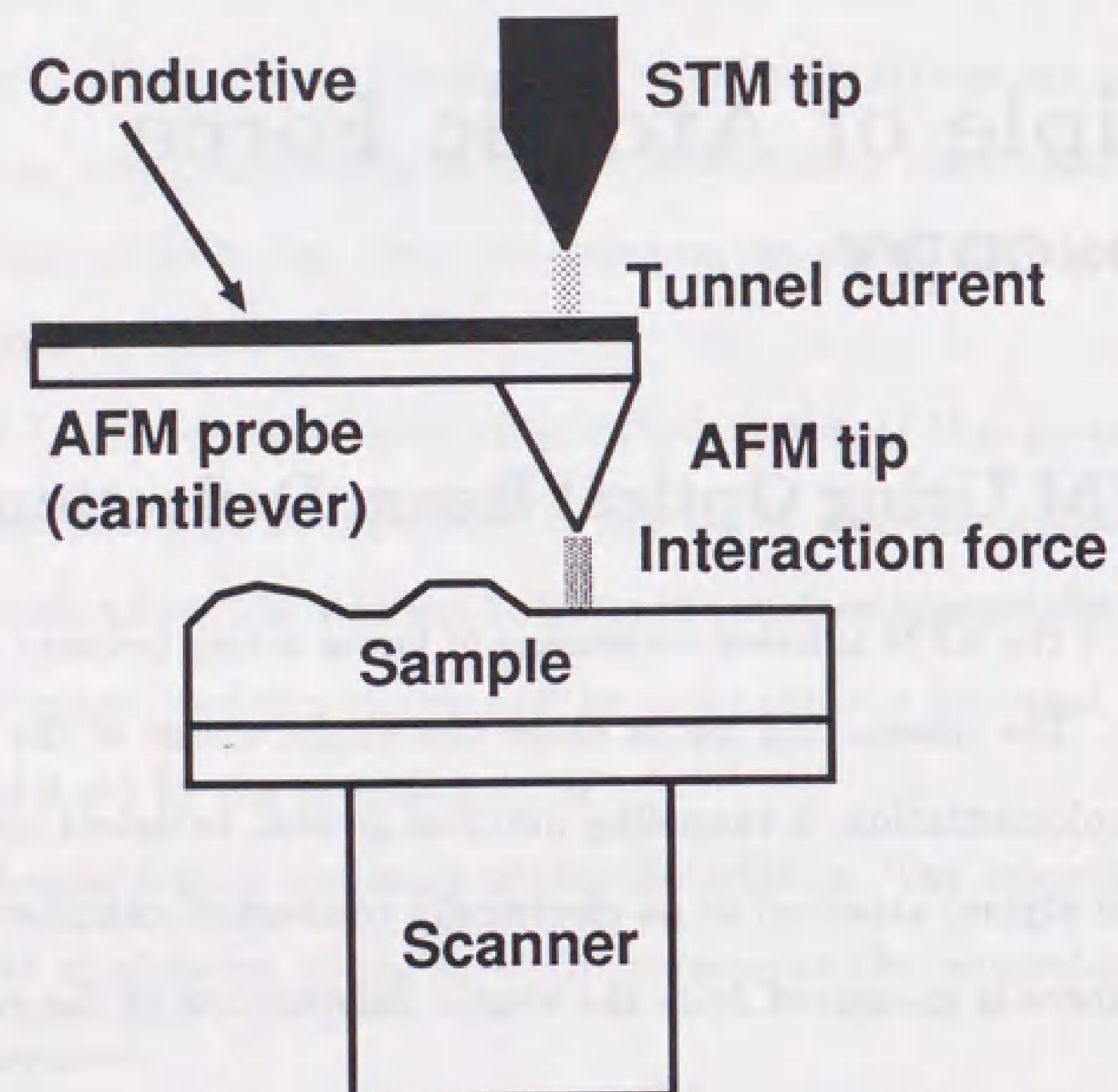

Figure 2.1: Atomic force microscopy using tunnel displacement sensor. Rear surface of the cantilever must be conductive. An AFM probe deflects by a small force acting between a sample surface and an AFM tip. The deflection of the AFM probe is detected by a change of a tunneling current.

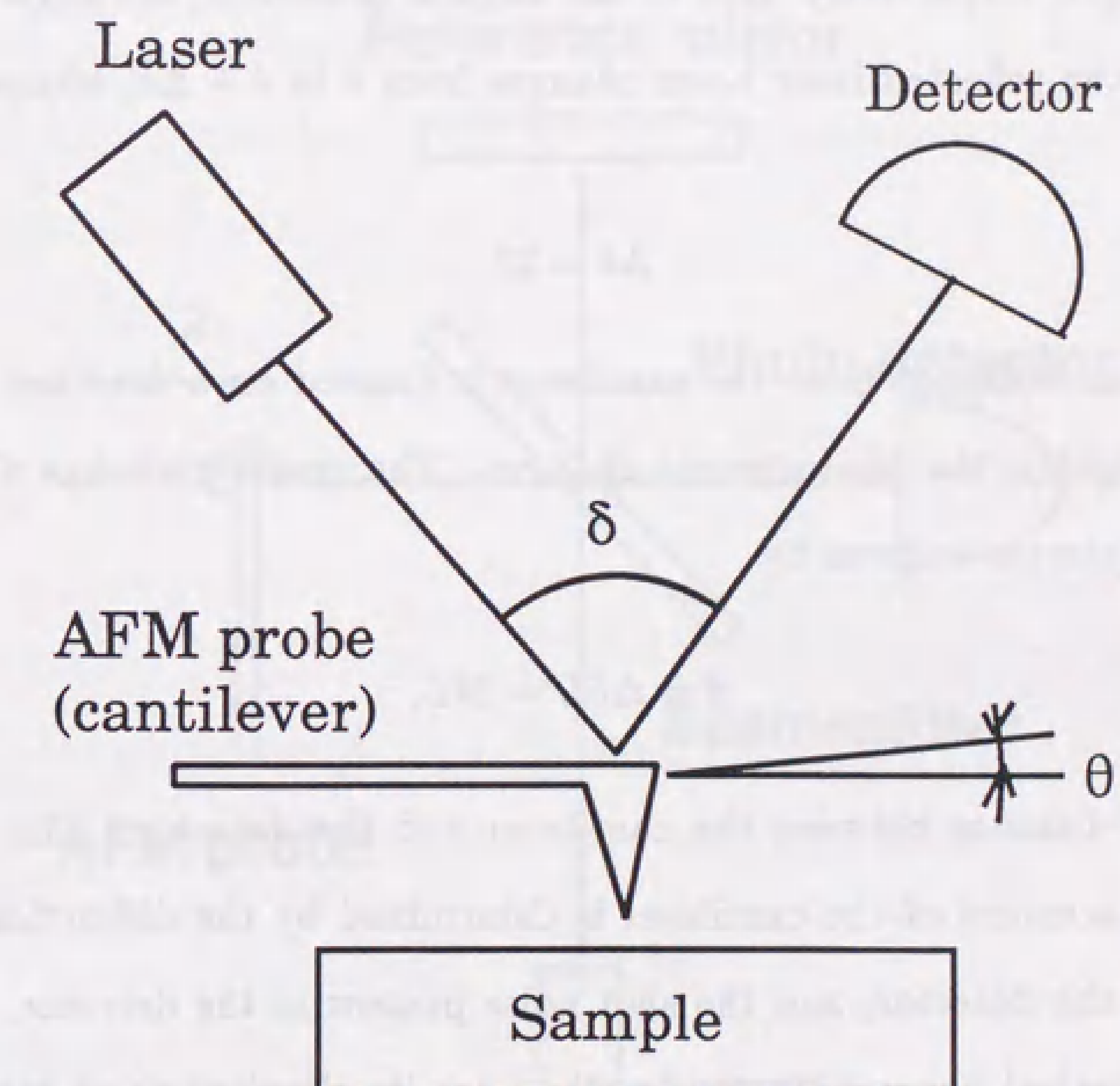

Figure 2.2: Schematic diagram of optical beam deflection method. The angle of the reflected laser beam changes slightly when the cantilever is deflected. The variation of the angle δ is detected with a detector.

imaging mode, a force exerted on the tip generates a small angular rotation θ of the free end of the cantilever,

$$\theta = \frac{z_c}{l}, \tag{2.1}$$

where z_c and l denote the displacement of the tip normal to the surface and the cantilever length, respectively. Due to this angular deflection, the angle between the incident and the reflected laser beam changes from δ to $\delta + \Delta\delta$, where $\Delta\delta$ is given by

$$\Delta\delta = 2\theta. \tag{2.2}$$

The laser beam reflected from the cantilever is focused on a detector. If the laser spot shifts slightly, the photocurrent changes. The position change d of the laser spot on the detector is given by

$$d = \Delta\delta L = 2\theta L, \tag{2.3}$$

where L is a distance between the cantilever and the detector. The smallest detectable displacement of the cantilever is determined by the diffraction size of the laser spot on the detector, and the shot noise present in the detector. The advantages of the optical beam deflection method are its simplicity and high reliability. The sensitivity is high enough to obtain atomic resolution.

2.2 AFM Using Interferometry

Optical interferometry is also used to detect the cantilever deflection. The basic set-up of the interferometer is shown in Fig.2.3. The beamsplitter splits a laser beam into two beams. The signal beam is reflected by the cantilever and the reference beam is

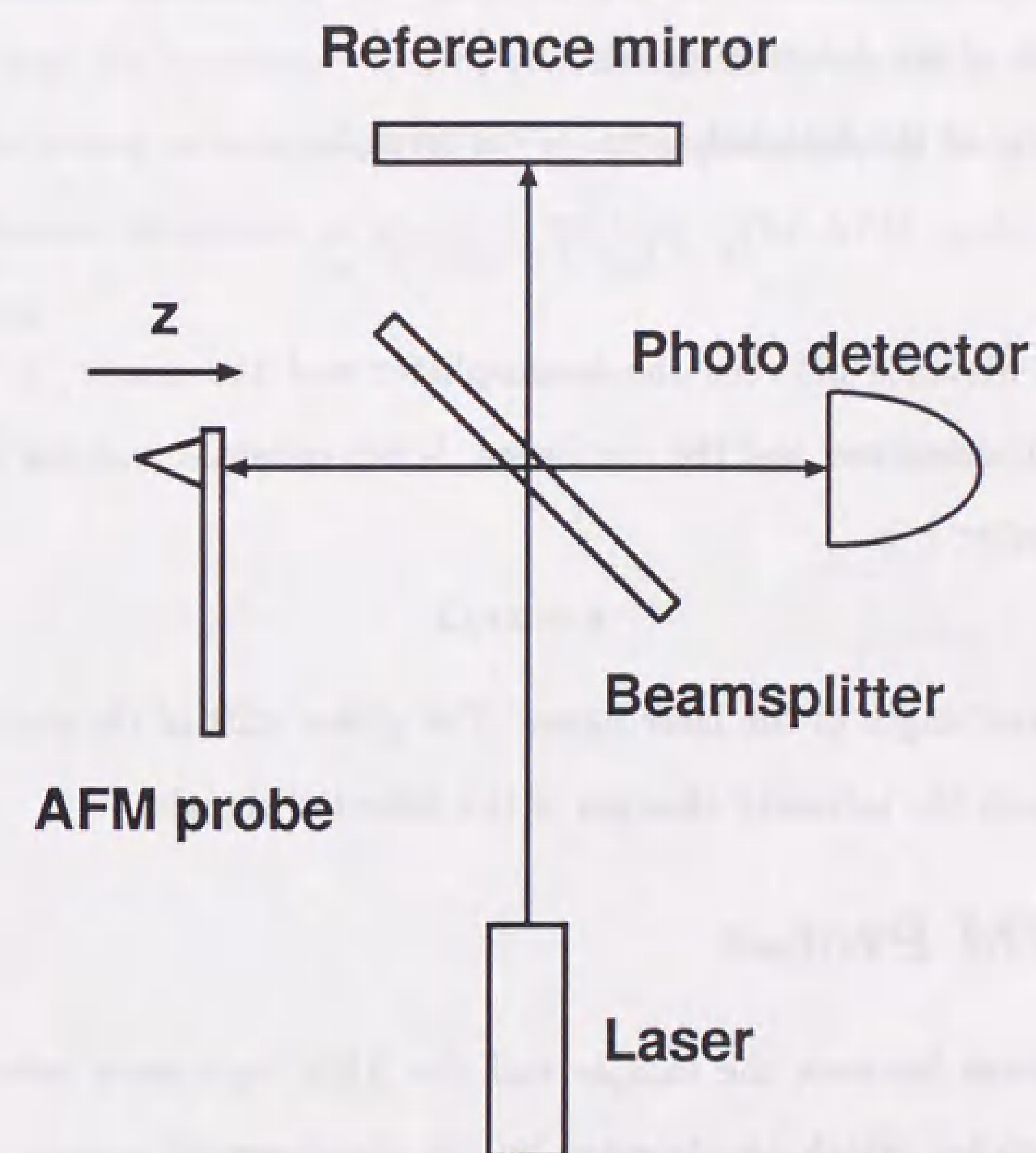

Figure 2.3: Schematic diagram of AFM using interferometry.

reflected by the mirror. After passing through the beamsplitter, the reference beam and the signal beam are combined, and the signal is detected by the photodetector. Displacement of the cantilever in the z-direction changes the phase of the reflected signal beam. The signal is detected with the photodetector and the photocurrent is amplified with an amplifier. The displacement of the cantilever is determined from the phase shift of the detected signals.

An intensity of the detected signal (I) is given by

$$I = I_0[1 + \cos 2k(l_1 - _2)], \tag{2.4}$$

where l_1 is a distance between the beamsplitter and the mirror, l_2 is a distance between the beamsplitter and the cantilever, I_0 is a constant and k is wave number. The wave number k is

$$k = 2\pi/\lambda \tag{2.5}$$

where λ is wave length of the laser beam. The phase shift of the detected signal is determined from the intensity changes of the detected signals.

2.3 AFM Probes

Interaction forces between the sample and the AFM tip causes minute deflection of the AFM probe, which are detected by the displacement sensor. A low spring constant ($\sim$ 1 N/m) is required for high sensitivity. A high resonance frequency ($>$ 10 kHz) of the cantilever is also necessary for noise filtering. These requirements were satisfied with skillfully prepared microprobes. A tungsten wire was etched electrochemically to form a sharp tip at one end. In other case, a mechanically cut platinum or other metal wires were used as the AFM probe. The top diameter of the

etched wire was a few tenth of micrometers and the length was a few millimeters. The spring constant and resonant frequency were $\sim 10^3$ N/m and $\sim$ 10 kHz, respectively.

Thin film cantilevers of the silicon dioxide with a glued diamond fragments as the tip were fabricated by surface micromachining. More recently, the AFM probe with an integrated tip were fabricated using a silicon nitride film. A polycrystalline silicon cantilever and a monocrystalline silicon cantilever are fabricated by the surface micromachining technique[49, 50]. The spring constant is about $\sim 10^{-3}$ N/m and the resonance frequency is about $\sim$ 20 kHz. The AFM probe is one of the micromachines.

Chapter 3

Atomic Force Microscope Used in This Thesis

In this thesis, two different types of the AFM are used. An AFM using the heterodyne interferometry is developed and used in chapters 4-6. An AFM using the optical beam deflection method is developed and used in chapter 7 in order to investigate the principle of the multiple probe AFM. Since the AFM using heterodyne interferometry is used in most of this study, it is described in detail in this chapter.

3.1 AFM Using Heterodyne Interferometry

A motion sensing technique using the heterodyne interferometry is capable of realizing a nanometer resolution. An AFM using the heterodyne interferometry is developed to detect an AFM probe deflection precisely. The schematic diagram of the developed AFM is shown in Fig.3.1. In the developed system, the AFM is combined with an optical microscope, which is used for rough positioning of a sample. The developed AFM system is placed on a vibration isolator (Herz, HG-107LM). Figure 3.2 shows a photograph of the developed system.

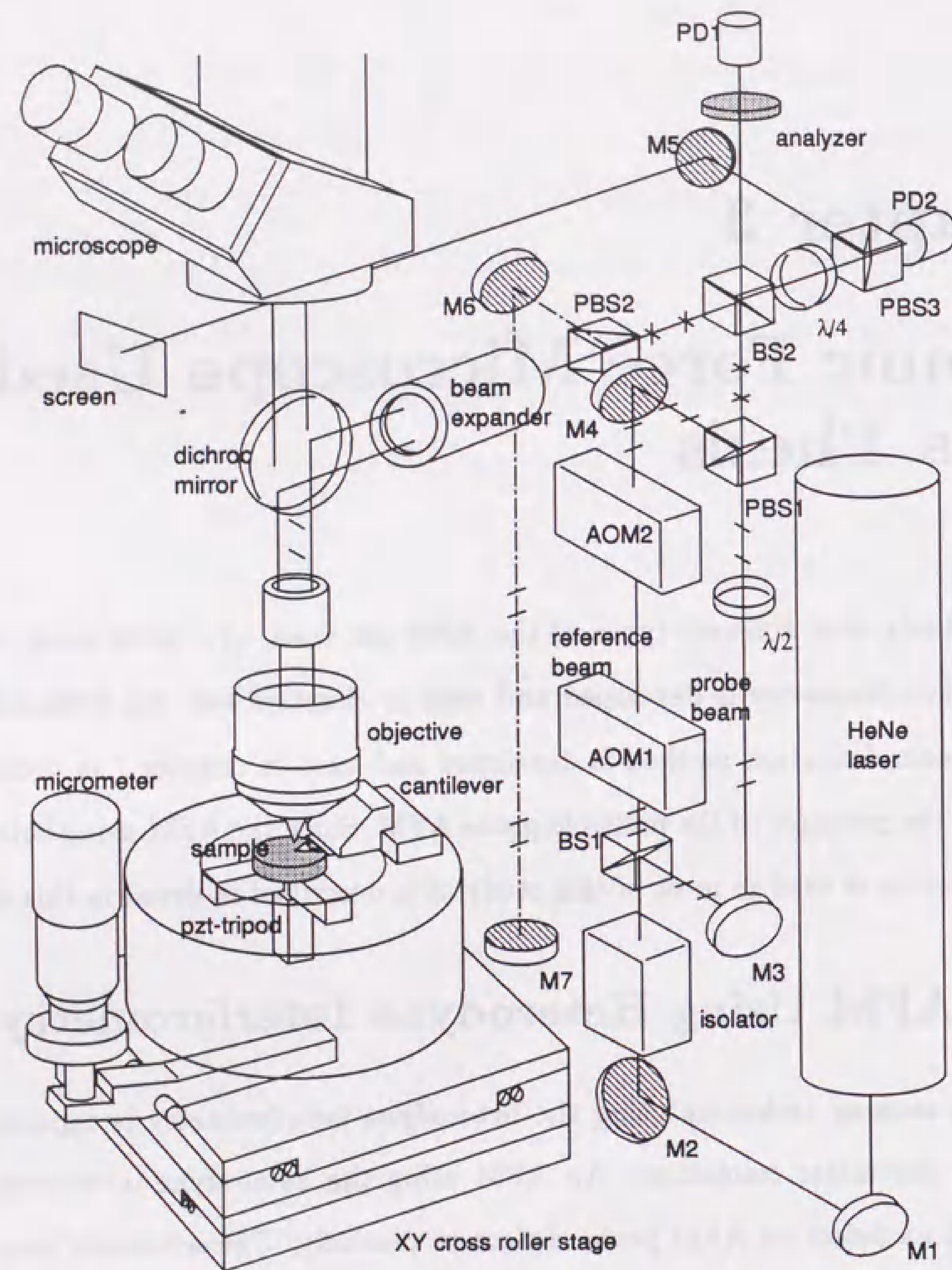

Figure 3.1: Schematic diagram of AFM using heterodyne interferometry.

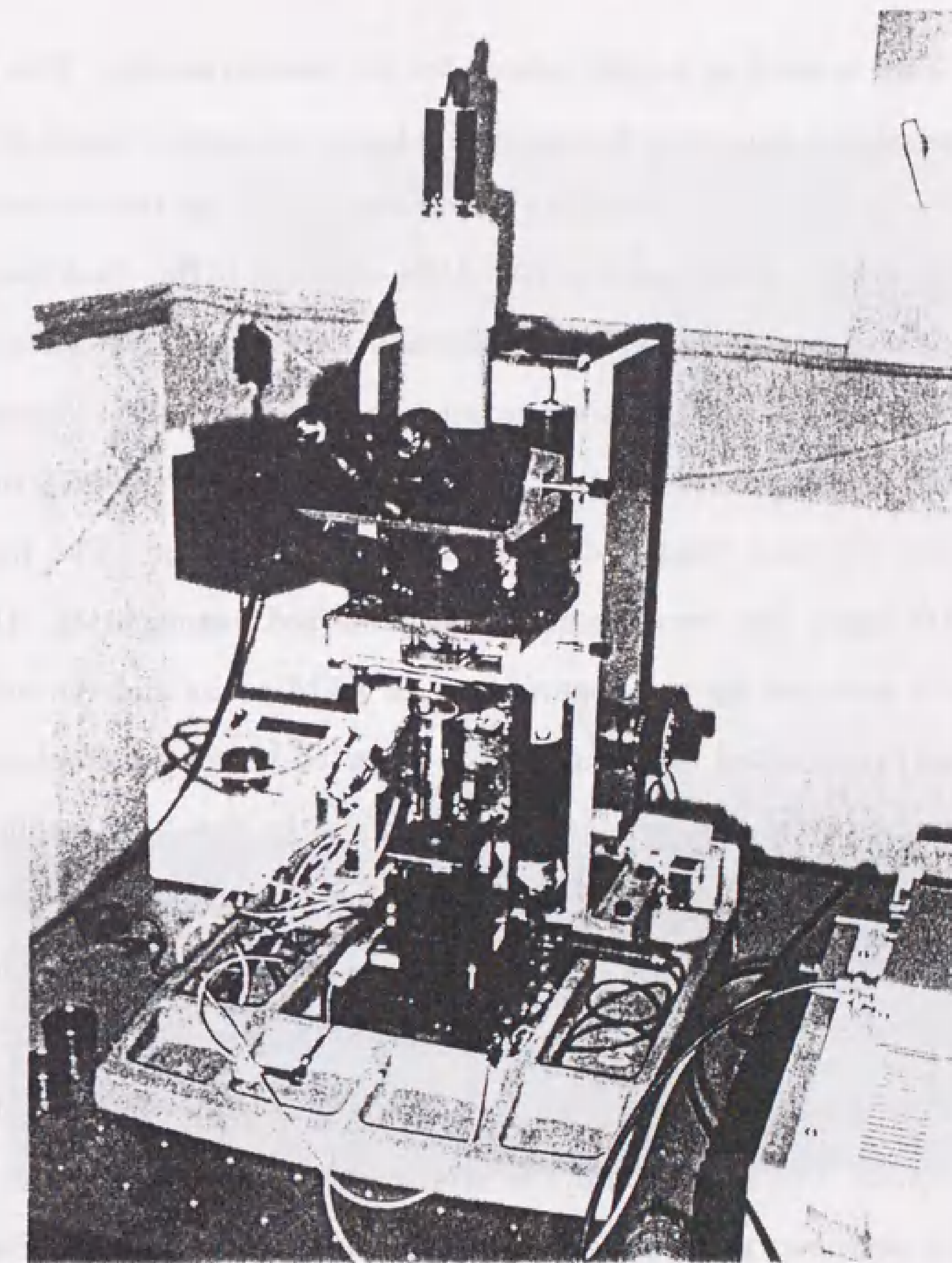

Figure 3.2: Photograph of AFM using heterodyne interferometry.

A He-Ne laser is used as a light source for the interferometer. The polarized incident beam is divided into two beams (signal beam / reference beam) by a beamsplitter. Frequency shift of the reference beam is generated by two acoustic optical modulators operated at frequencies of 80.0 MHz and 80.1 MHz. Beat frequency of the interfering two beams is 100 kHz. The signal beam passes a half-wave plate and the plane of the polarized signal beam is rotated by the angle of 90°. The modulated reference beam and the polarized signal beam are combined by the polarized beamsplitter, and the reference beat is detected by a photodetector. The recombined beam is divided again into two beams by the polarized beamsplitter. One beam (signal beam) is reflected by a rear surface of an AFM probe and the other beam (reference beam) is reflected by a mirror. The reflected beams are combined again. The interference beam, which is modulated in phase by the AFM probe motion, is detected by another photodetector. Deflection of the AFM probe changes the phase of the reflected signal beam. Both beat signals detected by the photodetectors are amplified by the respective photocurrent amplifiers. The displacement of the AFM probe is determined by the phase difference of the two signals obtained by two photodetectors. The resolution of the interferometer is approximately 0.3 nm.

A V-shaped cantilever made of Si_3N_4 by the surface micromachining (Park Scientific Instruments) is used as the AFM probe. Figure 3.3 shows an optical micrograph of the microcantilever. A pyramidal tip is formed near the edge of the cantilever.

A sample is mounted on a stage to move independently in x, y and z directions by a piezoelectric tripod, which consists of three piezoelectric actuators (NEC, AD050518). The movement of the stage is controlled by a computer. The movement of the stage is measured by the developed interferometry and the hysteresis of the

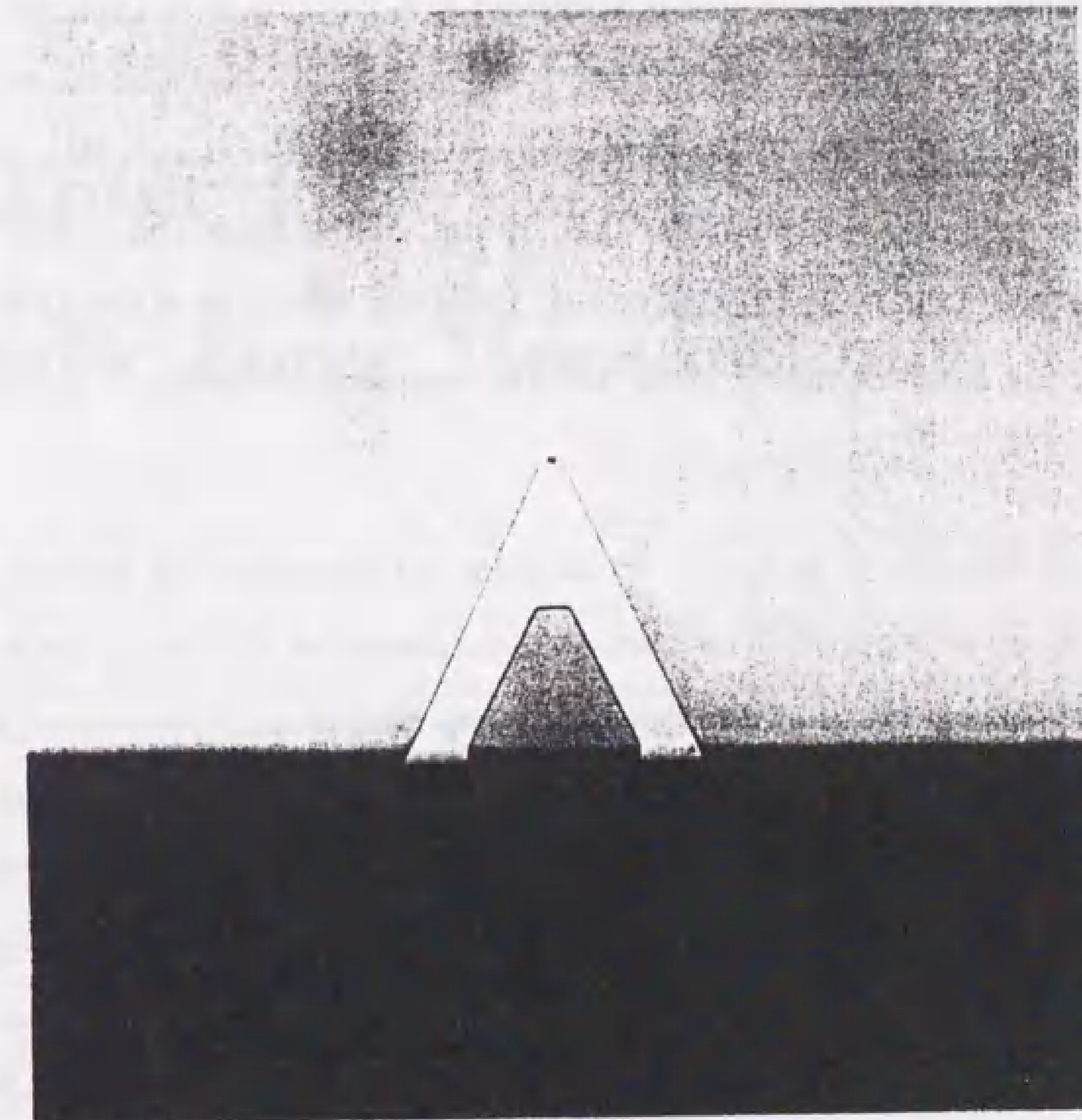

Figure 3.3: Optical micrograph of an AFM probe fabricated by surface micromachining. This micrograph shows a V-shaped microcantilever of 100 μm long, 18 μm wide.

piezoelectric actuators is compensated by controlling voltage applied to each piezoelectric element. The displacement is measured as a function of the voltage applied to the piezoelectric actuator. The voltage is controlled to obtain a linear movement of the stage. By this method, linearity with error of smaller than 1 % is obtained for the stage displacement of smaller than 10 μm. Using the x and y piezoelectric actuators, a sample is scanned horizontally. From the deflection of the AFM probe, the force acting between the AFM tip and the sample is obtained.

Chapter 4

Elastic Force Measurement

A new method for measuring the mechanical properties of micromechanical structures by using an AFM is reported in this chapter. A high resolution AFM system using a laser heterodyne interferometer is constructed. The interaction between an AFM tip and a sample is examined under the condition that a sample is so thin as to be deflected by an interaction force. An SiO_2 microcantilever is made by using the lithographic process and a spring constant is measured from a force curve. The spring constant is used to obtain the Young's modulus of a material. Moreover, the Young's modulus of thin aluminum film coated on a microcantilever is measured by this method. From these experimental results, it is shown that this method is simple and applicable to an elasticity measurement of the micromechanical structures.

4.1 Introduction

In 1970's, micromechanical structures, such as micro-bridge and micro-diaphragm, were fabricated for an integrated micromechanical sensors. In 1980's, a gear, a cantilever and a motor whose dimensions were in the range of hundreds micrometer

were fabricated as microactuators by the IC manufacturing techniques. Materials used for fabricating the micromechanical structures are mostly Si, Si compound and several thin film materials deposited on a flat substrate. Although electric properties of these materials have been well studied, mechanical properties of them are not fully studied. Therefore, it is necessary to study mechanical properties of those thin film materials in order to design the micromechanical structures [51][52].

Allen et al. measured the Young's modulus and residual stress of the polyimide thin films by using a bridge structure[22]. Petersen et al. obtained the Young's moduli of the thin film materials by the resonance frequency measurement[17]. Guckel et al. determined the compressive stress in thin poly-Si films by observing the buckling phenomenon of the thin films[21]. Sugiyama et al. measured the Young's modulus and the Poisson ratio of Si_3N_4 and poly-Si film by applying air pressure on a diaphragm[23]. Photothermal technique was also proposed for the non-destructive evaluation of small mechanical structures[25]. Although all those techniques are non-contact evaluation method, the samples with particular shape must be fabricated to evaluate the mechanical properties of the materials. In addition, since the force acting on the sample is indirect, it is not difficult to apply a localized force to a small portion of the micromechanical structure. Since the micromechanical parts fabricated by the IC technique are much fragiler than the mechanical parts fabricated by a conventional machining, it was difficult to obtain their mechanical properties by a conventional method. As a contact method, a surface profiler was used to obtain the Young's modulus of a material[53][54]. However, it is not applicable to a very fragile thin film structure, since the force applied to a sample by a surface profiler is in the millinewton range and the magnitude of the applied force

is not always changed continuously.

Recently, the AFM which detects an interaction force between a sharp tip of a probe and the sample surface has proved to be a powerful tool in an investigation of surface properties[55, 56]. In the repulsive type AFM, although the AFM probe is considered to be in contact with the sample, a force acting on the sample is in the range of nanonewton. Therefore, the test is non-destructive. A small force controlled in the range of 10^{-8} N can be applied to a small part of the sample by a sharp AFM tip[57]. The AFM has not been used for the evaluation of the mechanical properties of micromechanical structures, such as micro-bridges, micro-diaphragms, etc.

In this chapter, an elasticity evaluation method for micromechanical structures by using the AFM is described. First the interaction between an AFM tip and a sample is discussed under the condition that the sample is so thin as to be deflected by the interaction force. A force curve obtained from the deflection of the AFM probe as a function of the sample displacement is analyzed. Next, a high resolution AFM system using a laser heterodyne interferometer is described. In order to demonstrate the proposed technique, an elasticity of the microstructure is measured. The spring constant and the Young's modulus of an SiO_2 microcantilever are obtained. Moreover the Young's modulus of an aluminum thin film coated on the SiO_2 cantilever is measured. Since the force measured by the AFM is controlled in the region from nanonewton to micronewton, the AFM will be useful for the evaluation of elasticity of the self-sustained micromechanical structures.

4.2 Measurement Technique

Figure 4.1 shows a schematic diagram of an AFM probe and a sample. The AFM probe consists of a soft cantilever and a sharp tip. The AFM detects a small force acting between an AFM tip and a sample from a deflection of the cantilever. When the cantilever deflected upward in Fig.4.1, the displacement of the cantilever is defined as negative. From the deflection of the cantilever z_p and the spring constant $k_p(> 0)$ of the cantilever, we obtain the force $F = -k_p z_p$ acting on the cantilever from the Hooke's law.

Figure 4.2 shows an interaction force acting between the AFM tip and the sample as a function of a tip-sample distance. The vertical axis represents an interaction force F. The positive value corresponds to a repulsive force. The origin of the horizontal axis is a point that the attractive force acting between the sample and the probe balances with the repulsive force. Curve A represents the relation between the the interaction force F and tip-sample distance z_i. The relation between the force F and the cantilever deflection z_p is explained by line B in Fig.4.2. In the previous works, the deformation of the sample itself has not been considered in the AFM measurement. However, in the case of the sample made of self-standing thin film, the sample itself is deformed by applying a small force with the AFM tip. The relation between the force F and the sample deformation z_s is given by line C in Fig.4.2. In the region $z_i < 0$, the decrease of curve A in Fig.4.2 is more rapid than that of line B and line C, and thus, the distance z_i is assumed to be zero.

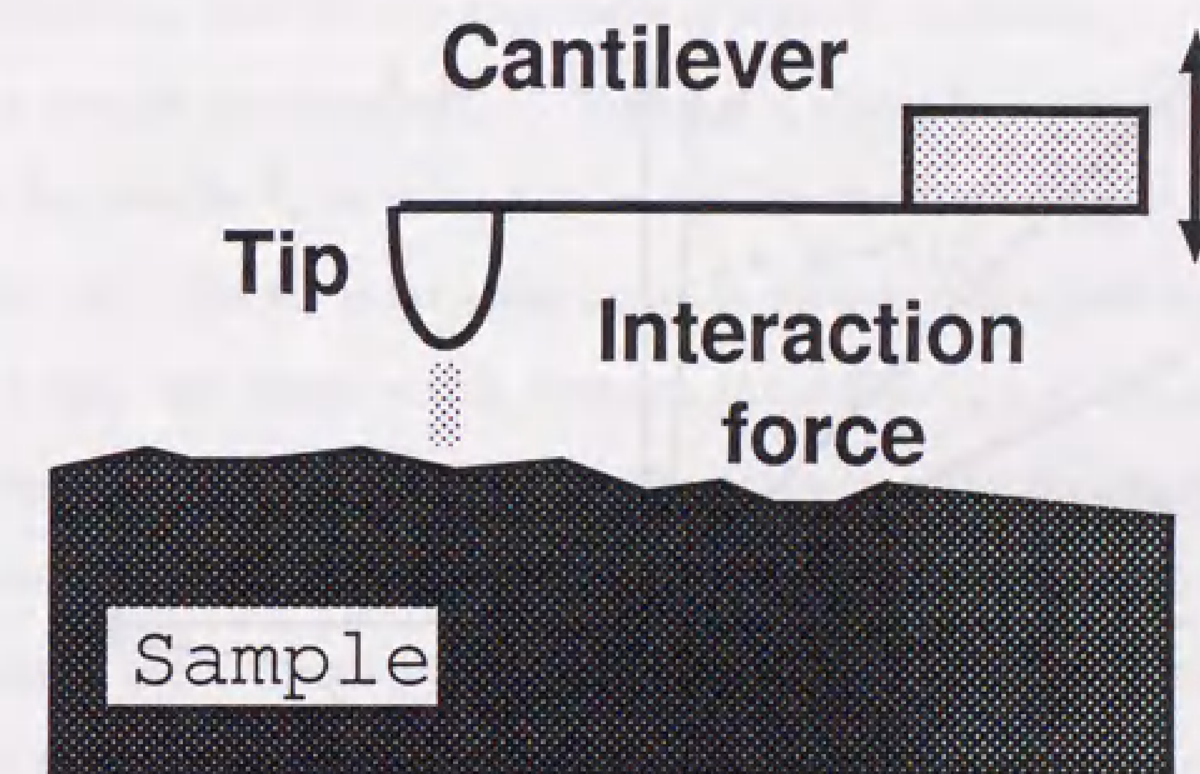

Figure 4.1: Schematic diagram of the AFM probe and the sample.

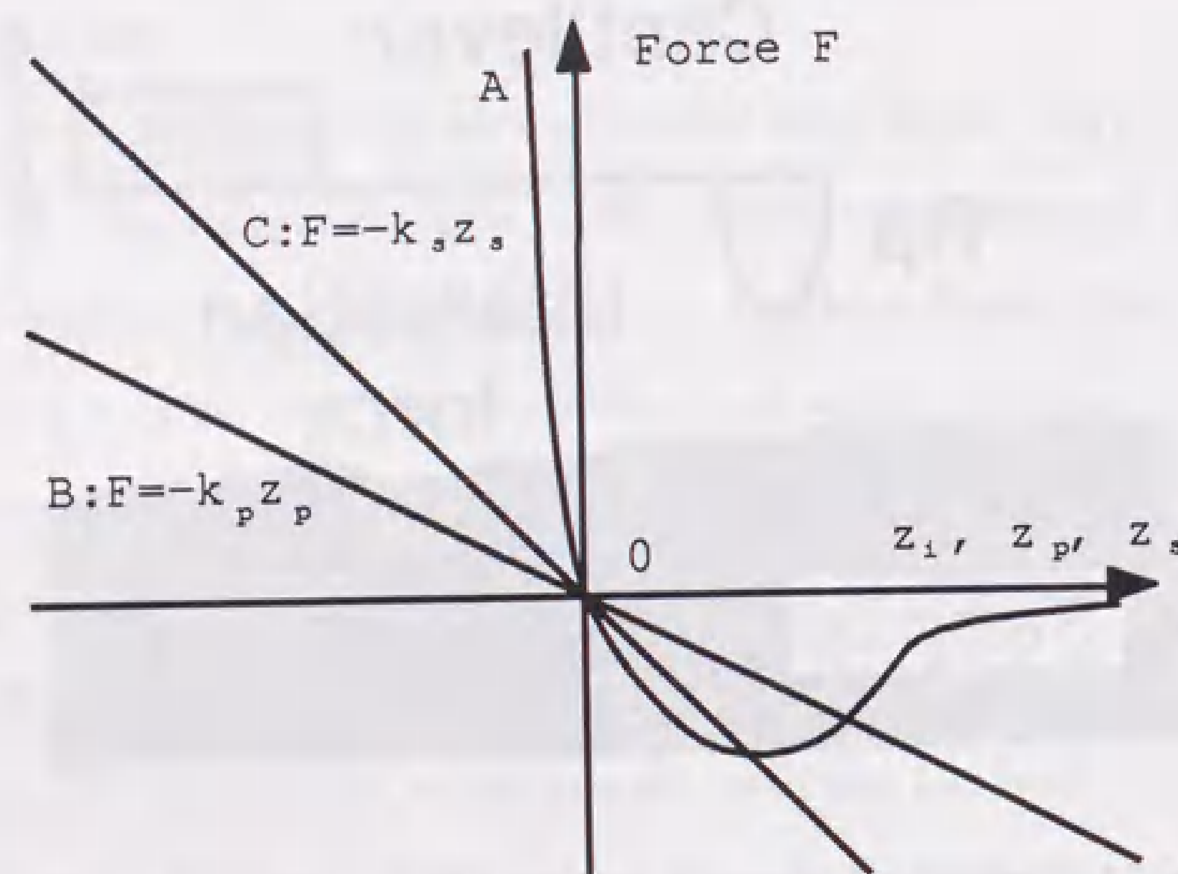

Figure 4.2: Curve A: Interaction force between the AFM tip and sample surface as a function of the distance z_i between them, Line B: force acting on the AFM tip as a function of the probe deflection z_p, Line C: force acting on the sample as a function of the sample deflection z_s.

The force curve (force as a function of sample displacement) for a deformative sample is different from a conventional force curve. Schematic diagram of a self-standing cantilever which is used as a sample in this experiment is shown in Figure 4.3. The cantilever made of a thin film material is assumed to be soft enough to be deformed. The cantilever is distorted downward, when a force applied to the top of the cantilever with an AFM tip.

Figure 4.4 shows typical force curves. Since the force is directly proportional to the probe deflection, the vertical axis denotes a probe deflection z_p. The horizontal axis shows a sample displacement z_s. Figure 4.4 shows force curves for the spring constant of the sample $k_s = \infty$ and $k_s = k_p$. At the beginning of the force curve measurement, the AFM tip is far away from the sample and z_s and dz_p/dz_s are zero, since there is not any forces acting between the AFM tip and the surface. When the sample approaches to the AFM tip, the probe is attracted by the sample and dz_p/dz_s becomes negative (point A). Although the attractive force is van der Waals force in vacuum, the attractive force generated by water layer covering a surface is predominant in air[58]. The AFM probe is deflected downward by the attractive force. Then the restoring force was generated by the deflection, and a distance between the tip and the sample surface become smaller and the probe is moved to a stabilized point. As the stage of the sample is moved closer to the probe, the force changes from attractive to repulsive. In the repulsive region, the distance between the sample and the AFM probe is very small and it is considered to be in contact. If the sample, which contacts with the probe, moves toward the probe, the probe and the sample deflect by the repulsive force and dz_p/dz_s becomes positive as shown in Fig.4.4. Since the force detected by the AFM probe is equal to that applied to the

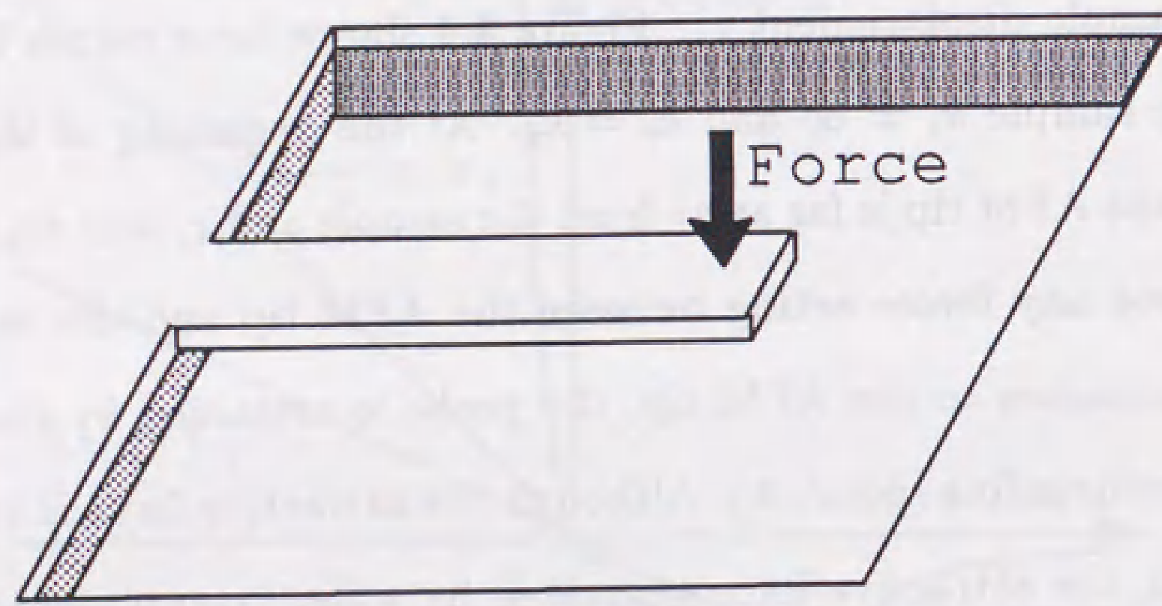

Figure 4.3: Schematic diagram of the cantilever.

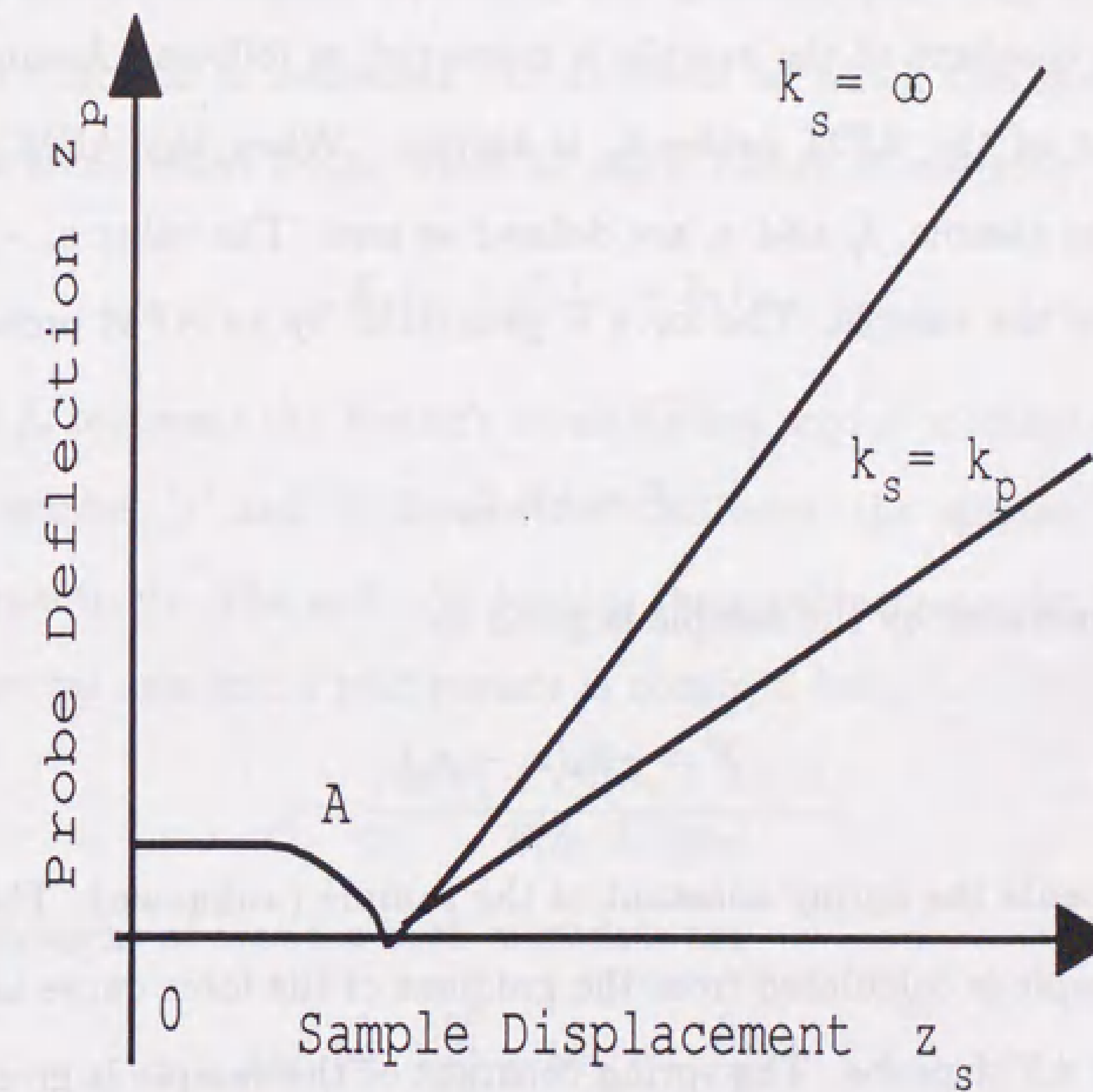

Figure 4.4: Force curves (probe deflection z_p as a function of sample displacement z_s) calculated for the sample having the spring constant of $k_s = \infty$ and k_p.

sample, the deflections of the sample and the probe are obtained by using Fig.4.2. If the sample is considered as a rigid body ($k_s = \infty$), the displacement of the sample is equal to the deflection of the probe and the gradient (dz_p/dz_s) becomes unity as shown in Fig.4.4. When the deformative sample is used as a sample, the gradient in the force curve becomes less than 1. One example ($k_s = k_p$) is shown in Fig.4.4.

The spring constant of the sample is measured as follows. Assuming that the spring constant of the AFM probe k_p is known. When the AFM tip comes in contact with the sample, z_p and z_s are defined as zero. The value $z_s - z_p$ represents the deflection of the sample. The force F generated by an AFM probe is obtained from

$$F = -k_p z_p. \tag{4.1}$$

The force F generated by the sample is given by

$$F = -k_s(z_s - z_p), \tag{4.2}$$

where k_s represents the spring constant of the sample (unknown). The spring constant of the sample is calculated from the gradient of the force curve and the spring constant of the AFM probe. The spring constant of the sample is given by

$$k_s = k_p \frac{z_p}{z_s - z_p} = k_p \frac{c}{1-c}, \tag{4.3}$$

where z_p/z_s is replaced by c.

A rectangular cantilever shown in Fig.4.3 is considered as an sample in this work. The theoretical spring constant is given by

$$k_s = \frac{3EI_z}{l^3} = \frac{Ebh^3}{4l^3}, \tag{4.4}$$

where b, h, l, E, I_z represent width, thickness, length, Young's modulus of the material and the second moment of area, respectively. The Young's modulus is calculated by using Eqs. (4.3) and (4.4).

$$E = \frac{4l^3}{bh^3} k_s \tag{4.5}$$

Next, the cantilever coated with thin film is considered. The Young's modulus of the coated thin film is measured. A cantilever on which thin film was coated is considered as a combined beam. From strength theory of materials, we obtain

$$E_s I_{zs} = E_1 I_{z1} + E_2 I_{z2}, \tag{4.6}$$

where E and I_z represent the Young's modulus and second moment of area, respectively. The number '1' and '2' denote the cantilever, the material coated on the cantilever respectively. The suffix 's' denotes the combined sample. The distance $\bar{y}$ between a neutral axis and a rear surface is obtained from,

$$\bar{y} = \frac{1}{2} \frac{E_1 h_1^2 + E_2(h_2 + 2h_1)h_2}{E_1 h_1 + E_2 h_2}. \tag{4.7}$$

The second moment of area for both materials are

$$I_{Z1} = \frac{bh_1^3}{12} + bh_1(\bar{y} - \frac{h_1}{2})^2, \tag{4.8}$$

$$I_{Z2} = \frac{bh_2^3}{12} + bh_2(\bar{y} - h_1 - \frac{h_2}{2})^2 \tag{4.9}$$

From Eqs.(4.6)-(4.9), we obtained the quadratic equation on E_2,

$$AE_2^2 + BE_2 + C = 0, \tag{4.10}$$

where

$$A = bh_2^4,$$

$$B = E_1 b h_1 h_2 (4h_1^2 + 6h_1 h_2 + 4h_2^2) - 12 E_s I_{Zs} h_2,$$
$$C = E_1^2 b h_1^4 - 12 E_s I_{Zs} E_1 h_1.$$

The values E_1, b, h_1, h_2 and l are known. The value of $E_s I_{zs}$ is obtained from the force curve measurement of the combined beam by Eqs.(4.3) and (4.4),

$$E_s I_{zs} = \frac{l^3}{3} k_s = \frac{l^3}{3} \frac{c}{1-c} k_p. \quad (4.11)$$

The Young's modulus E_2 of coated thin film is calculated by Eq.(4.10).

4.3 Experiments

The experimental setup was described in chapter 3. A V-shaped cantilever (Park Scientific Instruments) was used as an AFM probe. The cantilever used in this chapter is 200 μm long, 36 μm wide and 0.6 μm thick. A spring constant of the AFM probe is 0.064 N/m (catalogue value). The spring constant was confirmed. A small particle was attached to an end of the probe and a deflection of the probe was measured.

Deflection of the cantilever is measured by a heterodyne interferometer. A He-Ne laser is used as a light source for the interferometer. Beat frequency of the interference signal generated by two acoustic-optical modulators is 100 kHz. An incident beam is divided into a signal beam and a reference beam. Two divided beams are polarized perpendicularly to each other using half wavelength plates. A signal laser beam is focused on an end of the AFM probe. The signal beam interferes with the reference beam and a phase difference is counted by the pulse counting method. The resolution corresponding to the probe displacement is 0.3 nm.

A sample mounted on a stage is moved independently to x, y and z directions by three piezoelectric actuators. Movement of the stage is controlled by a computer. In order to avoid the hysteresis of the piezoelectric actuators, the displacement as a function of the voltage applied to the piezoelectric actuators was measured and the controlled voltage which was subject to obtain a linear movement of the stage was determined. By this method, the stage moves linearly with the accuracy of 1 % for the displacement smaller than to 10 μm.

The probe deflection z_p is measured as a function of the sample displacement z_s. The value z_p was obtained through an AD converter and was processed by a computer. The time necessary to measure the force curve is approximately 10 seconds. Since the stage moves in the range of 10 μm with 0.01μm resolution, the force applied to the sample by the probe is smaller than 0.6 μN and the resolution is 0.6 nN.

In the experiments, self-standing cantilevers made of an SiO_2 thin film were fabricated as samples. An SiO_2 layer which was grown on $< 100 >$ Si wafer was patterned by a HF:NH_4F solution with a photoresist. After stripping the photoresist, the wafer was immersed into a KOH solution. By etching Si anisotropically, a cantilever array of SiO_2 thin film was fabricated. Figure 4.5 shows the rectangular cantilever array made of an SiO_2 thin film, which is coated with aluminum. Each cantilever is 200 μm long, 20 μm wide and 0.42 μm thick. The cantilevers of 40-200 μm long, 20/40 μm wide and 0.42 μm thick are also fabricated. The width and the width are measured by an optical microscope and the thickness is by the developed AFM.

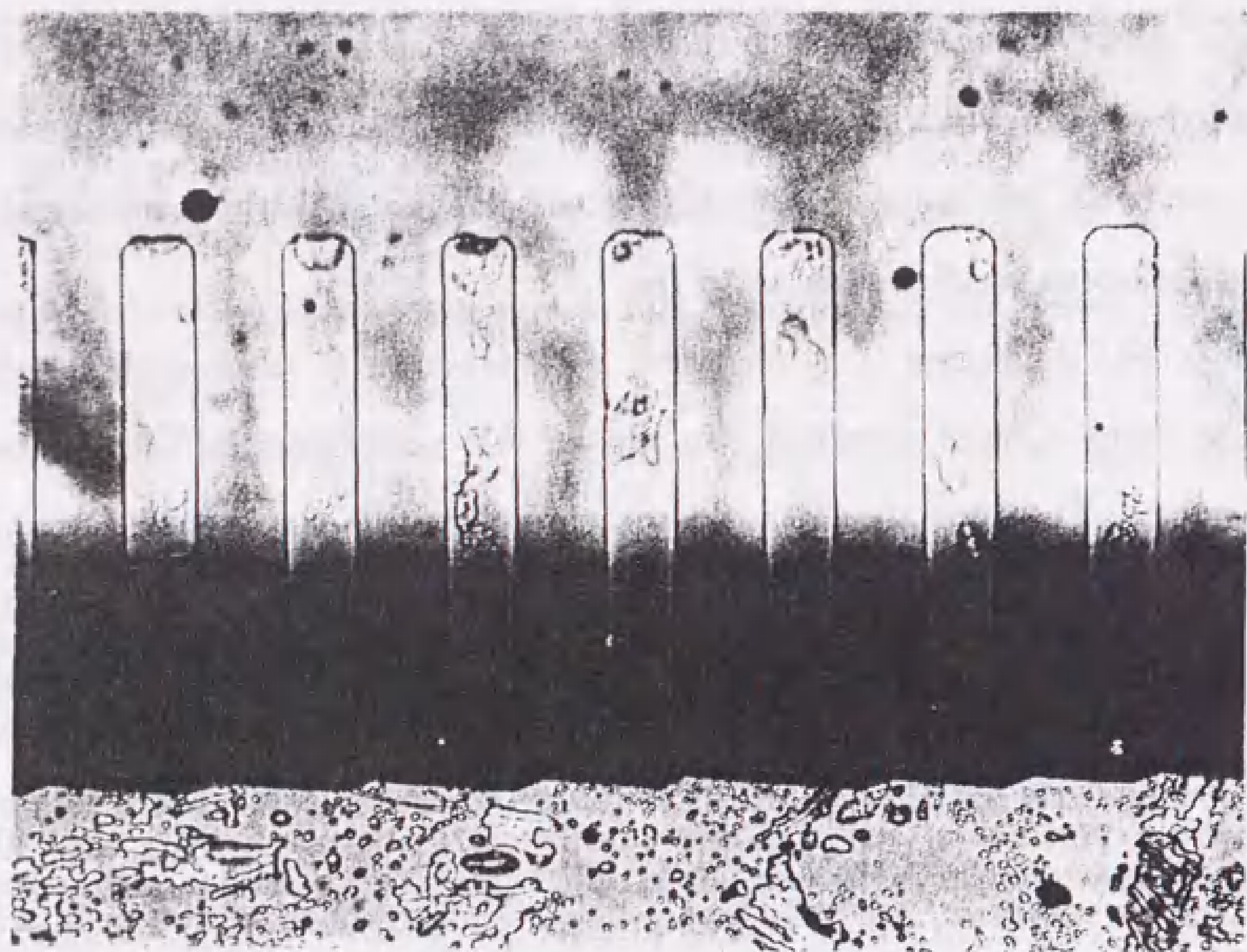

Figure 4.5: Fabricated cantilever array.

4.4 Results and Discussions

4.4.1 Elasticity Measurement of Microcantilever

The spring constant of a self-standing cantilever was measured. Typical results of the force curve are shown in Fig.4.6. When the sample approaches the AFM probe, the value z_s increases. The horizontal axis represents a stage displacement z_s, and the vertical axis represents a probe deflection z_p. The AFM probe first is attracted to the sample and comes into contact with the sample surface. The the AFM probe moves with the stage. The value c of Eq.(4.3) is obtained from the gradient of the curve shown in Fig.4.6, and then the spring constant k_s is calculated. In Fig.4.6(a), the spring constant k_s is calculated to be infinity by Eq.(4.3), since the gradient c of the force curve is equal to unity. Similarly, k_s obtained from the curve shown in Fig.4.6(b) is equal to k_p. In the case of Fig.4.6(b), $k_s = k_p/2$. By using the cantilevers of different length, the measurement was repeated. The results are shown in Fig.4.7. The horizontal axis represents the cantilever length and the vertical axis represents the spring constant k_s. In Fig.4.7, the results obtained by using 20 μm-wide and 40 μm-wide cantilever sample are shown. The measured spring constants k_s are nearly proportional to l^{-3}, where l is the length of the cantilever sample. These results agree with the fact that the spring constant is theoretically proportional to l^{-3} as shown by Eq.(4.4).

The Young's modulus of an SiO_2 thin film is obtained from the measured spring constant to be $(7.3 \pm 0.9) \times 10^{10}$ Pa. The error is calculated from the standard deviation of the measured values for each sample. The measured Young's modulus agrees with the value of a silica glass (7.31×10^{10}Pa[59]). Therefore the Young's

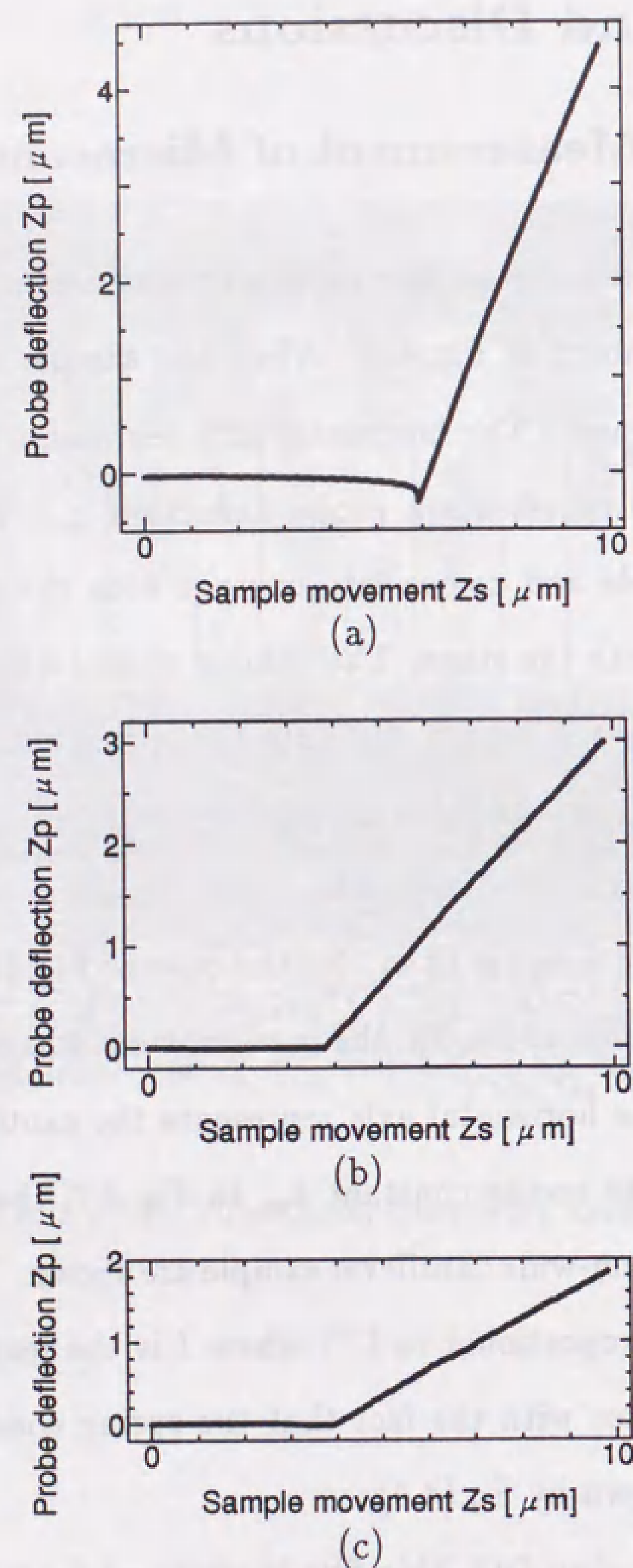

Figure 4.6: Measured force curves (probe deflection z_p as a function of sample displacement z_s).

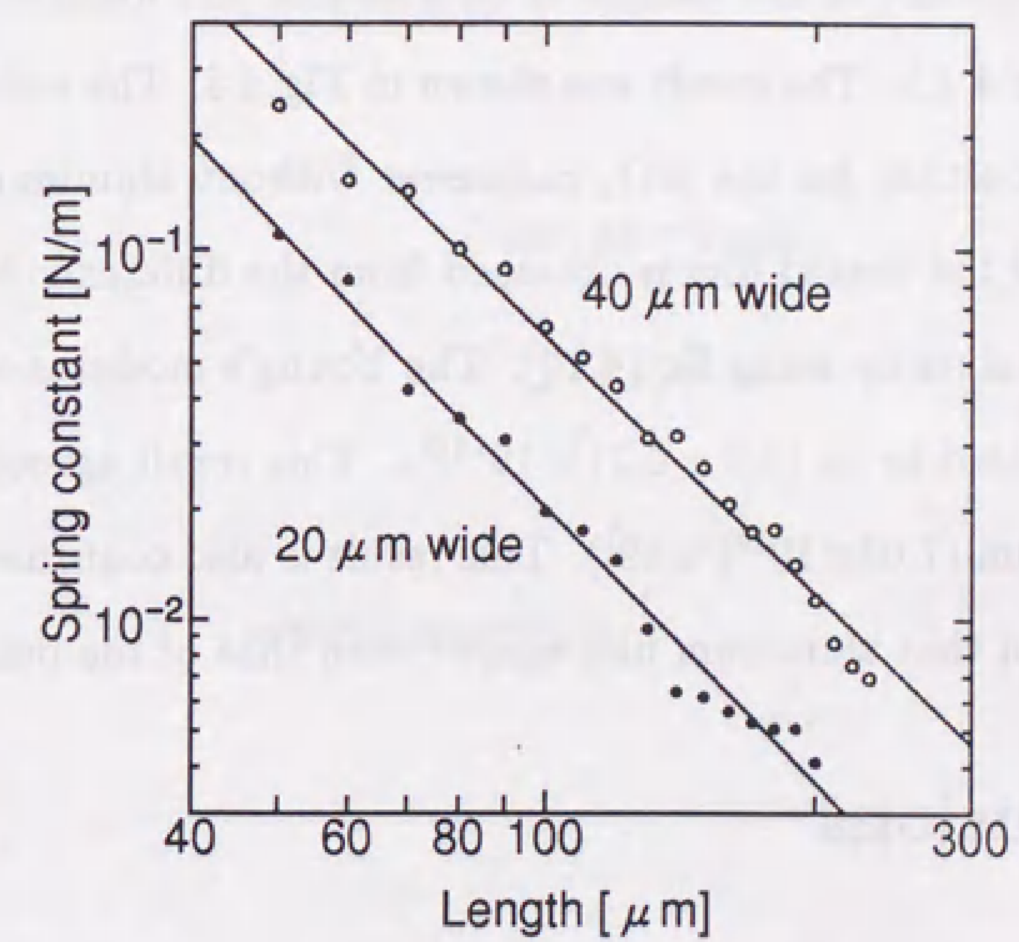

Figure 4.7: Spring constant of the SiO_2 cantilever measured as a function of the length.

modulus of the thin SiO_2 film is not different from the value of bulk material.

4.4.2 Measurement of the Young's Modulus of PVD Thin Film

The same cantilever used in the previous experiment was coated with vaporized aluminum. The thickness of aluminum is measured with the AFM to be 84 ± 7 nm. The spring constant of the sample is obtained in the manner similar to that described in section 4.4.1. The result was shown in Fig.4.8. The solid line in Fig.4.8 shows the spring constant for the SiO_2 cantilever without aluminum coating. The Young's modulus of the coated film is obtained from the difference between the line and the measured values by using Eq.(4.10). The Young's modulus of the aluminum thin film was evaluated to be $(6.9 \pm 0.2) \times 10^{10}$Pa. This result agreed well with that of the bulk aluminum (7.03×10^{10}Pa[59]). This result is also confirmed by the report that the elasticity of thin aluminum film agreed with that of the bulk materials[60].

4.5 Conclusions

For practical fabrication of the micromechanical systems, it is necessary to know mechanical properties of thin film materials. In this chapter, the spring constants of micromechanical structures were directly measured with the AFM. The AFM system using the heterodyne interferometry was developed in order to measure a probe deflection with high accuracy. A small force controlled in the range of nanonewton was applied to the sample by the AFM probe. The spring constant and the Young's modulus of self-sustained thin films were measured by the proposed method. The spring constants of micromachined cantilevers coated with thin aluminum films were

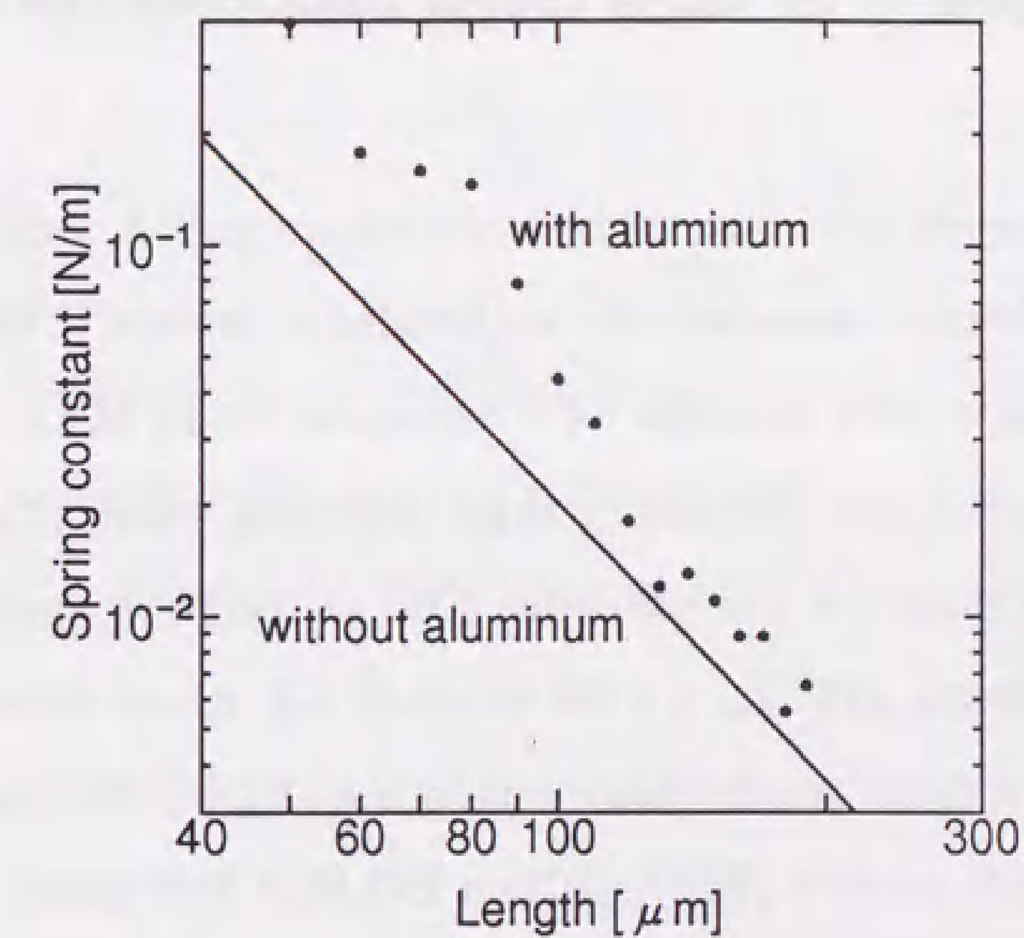

Figure 4.8: Spring constant of the cantilever (20 μm wide) measured as a function of the length. The SiO_2 cantilever is coated with aluminum (84 nm thick).

also measured, and the Young's modulus of the film was obtained. The proposed technique will be useful for the measurement of elasticity of the thin film and the measurement of the spring constant of the micromechanical structure. The merits of the proposed method is as follows. The measurement is nondestructive. An elasticity force of the micromechanical structure can be measured. A small force in the range of nanonewton can be applied to a small region in the nanometer range. The magnitude applied to the sample changes continuously from nanonewton to micronewton.

Chapter 5

Adhesive Force Measurement

The adhesive force acting on microstructures has been investigated by using an AFM. In the AFM system, a heterodyne interferometer is used to measure the deflection of the AFM probe precisely. The adhesive force (capillary force) acting between an Si_3N_4 probe and some kinds of material used for micromachining processes is investigated. When an SiO_2 substrate and five kinds of solution are used, the adhesive forces are in the range 10 nN - 1 μN. The adhesive forces generated by C_2H_5OH and CH_3COCH_3 are smaller than others, which is consistent with the result that the rinse with C_2H_5OH or CH_3COCH_3 reduces the pinning of surface-micromachined cantilevers to a substrate. The results are discussed on the basis of the macroscopic adhesive theory. The adhesive force is independent of the repulsive force applied to the sample surface in the force range from 10 nN to 6 μN and is almost uniform in the measured area (6 μm$\times$6μm). In addition, the adhesive force of solid bridging, which occurs by the deposition of insoluble impurities present in a small gap of the microstructures after drying process, has been tested by peeling off a microcantilever pinned to the dried substrate.

5.1 Introduction

It is important to evaluate quantitatively the adhesive force acting in the microscopic region, since microstructures fabricated by silicon anisotropic wet etching or by sacrificial layer etching are often plagued by the problem of adhesion to the substrate. In addition, the adhesive force as well as the frictional force often affects the movement of microstructures having the contact slide mechanism.

Linder and de Rooij investigated the sticking of polysilicon microbeams fabricated by using silicon dioxide as a sacrificial layer, and reported that it is caused by an electrostatic force[35]. Using micromachined test vehicles especially designed to evaluate the adhesion, Alley et al. measured the pull-off force[38]. Silica residues were considered to be responsible for the adhesion. Mastrangelo and Hsu presented a simple experimental technique for the measurement of the adhesion of microstructures[41, 42]. Cantilevers different in length and thickness were fabricated, and the adhesion was investigated by the measurement of the detachment length of the cantilever. The surface energy was evaluated to be 140mJm^{-2} for the combination of a polysilicon beam and silicon substrate. Scheeper et al. investigated the adhesive force acting between a PECVD silicon nitride cantilever and silicon dioxide substrate. It was concluded that the sticking of the cantilever was due to the adsorption of water molecules[39].

On the other hand, the AFM has proved to be a powerful tool for evaluating the force acting in a very small region[44]. The interactions between the AFM probe and the surface include the van der Waals force, electrostatic force and capillary force of liquids present in the gap. These respective forces can be evaluated by an

AFM with a resolution surpassing that of currently available techniques. There is also a high level of interest in adhesion measurement using the AFM[58, 28, 61].

In this paper, the properties of the adhesive force acting in the materials used for micromachining were investigated by an AFM. A high resolution AFM system using a laser heterodyne interferometry was constructed. We measured the adhesive force (capillary force) acting between silicon nitride probe and several kinds of substrate, which were covered with different solutions. Moreover, the adhesive force due to solid bridging was examined by palpating the micromachined structures pinned to the substrate with the AFM probe The micromachined cantilevers were pinned to the substrate by the deposition of insoluble impurities after they were dried completely. The AFM probe was placed below the micromachined cantilevers, then was moved upward to peel off the cantilevers pinned to the substrate.

5.2 Experiments

The AFM probe consists of a sharp tip and a cantilever having a low spring constant. The motion of the cantilever is monitored as a function of the sample translation. From the deflection of the cantilever, the force acting between the tip and sample surface is obtained. In the case of the adhesion measurement, the adhesive force is measured from the magnitude of the transition appearing in the force curve (force vs. sample-translation curve)[61]. When the probe is in contact with the sample surface, the repulsive force increases linearly with the increase of sample displacement. On retracting the probe, the repulsive force decreases. On further withdrawal, the pull-off force increases. When it overcomes the adhesive force acting between the sample and the probe, the probe suddenly separates from the surface. The adhesive force

is determined from the transition.

The experimental setup is described in chapter 3. The deflection of the cantilever is measured by heterodyne interferometry. A He-Ne laser is used as a light source for the interferometer. The incident beam is divided into a signal beam and a reference beam. The signal beam is focused on the rear surface of the probe and the phase difference between the reflected signal beam and the reference beam is detected. The resolution of the interferometer is approximately 0.3 nm. A V-shaped cantilever made of silicon nitride (Park Scientific Instruments) is used as a probe. The cantilever is 200 μm long, 36 μm wide and 0.6 μm thick and the spring constant of the probe is 0.064 N/m. A small sharp tip is formed near the edge of the probe. The scanning electron micrograph of the AFM tip is shown in Fig.5.1. A pyramidal tip is formed near the edge of the probe. Small latex spheres of 500 nm diameter, which are widely used in calibrating the SEM, are used as a size standard. Both the base length and the height of the pyramidal tip are approximately 4 μm. The top radius of the tip is evaluated from observation with a scanning electron microscope to be approximately 50 nm. The sensitivity for the force measurement is approximately 20 pN. A sample mounted on a stage is moved independently in x, y and z directions by three piezoelectric actuators. The hysteresis of the piezoelectric actuator is compensated by controlling the voltage applied to the piezoelectric element. The stage is moved linearly with an uncertainty less than 1%. In the adhesive force measurements, five kinds of liquid (purified water, H_2O ; 99% acetone, CH_3COCH_3 ; 99.5% ethanol, C_2H_5OH ; 4% potassium hydroxide, KOH ; 99% carbon tetrachloride, CCl_4), and four kinds of substrate (slide glass, SiO_2 ; silicon wafer, Si; CVD polysilicon film, poly-Si; and CVD silicon

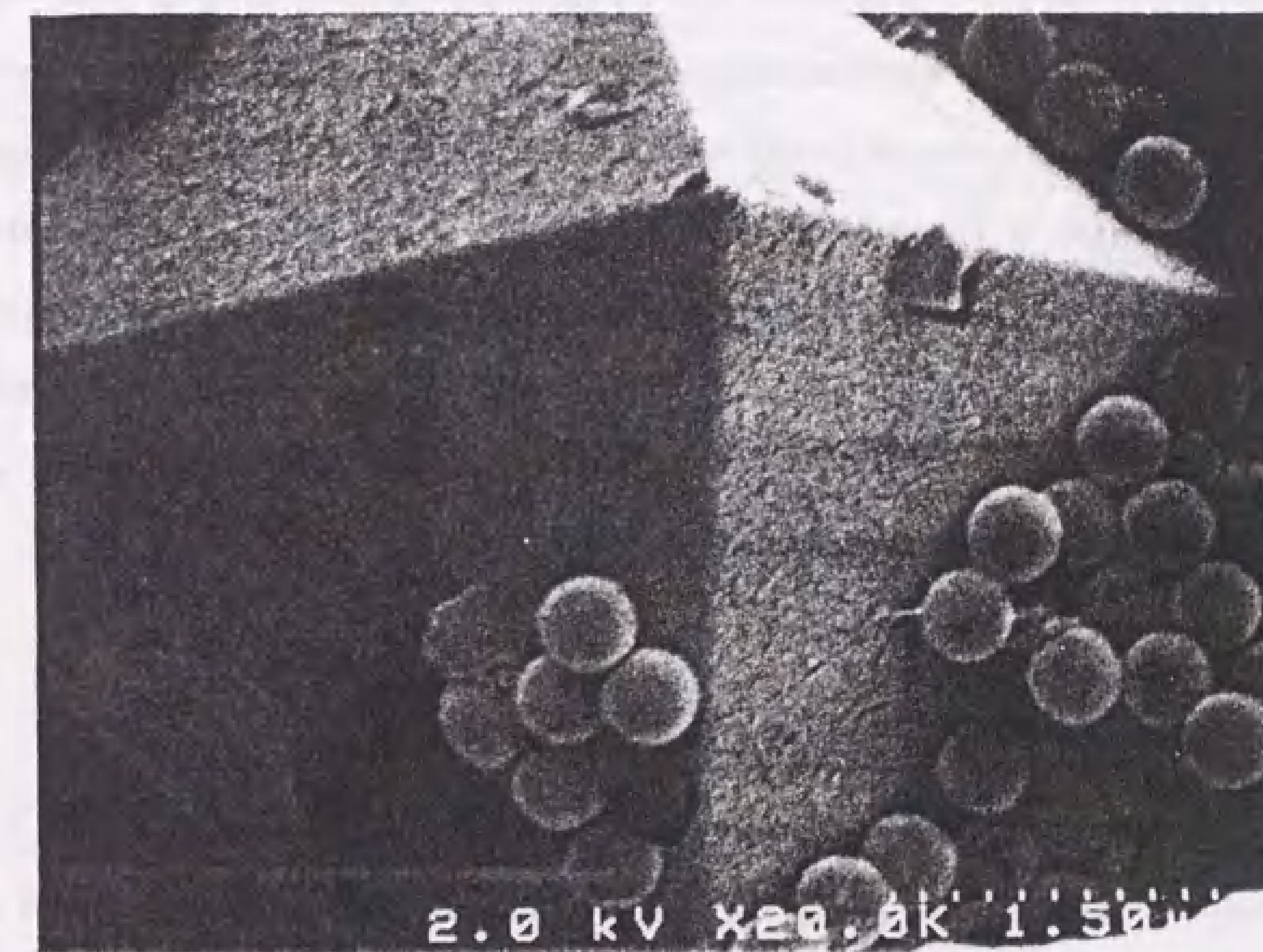

Figure 5.1: Scanning electron micrograph of an AFM tip. Top radius is approximately 50 nm.

nitride film, Si_3N_4) were used. The substrates were immersed in the liquids and were dried by a heater at 50 °C for five minutes.

In addition, we carried out another experiment to measure the adhesive force due to solid bridging. The micromachined cantilevers were pinned to the substrate by the deposition of insoluble impurities after they were dried completely. The AFM probe was placed below the micromachined cantilevers, then it was moved upward to peel off the cantilevers pinned to the substrate as shown in Fig.5.2. In this case, the AFM was used as a manipulator for palpation. When the pinned structure was released by the increase of the pull-off force, the adhesive force of the pinning was determined from the deflection of the AFM probe. The deflection of the probe was measured by the interferometer. A pinned microcantilever array, which was fabricated from thermally oxided silicon thin film, was used as the sample.

5.3 Results and Discussions

Figure 5.3 shows the typical force curve obtained for an SiO_2 sample with thin H_2O layer at a sample temperature of 22 °C and 40 % humidity. Two transitions are shown in the force curve. At the first transition point (point A in Fig.5.3), the probe touches the sample surface, At the second transition point (point B in Fig.5.3), the probe separates from the sample surface and returns to the original position. The adhesive force is determined from the second transition, where the adhesive force (F_{cf}) is equal to the distortional force of the AFM probe. The distortional force is calculated by kz_c, where k is the spring constant of the AFM probe ($k = 0.064$ N/m) and z_c is the deflection of the AFM probe at the second transition. Therefore, force balance is given by $F_{cf} = kz_c$. Since the second transition occurs under a critical

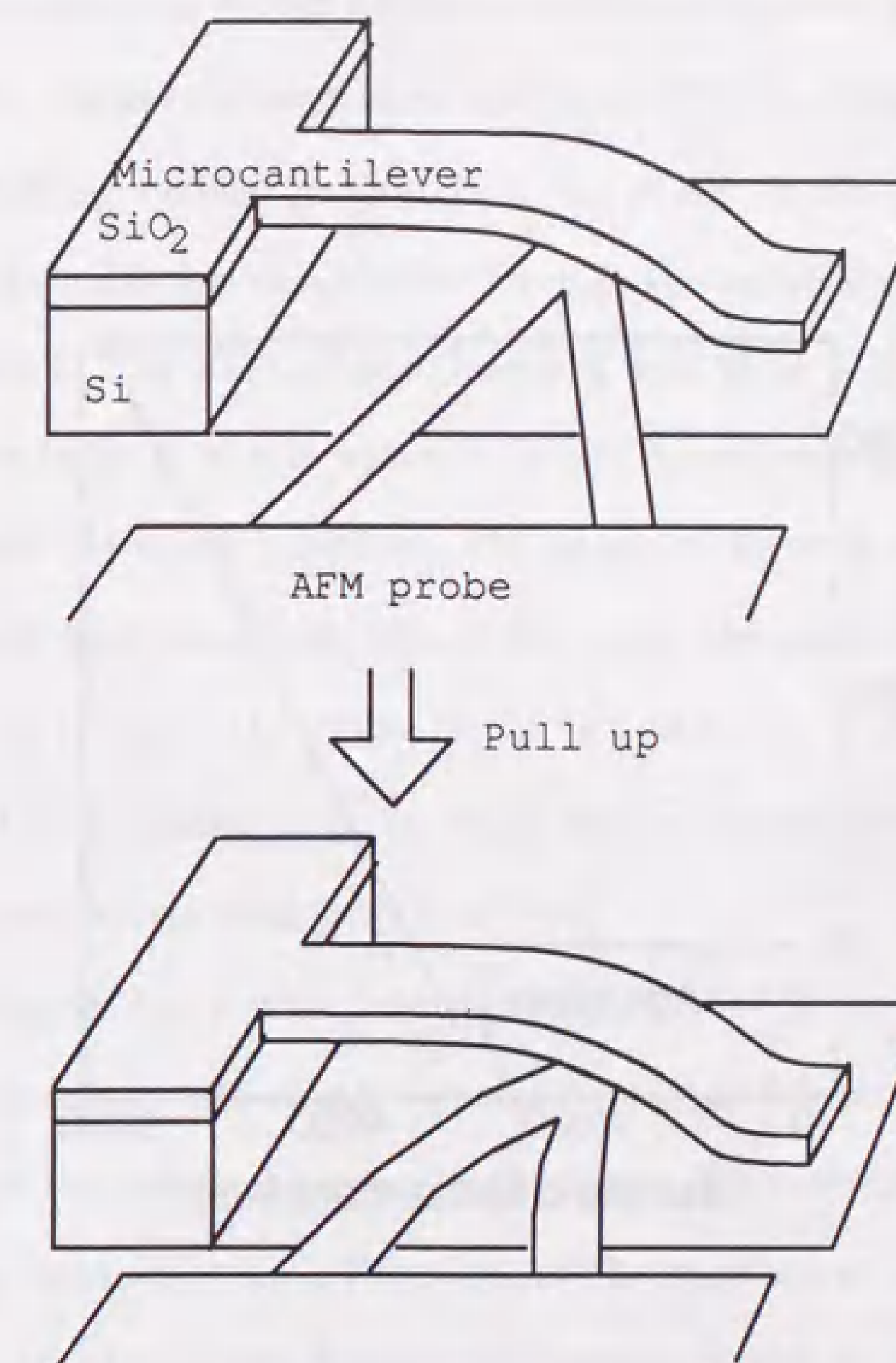

Figure 5.2: Schematic diagram of a peel-off sequence of a microcantilever pinned to a substrate.

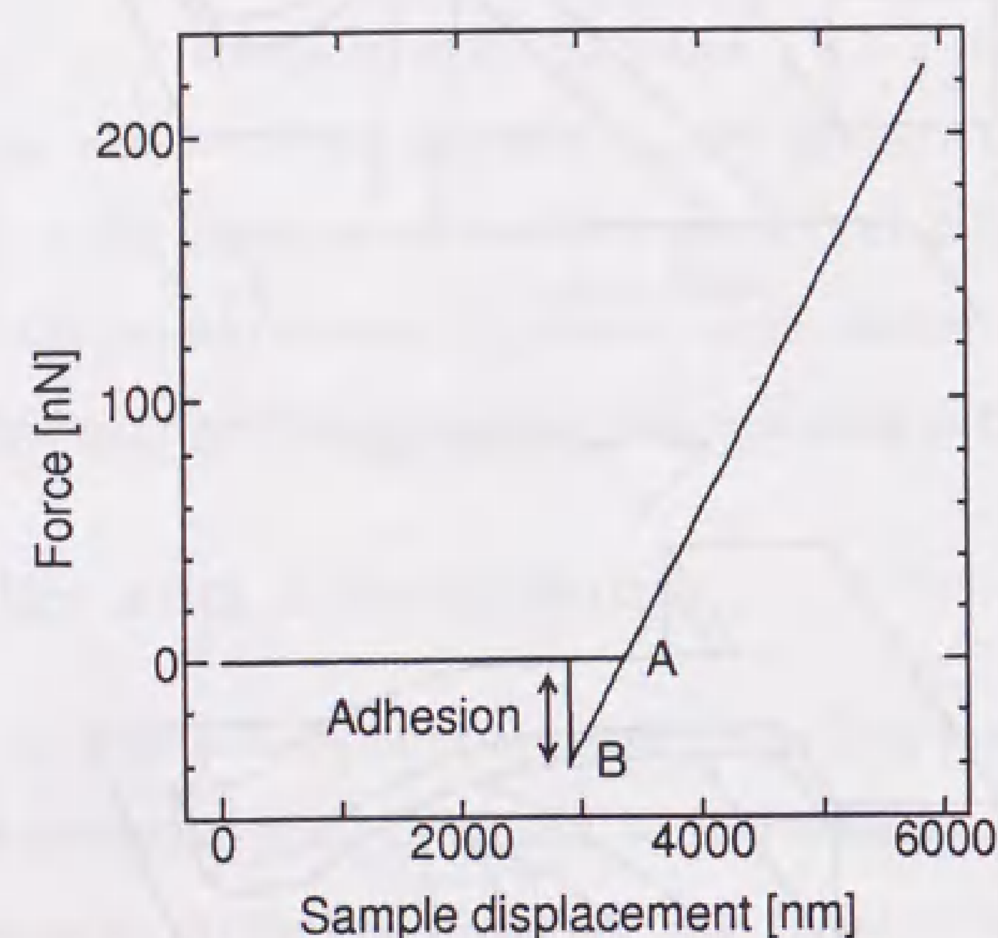

Figure 5.3: Typical force curve obtained for SiO_2 sample and H_2O solution. The temperature was 22 °C and the humidity was 40 %.

condition of the force equilibrium, the measured values of the adhesive force are somewhat scattered. We repeat the force curve measurement more than 50 times, and an average value is obtained.

The spatial distribution of the adhesion was investigated for an SiO_2 substrate. An example of the measured results is shown in Fig.5.4. Figure 5.4(a) shows the topography of the SiO_2 surface measured in the static mode of AFM. Figure 5.4(b) shows the spatial distribution of adhesive force in the same area. The sample surface is covered with H_2O. The surface roughness is less than 1 nm in the 6 μm$\times$6μm area. The adhesive force is nearly uniform in the measured region, and the averaged magnitude is 45 nN. At some positions, the adhesive force is smaller than the averaged value. It seems that small particles existing on the surface reduce the adhesion. From the magnified images, the diameter of the particles is estimated to be on the order of 10 nm. The particles may be small silica impurities that are produced in the wet etch process as reported previously[38].

When the adhesive force was determined from the force curve measurements, the probe was pressed to the sample surface. The influence of the pressing force (repulsive force) on the measurement of adhesion was investigated. Figure 5.5 shows the adhesive force measured as a function of the maximum repulsive force, which is applied to the sample surface before the measurement of the adhesive (pull-off) force. The sample used in the experiment is a flat fused SiO_2 substrate (Matsunami Ltd., S-1225) placed in the atmosphere (temperature 17°C , humidity 38%). The flat SiO_2 substrate was cleaned without polishing. The roughness of the sample surface is smaller than 1 nm. The measured adhesive force increases slightly in the force region smaller than 5000 nN. The rate of the increase is 5×10^{-4} nN/nN.

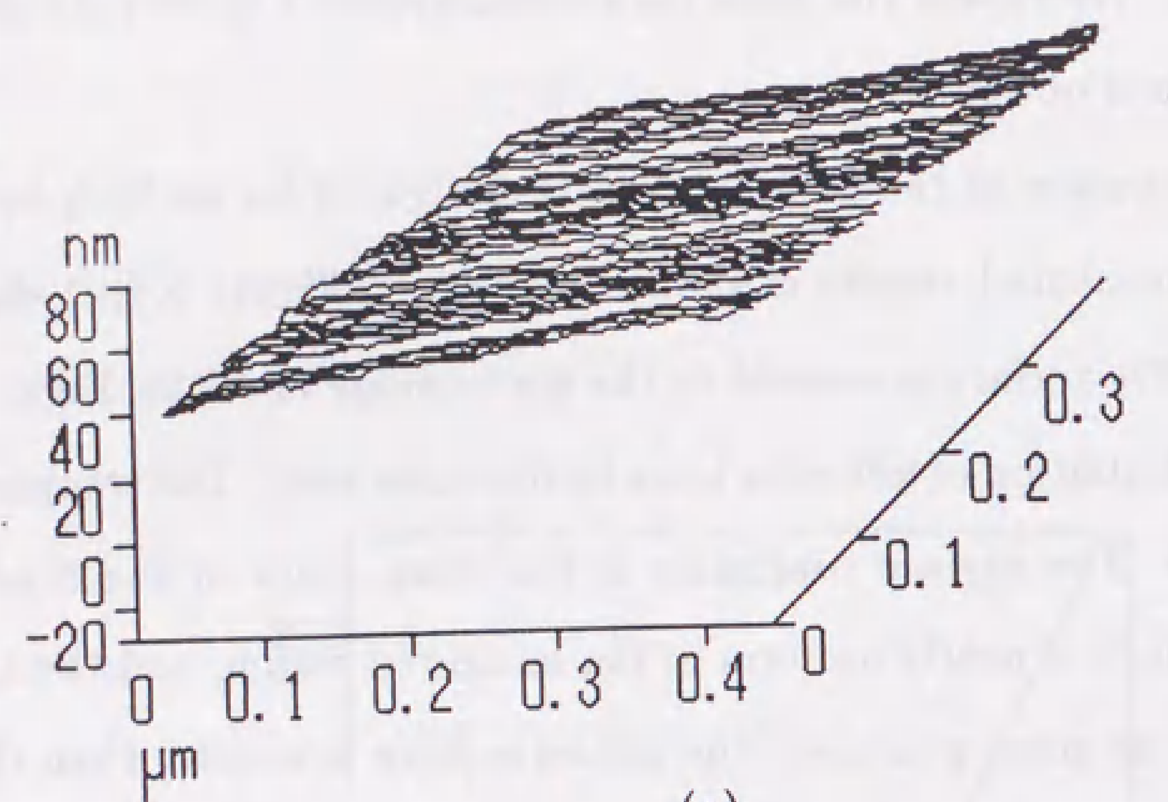

(a)

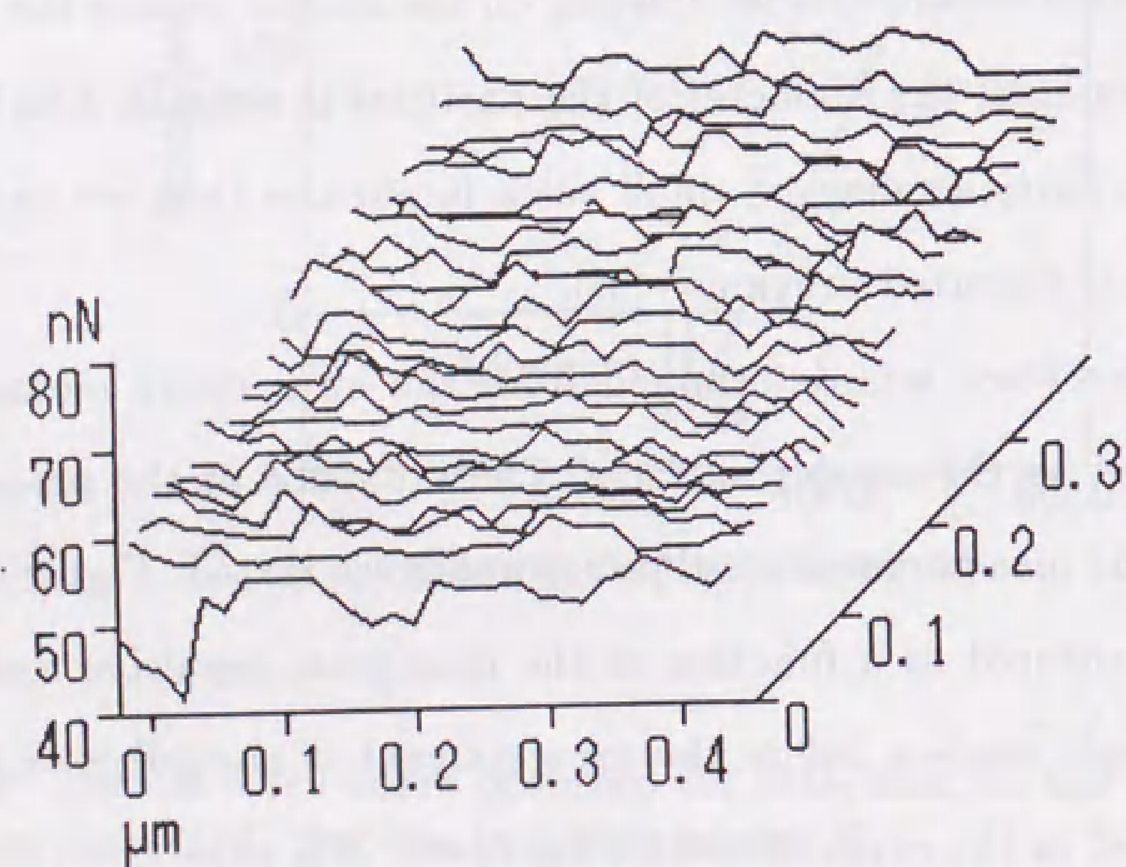

(b)

Figure 5.4: (a) Surface topography of SiO_2 substrate, (b) spatial distribution of adhesive force in the same area as shown in (a).

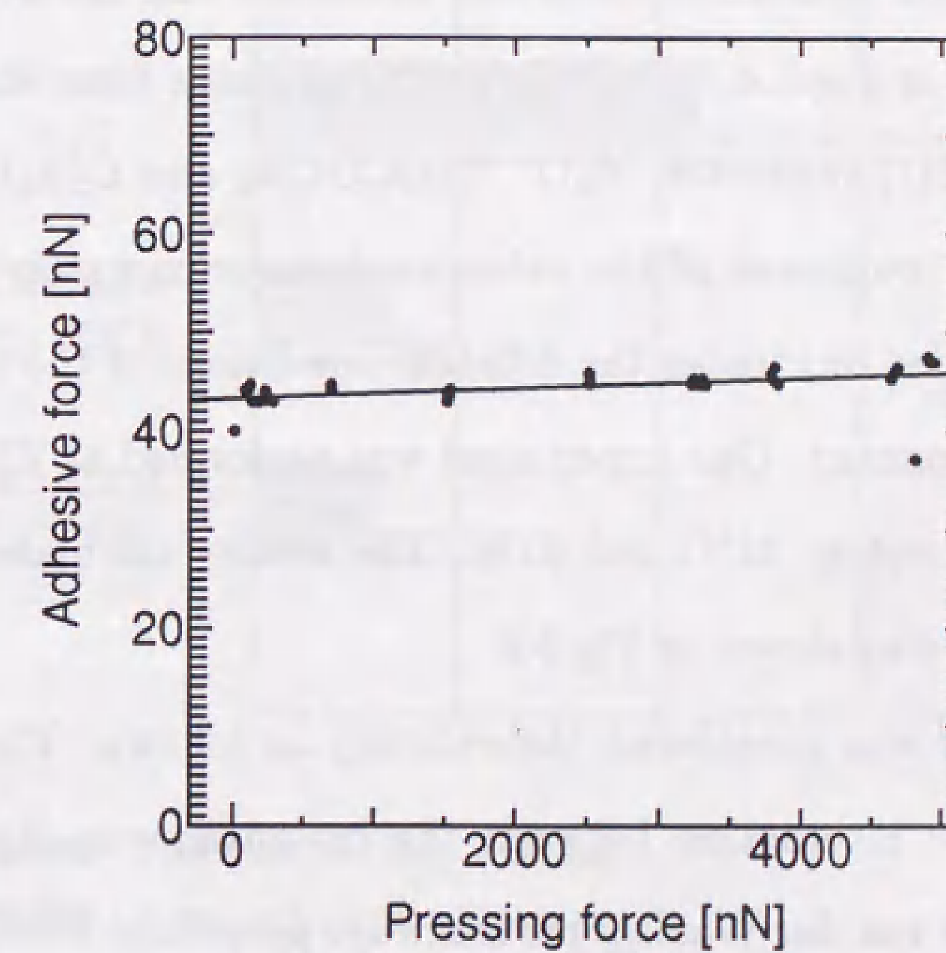

Figure 5.5: Adhesive force measured as a function of the repulsive force (pressing force) applied to a sample.

We believe that the slight increase is caused by the increase of the contact area. However, the adhesive force measurements were carried out mostly in the repulsive force region smaller than 300 nN. Therefore, the influence of the repulsive force on the adhesive force measurement was negligible when compared with the scattering of the measured values.

With the above experimental results in mind, we carried out the adhesive force measurement for several combinations of the substrate and the solution. A set of results is summarized in Fig.5.6, which shows the adhesive force acting between an Si_3N_4 probe and an SiO_2 substrate. H_2O , CH_3COCH_3 and C_2H_5OH were used as the test liquids. The roughness of the substrate is approximately 1 nm. The two experiments were carried out under the different conditions of the temperature and humidity of the environment. One experiment was performed at 23°C and 26% and the other was carried out at 21°C and 61%. The results calculated by the Eq.(2) (described below) are also shown in Fig.5.6.

The adhesive force was considered theoretically as follows. The van der Waals force is caused by the interaction between the instantaneous dipole moments of atoms[38, 62, 63]. The van der Waals force is always present to some degree, but can be reduced by using surface layers having lower surface energy, such as hydrocarbon or fluorocarbon monolayers. The van der Waals force F_{vdw} is given by

$$F_{vdw} = \frac{AS}{6\pi d^3}, \tag{5.1}$$

where A is the Hamaker constant of the surfaces with no surface layers and an intervening air gap is 1.7 eV, d is a distance between two flat surfaces, and S is an effective contact area. The van der Waals force acting between two flat Si

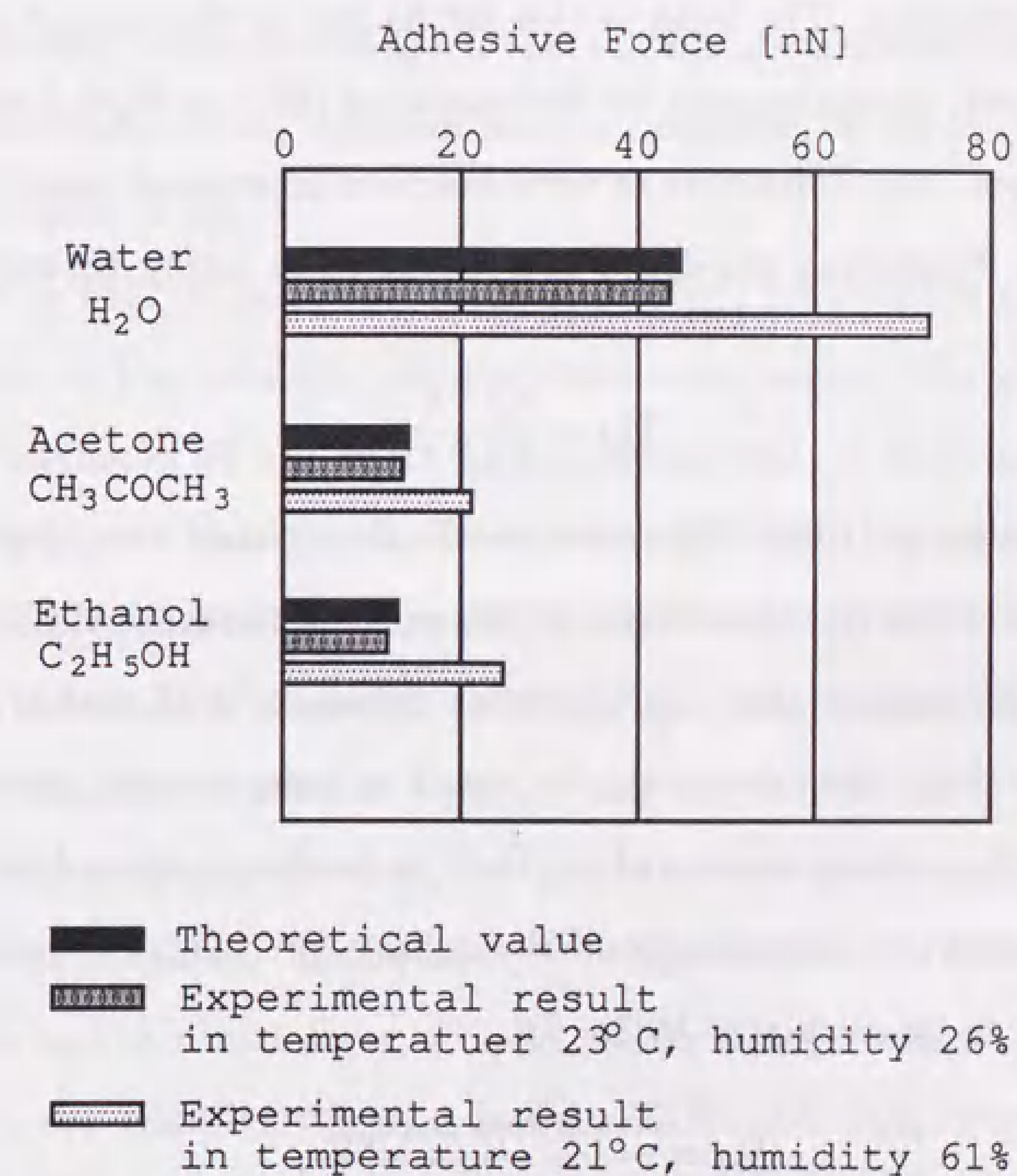

Figure 5.6: Adhesive forces measured for different kinds of liquid. Theoretical values were calculated by capillary theory.

surface (10 nm^2 area and 10 nm separation) is calculated to be 0.1 pN. On the other hand, an electrostatic force may arise because of the difference in the work function of the opposed surfaces[38, 63]. The electrostatic force can be generated by the electric charging due to etching, rinsing and drying wafer. However, the wafer is discharged with time. The wafer is also discharged by the contact of conductive surfaces. However, charge trapped on the insulators (SiO_2 or Si_3N_4) may cause the electrostatic force. The differences of work function generate at most 1 V potential in equilibrium. Neglecting the space charge, the force acting between surfaces is given by

$$F_{cf} = \frac{\varepsilon_0 U^2 S}{2d^2}, \tag{5.2}$$

where U, S, d, ε_0 are potential difference, an effective contact area, gap between the surfaces and permittivity, respectively. A difference on the order of 1V generates an electrostatic force smaller than 1 pN between the areas of 10 nm^2 at the distance of 10 nm. Therefore, those forces are too small to compare with the experimental results. Since the surface is covered by H_2O molecules condensed on the surface under the atmospheric environments,[58] capillary force (F_{cf}) is generated. The capillary force can be calculated by[38, 63]

$$F_{cf} = \frac{\gamma(\cos\theta_1 + \cos\theta_2)S}{d}, \tag{5.3}$$

where θ_1 and θ_2 are the contact angles between the condensed liquid surface and the two solid surfaces, which approach 0° for a hydroxylated chemical oxide surface. The symbols γ and S are the surface tension and the shared area of the parallel surfaces. Assuming that the contact angles are small ($\theta_1 \simeq \theta_2 \simeq 0$), and that the distance between the two surfaces is much smaller than the radius R of the tip,

Eq.(5.3) is simplified to

$$F_{cf} = 4\pi\gamma R. \tag{5.4}$$

Here the cross section S is replaced by $S = \pi x^2 \simeq 2\pi R d$. The capillary force is calculated to be of the order of 10 nN. Therefore, the capillary force is considered to be predominant under the condition that the surface is covered with liquid layer. The theoretical value of the adhesive force is calculated by Eq.(5.4), assuming the radius of the tip is 50 nm.

As shown in Fig.5.6, good agreement is obtained between the experimental results measured at low humidity and the theoretical results. The adhesive force of H_2O is approximately 40 nN, which is the highest value in the measured samples. This is caused by the fact that the surface energy of H_2O is higher than the other solutions. Since the adhesive forces of C_2H_5OH and CH_3COCH_3 are smaller, the solutions are more useful than H_2O to reduce the pinning effect of micromachined structures. The adhesive forces of C_2H_5OH and CH_3COCH_3 are in the region of 10 - 15 nN. At high humidity, however, the magnitude of the adhesion becomes larger than the theoretical value. The liquid layer in high humidity is thicker than that in low humidity, and this thick layer of liquid produces larger adhesion.

Moreover, the adhesive forces caused by KOH and CCl_4 solutions were also investigated under the same experimental conditions. The adhesive force of 4% KOH was between those of H_2O and C_2H_5OH . The adhesive force measured after immersing the substrate in CCl_4 was nearly equal to that of H_2O , since CCl_4 evaporated quickly and the surface was covered with the adsorbed H_2O again.

The effect of different substrate on the adhesion was investigated. Poly-Si, Si_3N_4 and SiO_2 substrates and H_2O , C_2H_5OH and CH_3COCH_3 solutions were used. Fig-

ure 5.7 shows the summarized results. The results calculated by Eq.(5.4) are also shown in Fig.5.7. The surface roughness of the poly-Si and Si_3N_4 substrates are less than 1 nm. As shown in Fig.5.7, the adhesive force seems to be independent of the kind of substrate. Since surface energy of a solid is typically much larger than that of a liquid, the surface tension of the solid does not affect the adhesion of capillary effect. The experimental results tend to be larger than the theoretical values for the C_2H_5OH solution. This is caused by the evaporation of the liquid and the condensation of H_2O molecular on the surface.

In addition, the adhesive force was measured to be 29 nN for the Si substrate (roughness < 1 nm) immersed in H_2O . On the other hand, the value for the smooth SiO_2 substrate (roughness < 1 nm) measured under the same experimental conditions was 27 nN. It was confirmed that the adhesive force for the Si substrate was nearly equal to that for the SiO_2 substrate, since the surface of the Si substrate was oxidized in the atmosphere.

If impurities are present in the etch and rinse solutions, they are deposited into very narrow gaps after drying. The adhesive strength resulting from these impurities is difficult to estimate quantitatively, since the amount of the impurities fluctuates widely[38]. In order to evaluate the adhesive force caused by solid bridging, an experiment to peel off a micromachined cantilever that is pinned to the substrate after the rinse process has been carried out. The sample is a cantilever made of a thermally oxidized Si film on Si substrate. A scanning electron micrograph of the pinned cantilevers coated with an evaporated aluminum film is shown in Fig.5.8. The free end of the cantilever adheres to the Si surface by the solid bridge. Using the AFM probe, the pinned cantilever is pulled upward as shown in Fig.5.2. The spring

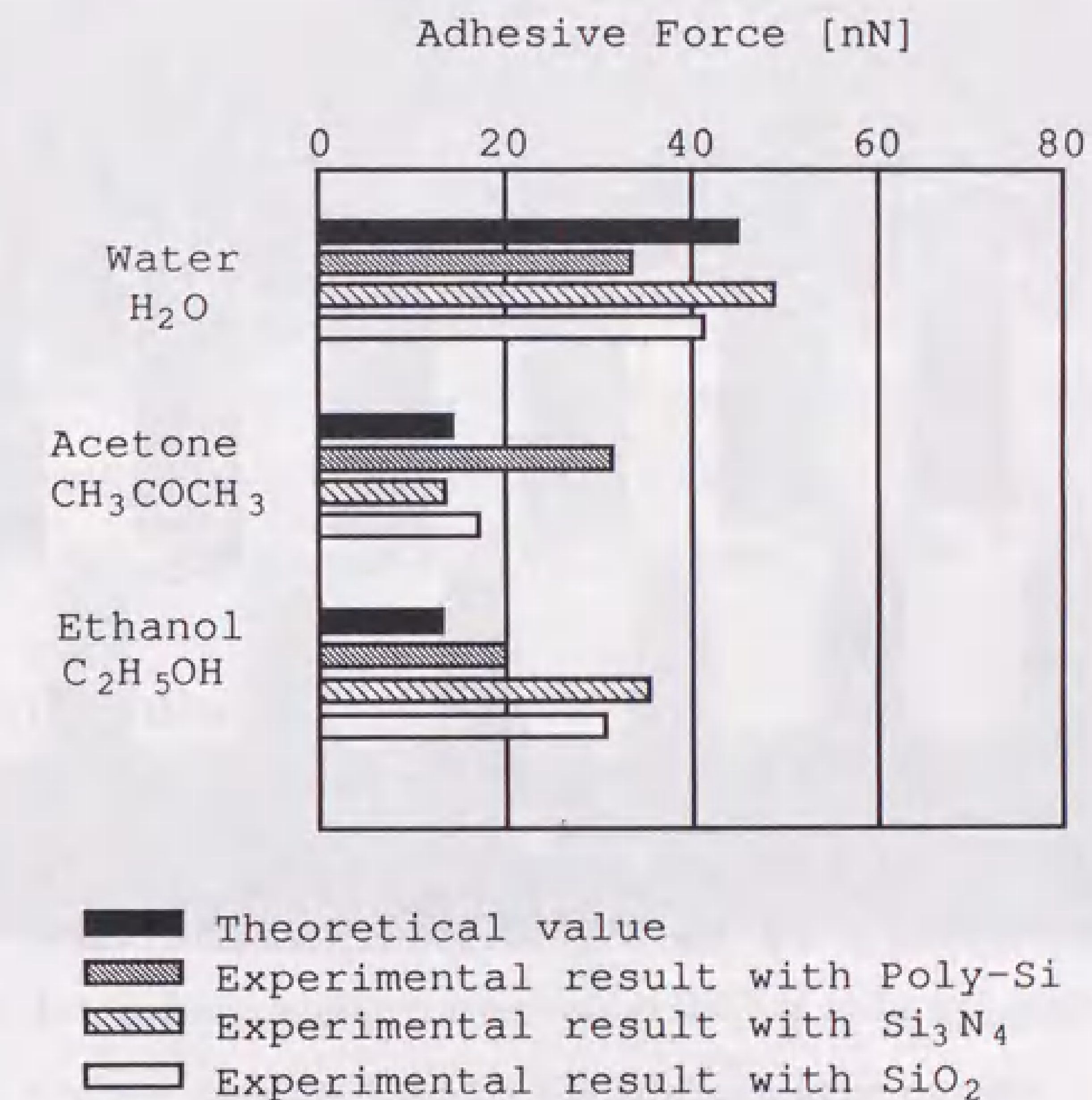

Figure 5.7: Adhesive forces measured for different kinds of substrate. Temperature was 20 °C and humidity was 30 %.

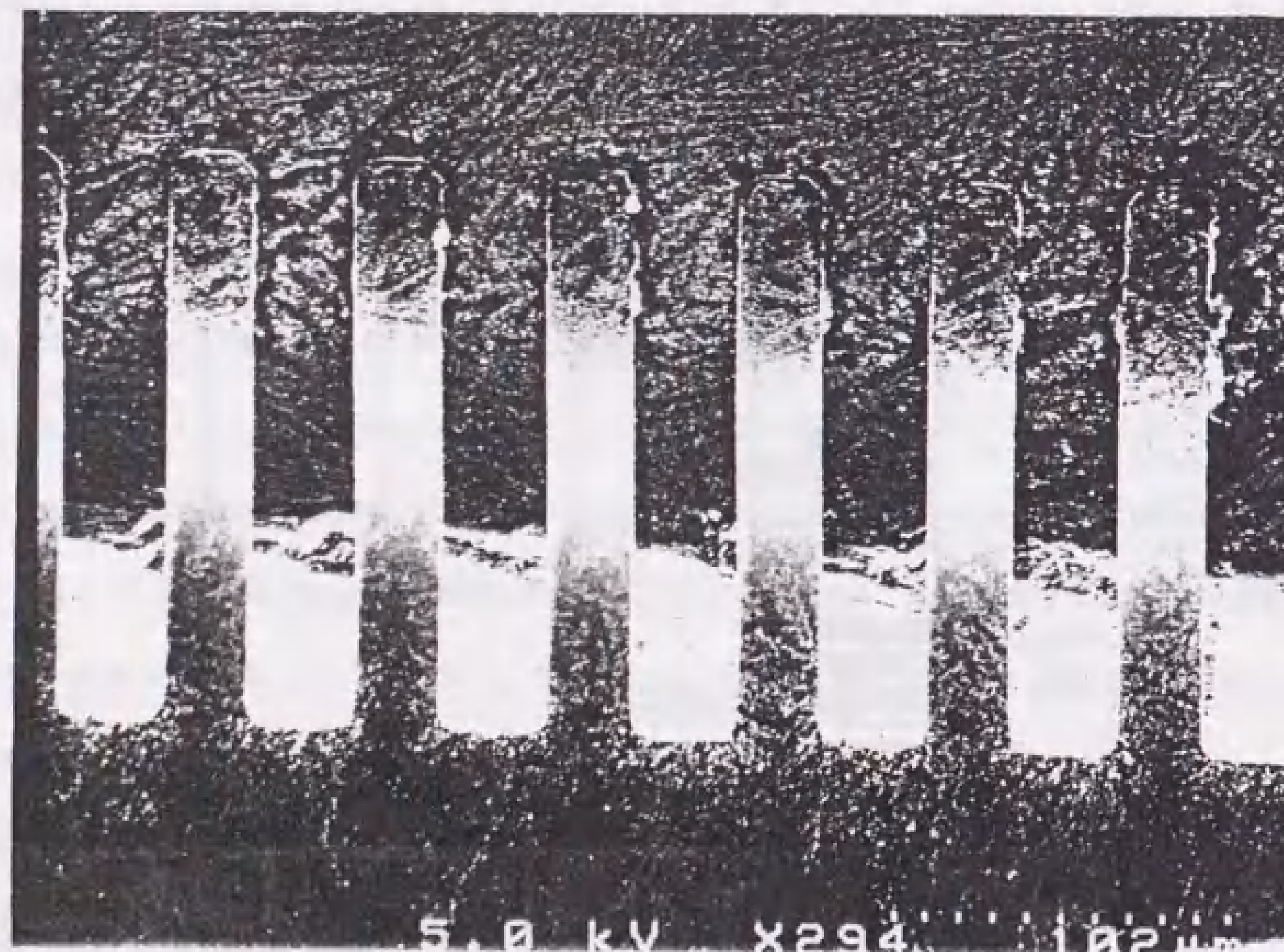

Figure 5.8: Scanning electron micrograph of the cantilever covered with aluminum film. The free end of the cantilever adheres to the substrate by solid bridging.

constant of the AFM probe used in this experiment is 1.3 N/m. Figure 5.9 shows an optical micrograph showing a location of the sample (cantilever adhering to the substrate) and the AFM probe. The AFM probe is located under the microcantilever adhering to the substrate. The cantilever used in the measurements is 150 μm long, 20 μm wide and approximately 0.4 μm thick. The area of the solid bridging is 10 μm $\times$ 20 μm. Figure 5.10 shows the force curve obtained by the peeling sequence. At the origin of the probe displacement shown in Fig.5.10, the AFM probe comes in contact with the rear surface of the pinned cantilever. With the increase of the probe movement, the pull-off force becomes larger. Increasing the force up to 3 μN, the cantilever is released as shown in Fig.5.10. Although the formation of solid bridge is dependent on the etch and rinse process, the adhesion by the solid bridge seems to be stronger than that by the capillary effect.

5.4 Conclusions

The adhesive force was measured from the transition of the force curve. The AFM using the heterodyne interferometer was employed in the measurements. The resolution of the heterodyne interferometer was evaluated to be approximately 0.3 nm. The influence of the pressing force on the adhesive force measurement was investigated. The adhesive force was independent of the pressing force in the range of smaller than 5 μN.

The adhesive forces acting between an Si_3N_4 probe (top radius of 50 nm) and four kinds of flat substrate (Si, SiO_2 , poly-Si, Si_3N_4) immersed into the etch and rinse solutions (H_2O , CH_3COCH_3 , C_2H_5OH , KOH , CCl_4) were measured. The measured adhesive forces were in the range of 10 nN - 1 μN. The adhesive

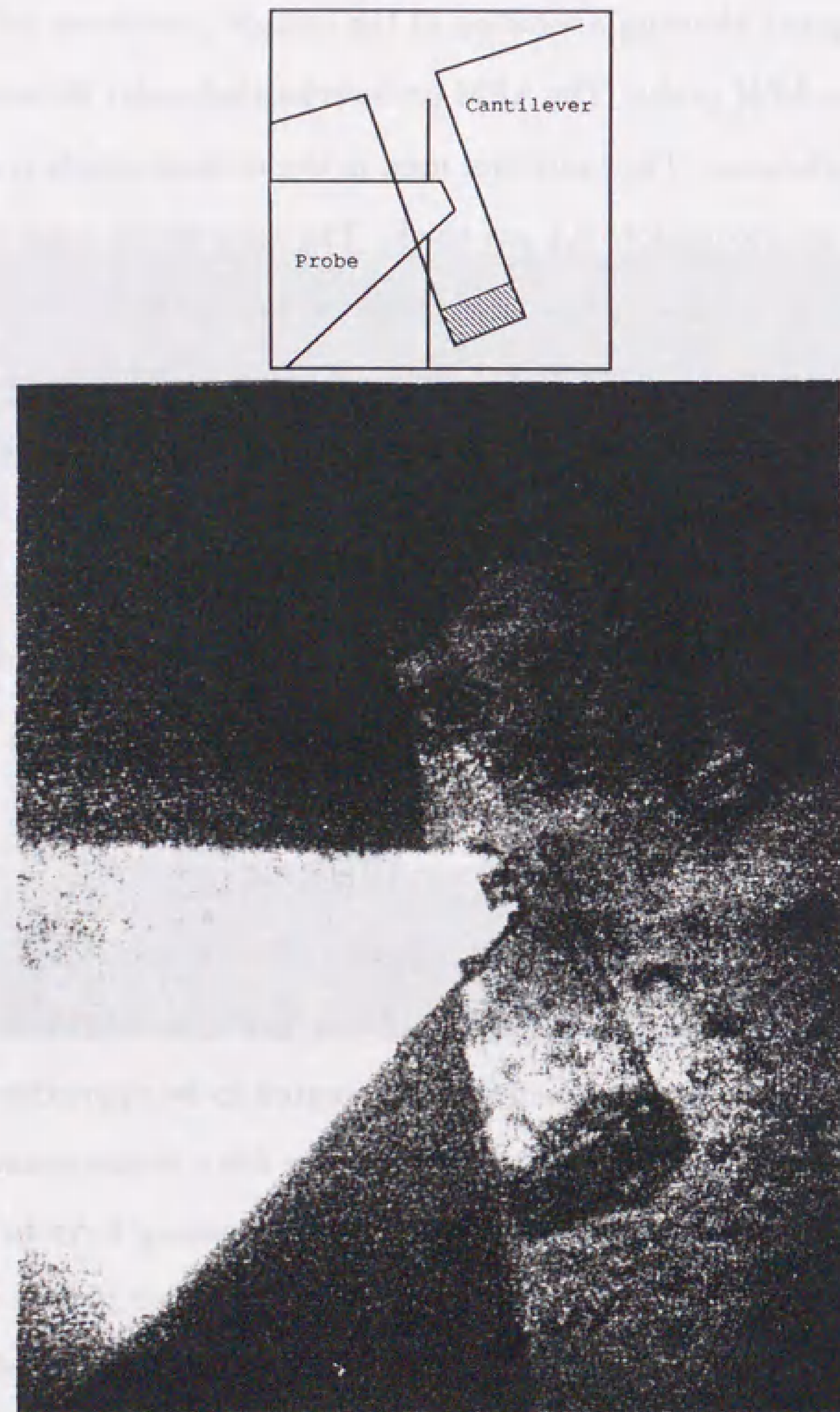

Figure 5.9: Optical micrograph of the sample (cantilever adhering to the substrate) and the AFM probe.

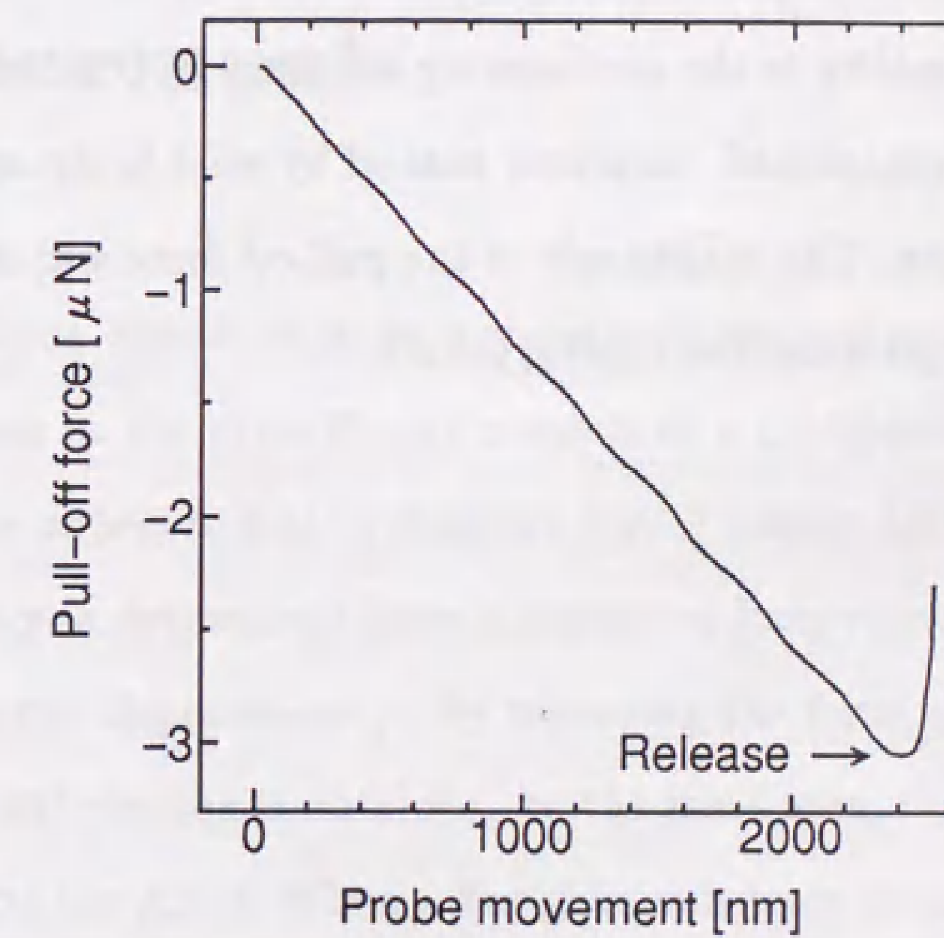

Figure 5.10: Force curve obtained in the peeling sequence. In this case, the force required to peel off the cantilever is obtained as negative.

forces generated by CH_3COCH_3 and C_2H_5OH were smaller than the others. This was consistent with the result that the rinse with CH_3COCH_3 or C_2H_5OH reduces the pinning effect of the surface-micromachined structures. The force acting on the microscopic region was discussed theoretically. The calculated capillary force agreed well with the experimental results when the humidity of the surrounding air was low (~26%). Therefore, for low humidity, the adhesive force was explained by the surface tension of the solution covering the sample. The measured adhesive force increased with the increase of humidity in the surrounding air, since H_2O molecules condensed on the surface. A micromachined cantilever pinned by solid bridging was pulled off by using the AFM probe. The magnitude of the pull-off force was approximately 3 μN. This value was larger than the capillary force.

Chapter 6

Adhesive Force Distribution Measurement

The adhesive force distribution on microstructures is measured by the AFM. An AFM probe used in the experiments consists of a cantilever and a micromachined sharp tip. The adhesive force (capillary force) acting between a sample surface and the AFM tip is determined from a measured force curve (probe deflection as a function of sample displacement). By repeating the force curve measurement, the adhesive force distribution is obtained. In the same area, the surface topography is also measured by the AFM. When a flat glass substrate (roughness < 1 nm) is used as a sample, the adhesive force distribution is structureless. However, the adhesive force is influenced considerably by the surface topography, when a grating sample and a latex sample are used. The relation between the topography and the adhesive force distribution is discussed in order to design micromechanical structures.

6.1 Introduction

It is important to evaluate quantitatively the adhesive force acting in the microscopic region, since microelectromechanical systems fabricated by anisotropic wet etching of silicon substrate or by sacrificial layer etching are often plagued by the problem of adhesion to the substrate. For example, free-standing microcantilever is often distorted by the adhesive force of liquid adsorbed in a small gap[64]. A spring constant of an SiO_2 microcantilever (200 μm long, 20 μm wide and 0.4 μm thick) fabricated by wet etching is 0.003 N/m as we previously measured[65]. If the distortion of the microcantilever is 10 μm, the distortional force is calculated to be 30 nN, which is smaller than the adhesive force due to a water capillary[64], and thus, the large distortional force is easily generated by the adhesion. Therefore, the knowledge of magnitude and property of the adhesive force is necessary to design the microelectromechanical systems.

Scheeper et al. investigated the adhesion of the silicon nitride cantilever beams and square diaphragms. They found that the adhesion of micromachined structures was caused by the adsorption of water molecules[39]. They also pointed out that the rinse with deionized water, ethanol and h-hexane, and a chemical surface modification with hexamethyldisilazane reduced the adhesion. A polysilicon microstructure with folded-beam butterfly suspension was used to evaluate the adhesion by the wet etching, rinse and dry processes[38]. The results were interpreted in term of particle adhesion theory. Mastrangelo et al. investigated the capillary force theoretically[41] and experimentally[42]. They fabricated various length of microcantilevers and determined the capillary force from a length of the released cantilever.

Moreover, the adhesive force often affects a movement of the microstructures with contact slide mechanism. Since the adhesive force generally depends on the condition of the surface contact position, it is important to investigate the spatial distribution of the adhesive force. The repulsive force distribution was obtained by an optical grating[66], the relation between the surface topography and the microscopic adhesive force distribution has not been investigated.

An AFM has proved to be a powerful tool for evaluation of a force acting in a very small region[44]. The adhesive force of the microscopic contact is measured by the AFM with a resolution surpassing that of currently available techniques. The adhesive force acting between an AFM tip and a sample surface, which is covered with the solution used in micromachining process, has been previously measured[64].

In this paper, the relation between the surface topography and the adhesive force distribution is investigated by the AFM. The force required to remove an AFM tip from the sample surface is measured at each point on the surface. The samples used in the experiments are a micromachined surface grating and ordered latex particles. The measured adhesive force is explained theoretically by the capillary force generated between the AFM tip and the microstructures covered with water molecules. The adhesive force depends on the surface topography. The relation between the surface topography and the adhesive force distribution is discussed in order to design the micromechanical structures.

6.2 Experiments

An AFM probe consists of a sharp tip and a cantilever with low spring constant. An interactive force acting on the tip is measured from the cantilever deflection.

The experimental setup was described in chapter 3. The deflection of the cantilever is measured by a heterodyne interferometer. A He-Ne laser is the light source for the interferometer. The incident beam is divided into a signal beam and a reference beam. The signal beam is focused on the rear surface of the probe and the phase difference between the reflected signal beam and the reference beam is detected. The resolution of the interferometer is approximately 0.3 nm. The probe used in the experiment is a V-shaped cantilever made of silicon nitride (Park Scientific Instruments). The cantilever is 200 μm long, 36 μm wide and 0.6 μm thick, and the spring constant of the cantilever was determined from the geometry and the Young's modulus to be 0.064 N/m, which was confirmed by calibration experiment[65]. The radius of the tip was measured from a scanning electron micrograph and it was approximately 50 nm. The sensitivity for the force measurement is approximately 20 pN.

A sample mounted on a piezoelectric tripod is moved independently in the x, y and z directions by computer control. Hysteresis of the piezoelectric tripod is compensated by adjusting the voltage applied to each piezoelectric actuator. The motion of the cantilever is monitored as a function of the sample translation. Using the x and y piezoelectric actuators, a sample is scanned horizontally. The sample approaches the AFM tip by the z (vertical direction) actuator. From the deflection of the cantilever, the force acting between the tip and the sample surface is obtained. In the case of the adhesion measurement, the adhesive force is measured from the magnitude of the transition appearing in the force curve (force vs. sample-translation curve)[61] when the AFM tip separates from the surface.

The relation between the topography and the adhesive force distribution can be

appreciated with the consideration of specific samples. The adhesion is measured for three samples, flat SiO_2 glass, periodic grating and ordered polystyrene latex particles. Roughness of the flat SiO_2 glass is less than 1 nm. The grating consists of 85 nm thick Cr film on flat SiO_2 substrate. The period of the grating is 4 μm. The adhesive force acting on the edge of the grating line (Cr film) is investigated in detail. The polystyrene latex particles of 500 nm diameter ordered on flat SiO_2 substrate is used to investigate the influence of the adhesive force on the convex surface topography. The experiment is carried out in air under atmospheric condition.

In the experiments, the surface is scanned in the conventional repulsive mode AFM to obtain surface topography. The force curve is measured at each point on the scanned area. The adhesive force is mapped to obtain the two-dimensional adhesive force distribution. As described in chapter 5, it was confirmed that the adhesive force was independent on the material under our experimental conditions.

6.3 Results and Discussions

The surface topography and the adhesive force distribution for an SiO_2 substrate are shown in Fig.6.1. The measured region is 0.4 μm × 0.4 μm. The surface roughness is 1 nm or less as shown in Fig.6.1. Although the measured values are somewhat scattered, the adhesive force distribution on the surface is considered to be uniform.

The adhesive force acting between a flat surface and a sphere of the radius, R, is theoretically given for the capillary force by,

$$F = 4\pi R\gamma, \tag{6.1}$$

where γ denotes surface energy. When the sample is placed in air and covered with

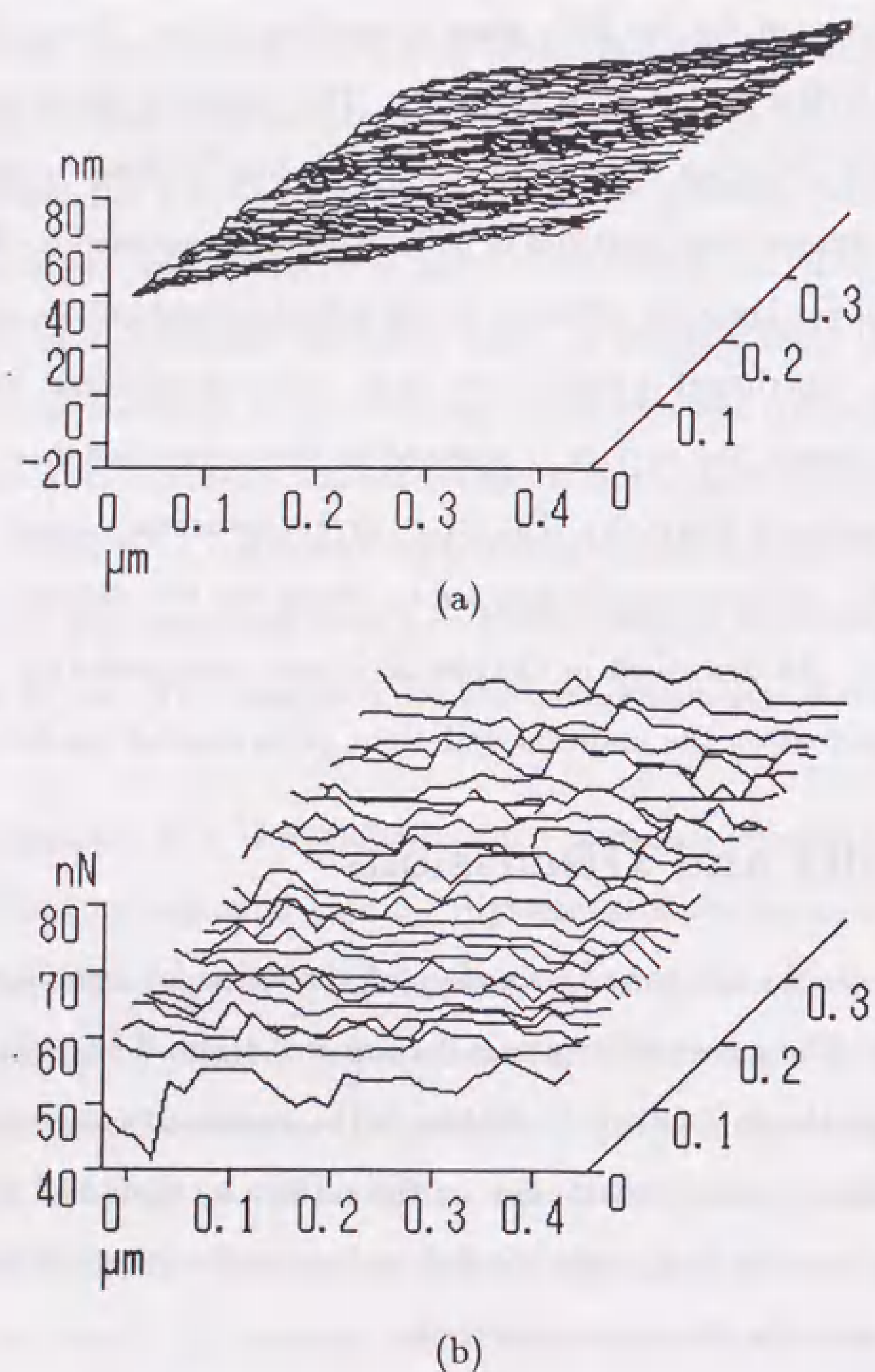

Figure 6.1: (a)Topography of the glass substrate and (b) adhesive force distribution in the same area.

water molecules, γ is 72.5 mJm^{-2}. Since the top radius R of the AFM tip used in the experiment is approximately 50 nm, the theoretical value of the adhesive force is calculated to be 45 nN by Eq.(6.1). The measured adhesive force for the SiO_2 substrate is approximately 60 nN. The theoretical value explains the measured value. The difference between the theoretical and the measured values is caused by the uncertainty of the measured radius of the tip.

The experimental results for the grating sample are shown in Fig.6.2. At the bottom of the grating groove (on the SiO_2 substrate) and at the top surface of the Cr film, the adhesive force is almost uniform. The magnitude of the adhesive force at the position on the Cr film and on the SiO_2 substrate is 60 nN, which agrees with the result for the flat SiO_2 substrate. At the edge of the Cr film, however, the measured adhesive force changes. The adhesive force decreases when the tip approaches to the edge of the Cr film from the center of the Cr line. The minimum adhesive force measured at the edge of the film is 20 nN. On the other hand, the maximum adhesive force is 200 nN, which is obtained at the position of 200 nm away from the position where the minimum adhesive force is obtained.

The results obtained with the grating can be explained by the capillary force of a water meniscus. The shape of the meniscus is illustrated in Fig.6.3. The radius r of the meniscus is given by Kelvin equation[67],

$$r = \frac{\gamma V}{RT \log(p/p_s)}, \tag{6.2}$$

where γ, V, R, T denote surface energy, mole volume, gas constant, and temperature, respectively. The value of $\gamma V/RT$ is calculated to be 0.54 nm for water[67]. When we consider the water vapor in air, p/p_s denotes the relative humidity. Since our

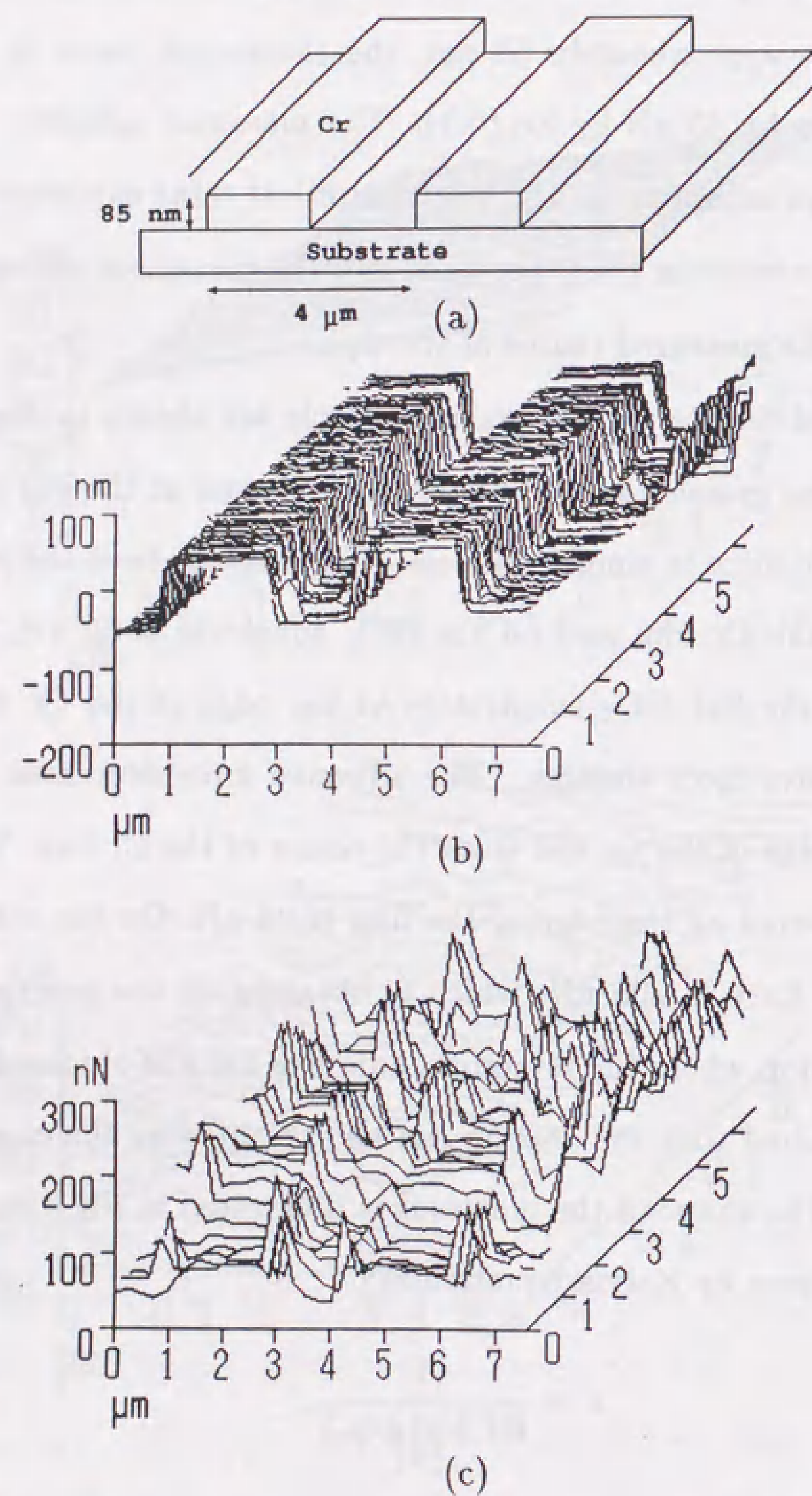

Figure 6.2: (a) Schematic diagram of the grating sample, (b) measured topography of the grating and (c) adhesive force distribution in the same area.

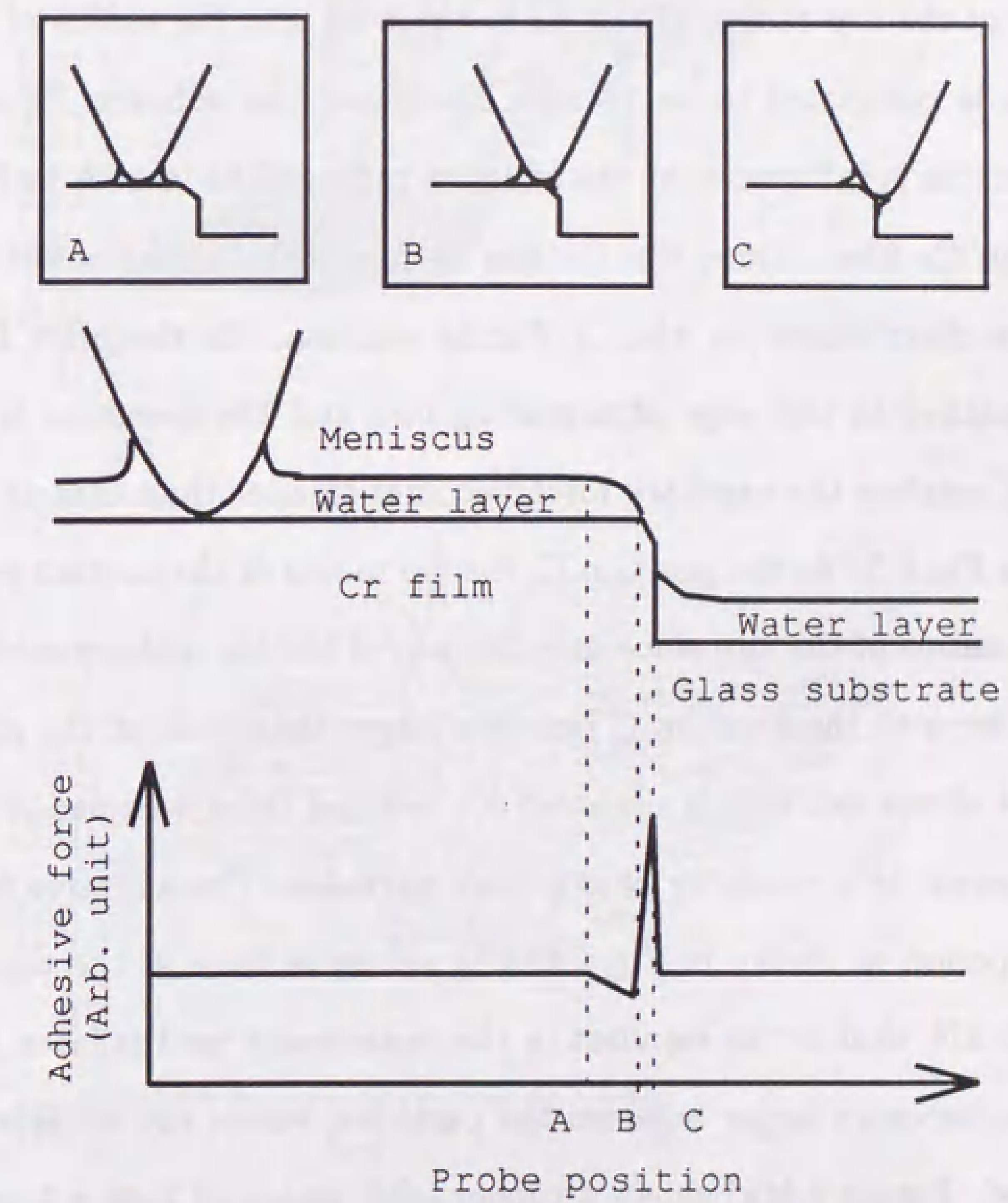

Figure 6.3: Schematic diagram of the edge of the grating sample.

experiments are carried out at 25 °C and 50 % humidity, the radius r of the meniscus is 1.8 nm. Effective contact area is approximately $2\pi Rd$, where d is the thickness of a water layer. Therefore, the radius of the effective contact area is equal to $\sqrt{2Rd}$. Since the thickness d of the water layer is approximately $2r$ ($\sim$ 3.6 nm) and the typical value of the top radius of the AFM tip is 50 nm, the radius of the effective constant area is calculated to be 19 nm. Therefore, the adhesive force due to the capillary meniscus is influenced by the effective radius. The inset A in Fig.6.3 shows the tip on the Cr film. Since the Cr film is considered to be a flat surface, the adhesive force distribution on the Cr film is uniform. In the inset B in Fig.6.3, the tip approaches to the edge of a grating line and the meniscus is not formed completely. Therefore the capillary force becomes smaller than that at the position A as shown in Fig.6.3. At the position C, the tip radius of the contact point is larger than the top radius of the tip, since only the top of the tip is sharpened. Therefore, the adhesive force at the position C becomes larger than that at the position A.

Figure 6.4 shows the results obtained for ordered latex samples. Periodicity of the image is equal to a diameter of the latex particles. The adhesive force changes by the same period as shown in Fig.6.4. The adhesive force at the top of the latex particles is 30 nN, that is the smallest in the experiment for the latex sample. The adhesive force becomes larger between the particles, where the adhesive force of 80 nN is obtained. Figure 6.5(a) shows a topographic image of 2μm $\times 2\mu$m area of the ordered latex particles in air. Figure 6.5(b) shows an adhesive force distribution on the same area. The hight variation in Fig.6.5(a) is approximately 0 nm (black) to 700 nm (white). The adhesive force variation in Fig.6.5(b) is from 20 nN (gray) to 50 nN (white). Although the measured value in Fig.6.5(b) is a little smaller than

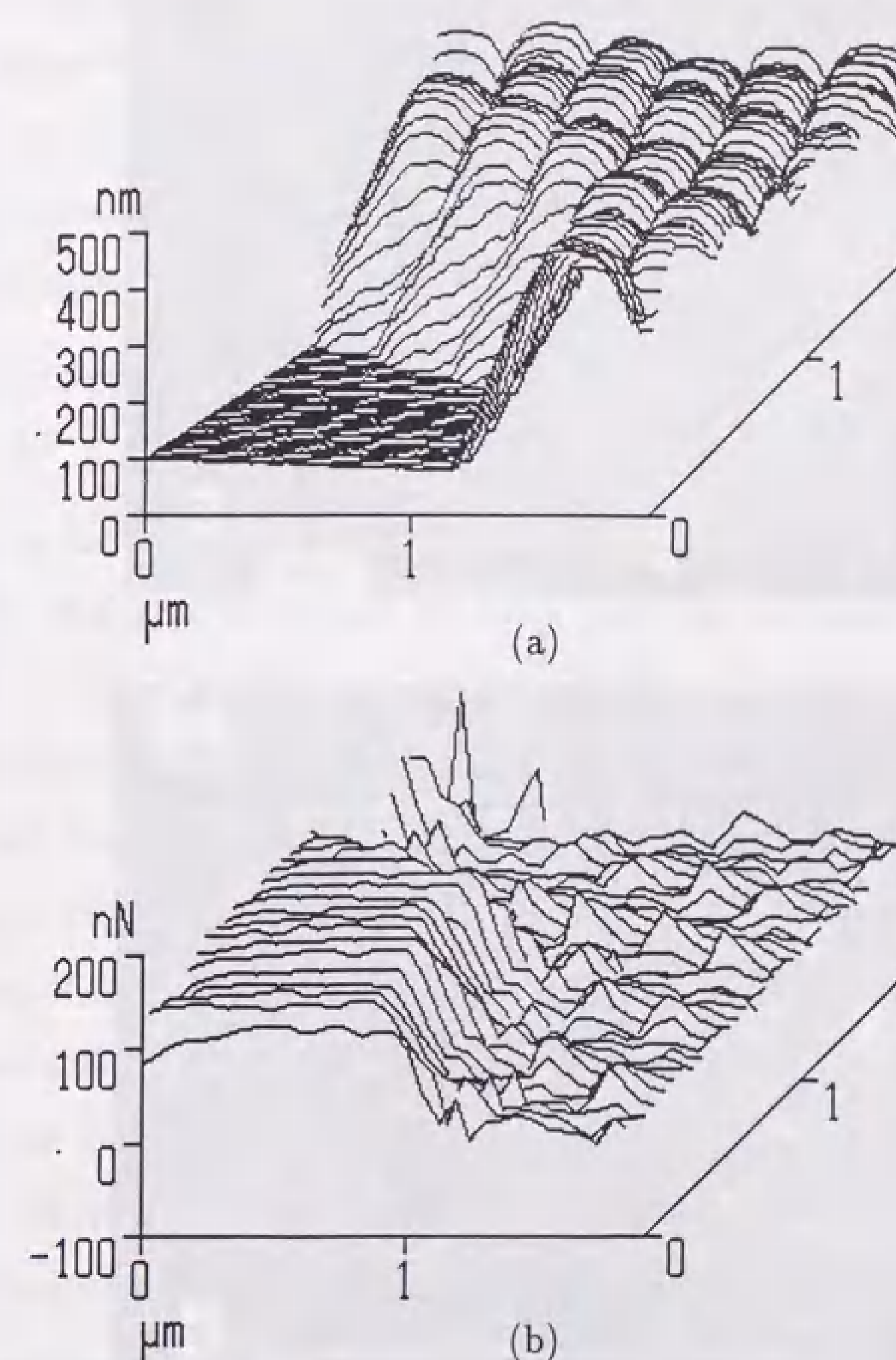

Figure 6.4: (a) Topography of the ordered latex particles and (b) adhesive force distribution in the same area.

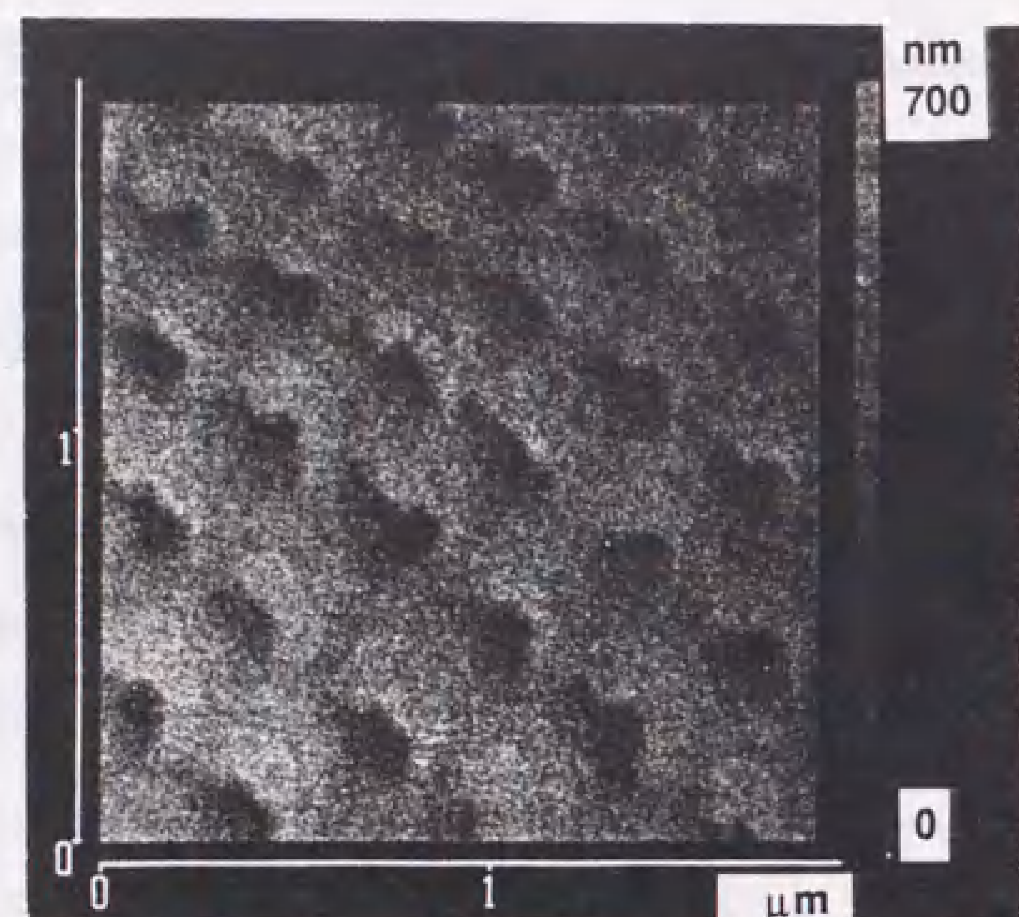

(a)

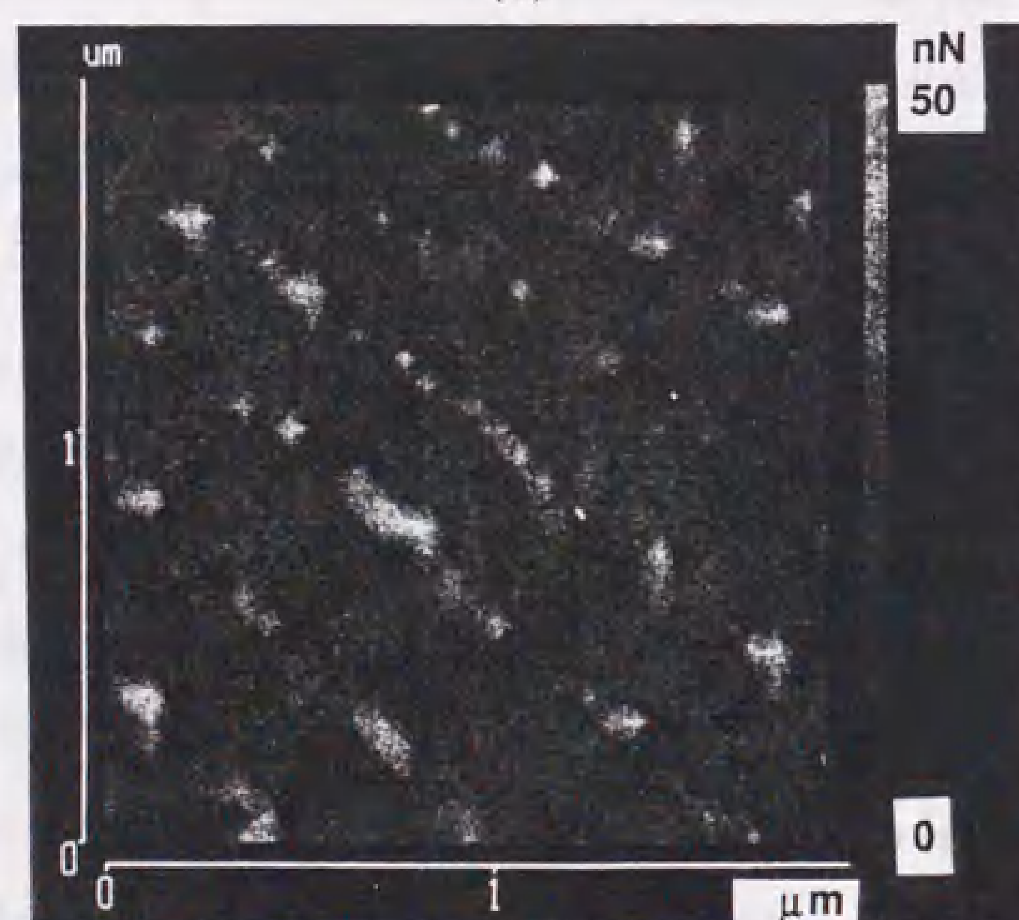

(b)

Figure 6.5: Top views of (a) the ordered latex particles and (b) the adhesive force distribution. The views were obtained on the same area.

the value in Fig.6.4(b), the relation between the topography and the adhesive force distribution is observed. Figure 6.5 is a reversal of Fig.6.5. This result also indicates that the adhesive force depends on the surface topography.

Similarly to the grating sample, the adhesive force for latex particles is also explained by taking the capillary force into account. The magnitude of the adhesive force acting between two spheres is obtained by

$$F = 4\pi \frac{R_1 R_2}{R_1 + R_2} \gamma, \qquad (6.3)$$

where R_1 is the radius of the AFM tip, and R_2 is the radius of the latex particle. The radius of the AFM tip and the latex particles were measured from an SEM images to be 50 nm and 250 nm, respectively. From Eq.(6.3), the adhesive force on the top of the latex particle is calculated to be 38 nN, which is 83 % of the adhesive force acting between the sphere and the flat substrate. The theoretical adhesive force agrees well with the measured value. The measured adhesive force on the flat surface was the 100 nN, which is somewhat larger than the theoretical value. That fact is now under investigation.

Since the number of the contact point of the tip increases between the latex particles, the adhesive force increases. The adhesive force between the particles is calculated as follows. When the AFM tip comes in contact with the latex particles at three points, the adhesive force becomes larger by more than the factor of 3. Although the absolute value of the measured force is somewhat larger than the calculated value, the adhesive force measured between the particles is roughly three times larger than that measured on the top of the latex particles. Therefore, the adhesive force between the particles is explained by the increase of number of the

contact points.

In general, the surface etched by the micromachining process is microscopically rough. Therefore, when we consider the adhesion between the micromachined surfaces, the total adhesion may be obtained by summing up the adhesive forces acting on the respective contact points. At a contact point, the adhesive force can be explained by the contact of the two spherical surfaces as shown by Eq.(6.3). Therefore, the magnitude of the adhesion decreases with the decrease of the radius of the surface curvature. This agrees with the experimental results for the ordered latex particles. In general, it is difficult to make contact between the two pointed tips. Therefore, the surface with relatively large curvature can be actually used to decrease the adhesive force in the microelectromechanical systems. The adhesive force was independent on the pressing force in the force region from 50 nN to 5000 nN previously described in chapter 5, when the adhesive force was measured with an AFM probe[64]. Decreasing the number of the contact points, the pressing force at each point increases. However, the adhesive force decreases with the decrease of the number of the contact points in a certain force range. Therefore, the combination of the sharp edge and the convex surface reduces the adhesive force. These considerations and the experimental results will be useful to design the microelectromechanical system.

6.4 Conclusions

The distribution of the adhesive force acting between an AFM probe (tip radius of 50 nm) and the sample surface was measured in air under atmospheric condition. The relation between the adhesive force and the surface topography was investigated.

The samples used in the experiments were a flat glass, a grating (4 μm pitch) fabricated by the lithographic process and ordered latex particles (500 nm diameter).

In the case of the flat glass (roughness < 1 nm), the adhesive force distribution was uniform. The magnitude of the measured adhesive force was approximately 60 nN. In the case of the grating, the maximum adhesive force was 200 nN and the minimum adhesive force was 20 nN. The adhesive force decreased when the AFM tip approached the edge of the grating lines, which was explained by considering formation of a water meniscus. The adhesive force for the ordered latex particles changed periodically with the topographic variation. The minimum adhesive force was 30 nN, which was obtained at the top of the latex particle. Therefore, the convex surface decreases the adhesive force. The relation between the adhesive force and the surface topography measured in this experiment will be useful to reduce the adhesive forces acting in the microelectromechanical system.

Chapter 7

Position Measurement

Position sensing technique using the AFM is studied in this chapter. By measuring the surface profiles of a lithographic grating and an ordered latex particles, the characteristics of the periodic signals obtained with the AFM are investigated. The response time of the probe is examined using the grating sample. The response time is proportional to the scan velocity when the vibrational frequency of the probe was less than the resonant frequency of the probe. The relation between the force applied to the probe and the scan velocity is investigated. The durabilities of the probe and the sample are also investigated. The feasibility of a position sensing technique using the principle of the AFM is studied to develop a new linear encoder. An AFM having a multiple probe is constructed using micromachined cantilevers and an optical multibeam detection system. The feasibility of the proposed encoder is investigated by means of the constructed multiple probe AFM. The displacement signals having different phases are obtained simultaneously. The results indicate that the proposed encoder will be a novel tool for precise linear displacement sensing if the high resolution inherent in the AFM is utilized advantageously.

7.1 Introduction

The STM invented recently is capable of imaging a solid surface with atomic scale resolution[43]. Similarly to the STM, the AFM is also a powerful tool for investigating the surface properties of conductive and non-conductive materials in the nanometer region[44]. In addition to physical evaluation of the surfaces, it is proposed that the STM and AFM can be useful for some metrological applications[68][69][46][47]. The STM with two tunneling units was developed to study the feasibility of displacement measurements using the highly oriented pyrolytic graphite (HOPG) images[46]. The HOPG images which had atomic scale hexagonal structures were used for the calibration of other sample images. More recently, polystyrene latex particles were used to calibrate the AFM instruments in the nanometer region[47].

On the other hand, a linear encoder is an indispensable instrument for the precise positioning of computer-controlled machines. To meet the recent demand to control systems in 0.1 μm regions for machining and 0.01 μm regions for IC fabrication, an instrument encoding the displacement in the nanometer region is required [70][71]. For conventional encoders, the optical and the magnetic techniques are widely used. In the optical encoder, two identical gratings are superimposed and the displacement is monitored from the intensity variation of the light transmitted through the gratings[72][73]. Although a displacement less than the pitch of the grating can be measured by the interpolation of the sinusoidal variation of the Moiré signal, the periodicity of the signal in the optical encoder is basically restricted to the wavelength of the light. In the magnetic encoder, it is not always easy to obtain displacement resolution of less than one micrometer.

In this chapter, position sensing technique using an AFM is investigated. The feasibility of a position sensing technique using the principle of the AFM is studied. In order to examine the fundamental characteristics of the proposed encoder system, a multiple probe force microscope was constructed.

In the following sections, first, the proposed design of the encoder utilizing the AFM is described. Next, the periodicity and the noise in the force microscope images of the samples having periodic surface structures are analyzed. In order to investigate the characteristics of the proposed encoder system, signals from the two probes of the multiple probe force microscope are measured under several experimental conditions. The maximum scan velocity of encoding and the sensitivity for the displacement are discussed from the point of view of the mechanical motion of the microcantilever.

7.2 Principle and Experiments

In the AFM, the surface is scanned by a small cantilever with a sharp tip under the condition of repulsive force. The surface corrugation is obtained from the instantaneous deflection of the cantilever (variable deflection mode), or from the voltage applied to the piezoelectric stage to keep the deflection constant (constant force mode). In the proposed system, a sample having a periodic structure is used as the scale reference. The multiple cantilever array is used to detect the periodic signal of the scale in the variable deflection mode. In our experiments, two microcantilevers are used to demonstrate the proposed system. Each cantilever works as an independent probe of the force microscope.

The following advantages will be obtained by using the multiple probe force

microscope as a position sensor. (1) A high resolution in position sensing will be obtained by using a cantilever having a sharp tip, since the resolution of the force microscope is not limited by the wavelength of the light. (2) Similarly to conventional encoders, periodic signals having different phases are obtained in the proposed encoder in order to detect the displacement direction and to sense displacements smaller than the signal periodicity. Therefore, it will be easy to construct an absolute address encoder using a coded sample as a scale. In addition, by averaging the signals obtained by the multiple probe, the noise due to the irregularity of the scale grating will be reduced. (3) In contrast with the STM, the multiplication of a probe is not difficult in the AFM. The multiple cantilever probe can be fabricated precisely by means of the conventional lithographic process. In addition, the distance between the probe and the scale sample is adjusted easily because of the elasticity of the microcantilever.

Figure 7.1 shows a schematic diagram of the proposed encoder system. In order to sense the deflections of the respective cantilevers located adjacently, the laser beam deflection technique combined with the grating beam splitter is proposed, as shown in Fig. 7.1. The collimated laser beam passes through the grating perpendicularly and is divided into several beams by diffraction. An objective lens is placed between the grating and the cantilever array.

The distance between the lens and the grating is set equal to the focal length of the lens, and the cantilever array is located at a distance nearly equal to the focal length from the lens. Therefore, the optical configuration is equivalent to the Fourier transform system with the grating as object. The amplitude transmittance $g(x_0)$ of the grating having the spatial frequencies multiple of $1/p$ is expressed in a

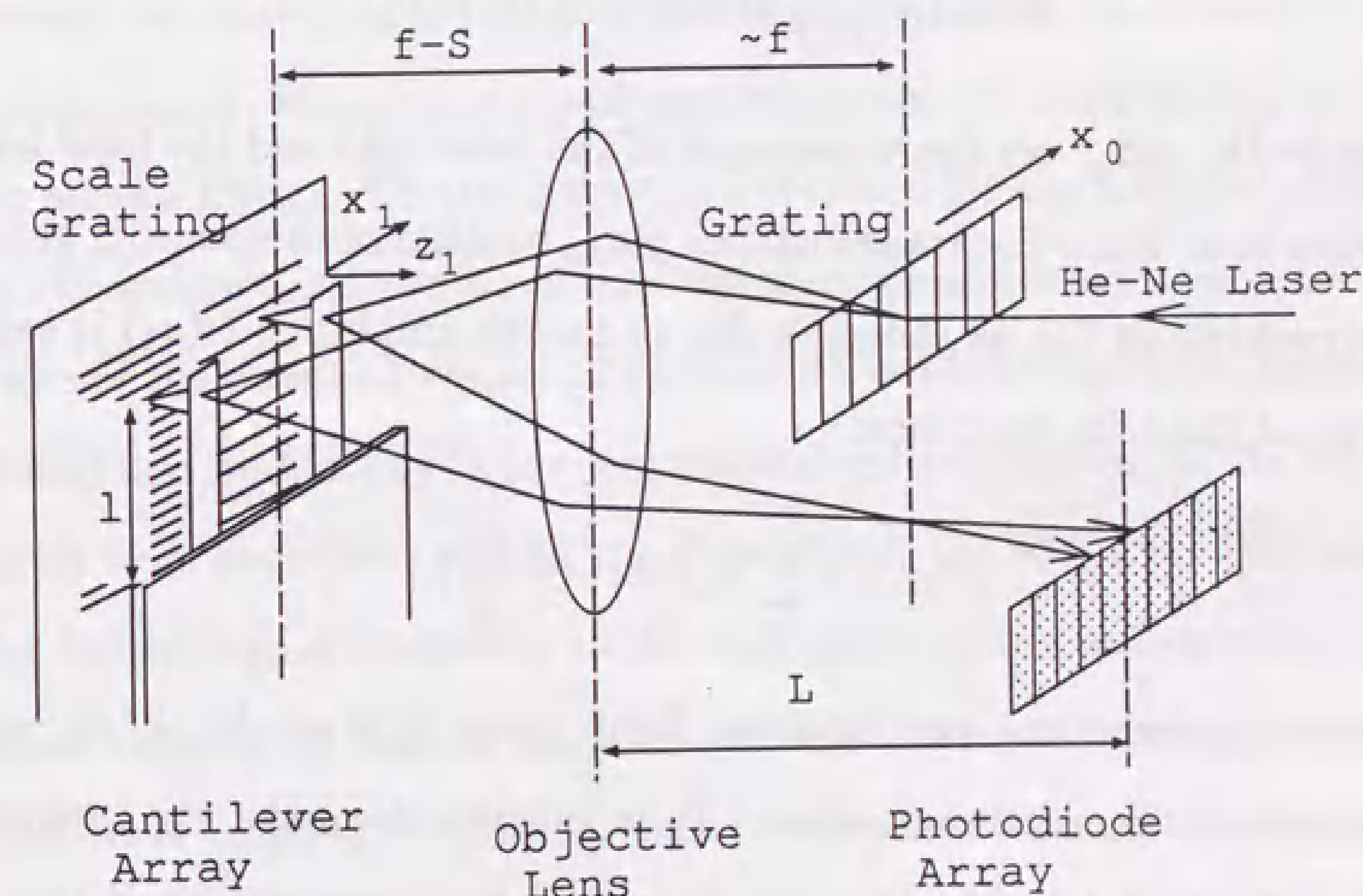

Figure 7.1: Schematic diagram of the multiple probe encoder.

Fourier series by

$$g(x_0) = \sum_n a_n \exp(i2\pi n \frac{x_0}{p}), \qquad (7.1)$$

where p, a_n and n denote the pitch of the grating, the Fourier coefficient and an integer, respectively. The amplitude $U(x_1)$ of the light on the focal plane of the lens along the x_1 axis is given by the Fourier transform of the transmittance $g(x_0)$,

$$U(x_1) = \frac{1}{i\lambda f} \exp(i2kf) F\{g(x_0)\}, \qquad (7.2)$$

where $\lambda(= 2\pi/k)$ and f are the wavelength of the laser light and the focal length of the objective lens. Since the transmittance $g(x_0)$ consists of components having the frequency multiple of $1/p$ as shown in Eq. (7.1), the amplitude $U(x_1)$ is expressed by an array of the delta functions:

$$U(x_1) = \sum_n a_n \delta(x_1 - n\frac{\lambda f}{p}). \qquad (7.3)$$

The distance between the two adjacent light spots is given by $\lambda f/p$, which is equal to that of the cantilever array. It is possible to make the intensities of the light spots equal to each other by designing the transmittance of the grating appropriately[74][75][76].

The beams reflected by the cantilevers pass backward along paths similar to those of the incident beam. The signal beams are detected by respective elements of a photodiode array. The deflection of the cantilever probe is measured from the intensity change of the laser spot on an element of a photodiode array (laser beam deflection method)[77].

Based on geometrical optics, the relation between the probe deflection z_1 and

the position change of the laser spot Δd on the photodiode array is expressed by

$$\frac{\Delta d}{z_1} = -2(\frac{LS}{f} + f - S)\frac{1}{l}, \qquad (7.4)$$

where L is the distance between the objective lens and the photodiode array, and l is the length of the cantilever. $f - S$ is the actual length between the lens and the probe.

Similarly to conventional encoders, the displacement can be encoded by means of the periodic signal. When the tip positions relative to the scale grating are different, periodic signals having different phases are obtained for the translation of the scale grating. Therefore the direction of the displacement is distinguished from the phase differences of the obtained signals. Displacement less than the signal periodicity can be obtained in a similar way to the conventional optical encoder[72]. In the case that the signals from respective probes are all in phase, the addition of the signals produces an output signal insensitive to the irregularity of the scale grating. Moreover, if the scale consists of various tracks of gratings having different periodicities, the displacement is encoded in a similar way to the conventional absolute-type optical encoder.

The experimental setup of the multiple probe AFM is shown in Fig.7.2. A He-Ne laser (Uniphase: model 1107P) is used as the light source. The objective lens and the optical grating constitute the optical system of the proposed force microscope. The focal length of the lens is 40 mm and the pitch of the grating is 25 μm. A photodiode array (Hamamatsu S2319-46Q, 46 elements) is used to detect the position changes of the beam spots. The distance from the objective lens to the photodiode array is approximately 1 m. A small force acting between the sample surface and the tip

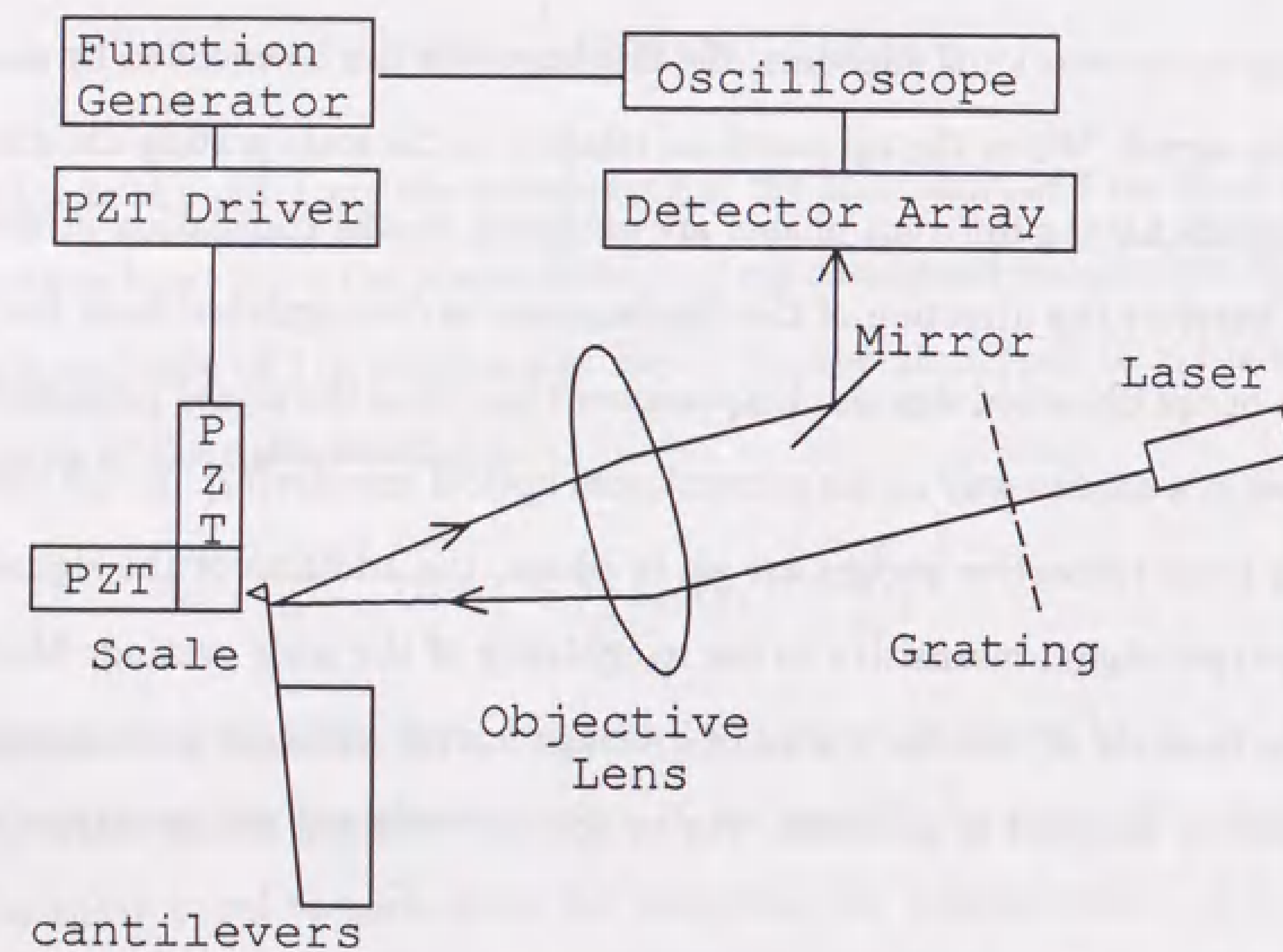

Figure 7.2: Experimental setup of the force microscope.

of the cantilever is monitored by the elastic deformation of the microcantilever. V-shaped microcantilevers (Park Scientific Instruments) are used in this experiment. The microcantilevers are made of an Si_3N_4 thin film and are fabricated on a silicon substrate by the lithographic process. Two cantilevers 1 mm apart on the substrate and the ±1st order beams of the diffracted light are used for the measurement. The cantilevers are 200 μm long and 600 nm thick, and one of them (probe 1) is 36 μm wide and the other (probe 2) is 18 μm wide. The spring constants of probes 1 and 2 are 0.064 N/m and 0.032 N/m, respectively. The theoretical resonant frequencies of the probes are 17 kHz. The magnification ($\Delta d/z_1$) of the probe deflection is calculated with Eq.(7.4) to be approximately 2800 (S~10 mm). The sensitivity for the deflection of the probe is estimated as approximately 2 nm from the output noise of the photodiode array. The piezoelectric scanner is used for translation of the sample. It consists of three piezoelectric actuators (NEC: 0.12 μm/V) mounted orthogonally. Micrometer screws are used for the rough positioning of the sample. The motion of the screw is reduced with a lever mechanism by a factor of 10. The tilt of the probes is also adjusted by the micrometer screws.

Another AFM described in chapter 3 is used to obtain the surface topography with a single probe[78], in which the interferometer is used to measure absolute value of the cantilever displacement. The cantilever probe is the same as that used for the multiple probe force microscope.

7.3 Results and Discussions

7.3.1 Single Probe Experiments

In order to investigate the characteristics of the AFM signals obtained using a sample having the periodic structure, two kinds of sample are used. In the first experiment, a grating as a scale reference is investigated, which was fabricated by the lithographic process. Since a highly precise periodicity is obtained by the lithographic process, the lithographic grating can be used for the scale of the proposed encoder. The grating consists of chromium film on a glass substrate. The pitch and the duty ratio of the grating are 4 μm and 0.515, respectively. Figure 7.3(a) shows the surface topography of the grating measured by the single probe force microscope. A rectangular wave signal is obtained as a function of the displacement in the direction perpendicular to the grating lines. As shown in Fig. 7.3(a), the intensity of the signal changes with the period of 4 μm, which is equal to the pitch of the grating. The difference between the high level and the low level of the signal is equal to 85 nm, which corresponds to the thickness of the chromium film. Figure 7.3(b) shows the Fourier-transformed signal of the rectangular wave signal shown in Fig. 7.3(a). The highest peak corresponds to the fundamental frequency of 0.23 /μm of the grating. The higher order components of the grating frequency are also shown in Fig. 7.3(b). The noise component averaged in the frequency region between 0 to 0.43 /μm is 8.0 % of the fundamental component. Thus, the signal-to-noise ratio calculated from the signal value at the fundamental frequency and the averaged noise is 12.5. By counting the repetition of the rectangular waves, the displacement can be measured incrementally. The grating will be useful as a scale reference since the signal has

(a)

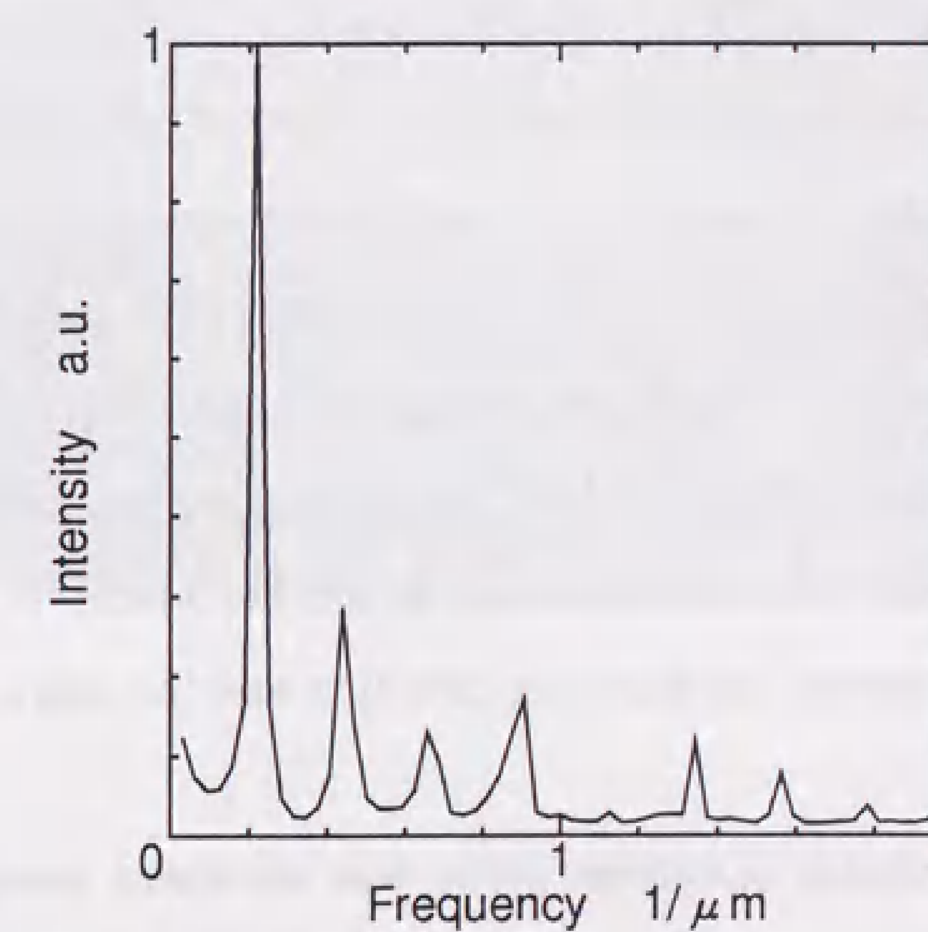

(b)

Figure 7.3: (a) Surface topography of the grating observed by the single probe force microscope; (b) Fourier-transformed signal of the surface topography.

good periodicity, as shown in Fig. 7.3.

The other sample are mono-disperse polystyrene latex particles of 500 nm diameter. Figure 7.4 shows the ordered latex particles on SiO_2 substrate. It is known that latex particles are ordered like a crystal under particular conditions. The polystyrene latex particles were used as a size calibration standard for the scanning electron microscope. The sample preparation method in our experiments is the same as that described by Li[47]. The typical signal obtained in our experiment is shown in Fig. 7.5(a). The periodic signal due to the ordered latex particles is obtained. The signal period of 550 nm is nearly equal to the diameter of the particles. The ordered latex particles will be useful as a scale reference since the obtained signal shows good periodicity. As the size of the latex particles commercially available ranges from 50 nm to 3 μm, higher periodicity is possible. An example of the Fourier-transformed signal is shown in Fig. 7.5(b). The fundamental frequency component is equal to 1.8 /μm. The width of the fundamental frequency component, however, is somewhat larger than that obtained using the grating sample. From repeated measurements, it was found that the distortion in the periodicity of the signal is caused by misalignment between the scanning direction and the axis of the ordered particles.

The operation of a multiple cantilever probe was simulated using the signals obtained with the single probe force microscope. Figure 7.6(a) shows the signals obtained by scanning the grating surface horizontally. The same sample as used before is scanned in the X direction perpendicular to the grating line for the distance of 30 μm. The single scan is repeated after translating the sample in the Y direction by a step of 1 μm. The start points of the respective X-scans are shifted by a step of

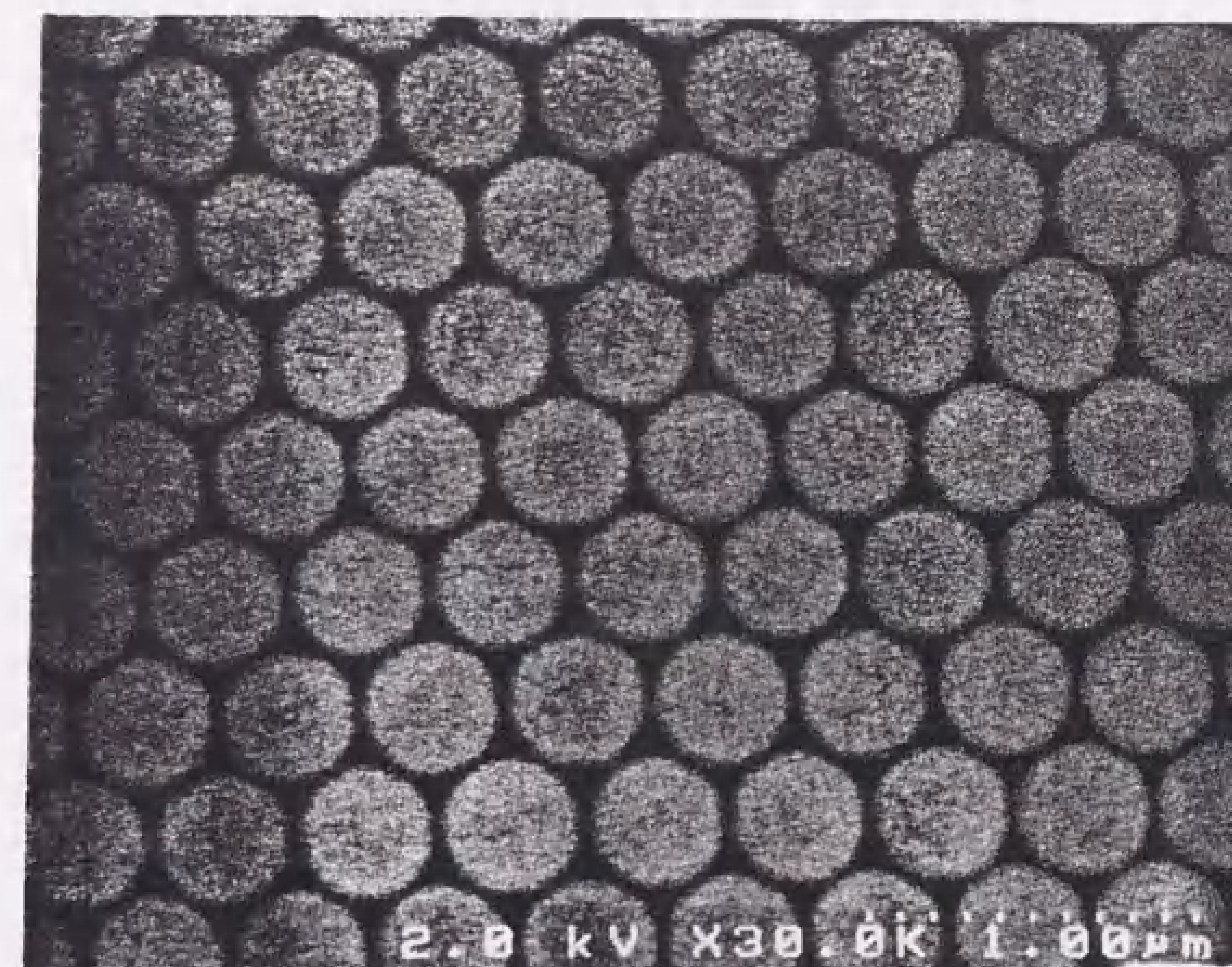

Figure 7.4: Scanning electron micrograph of the ordered latex particles on a flat SiO_2 substrate. These particles are coated with thin aluminum. The diameter of the particle is 500 nm.

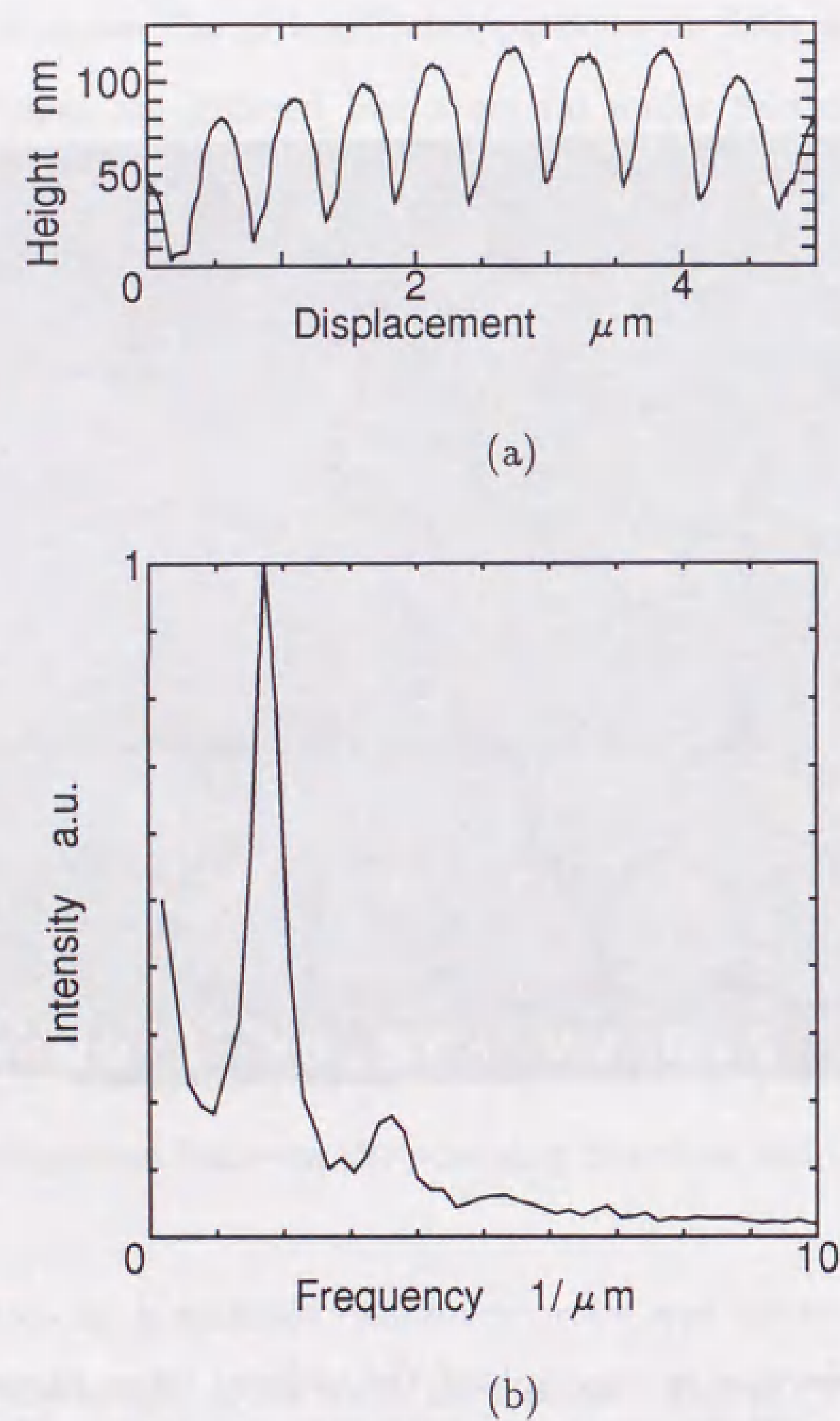

Figure 7.5: (a) Surface topography of the ordered latex particles observed by the single probe force microscope; (b) Fourier-transformed signal of the surface topography.

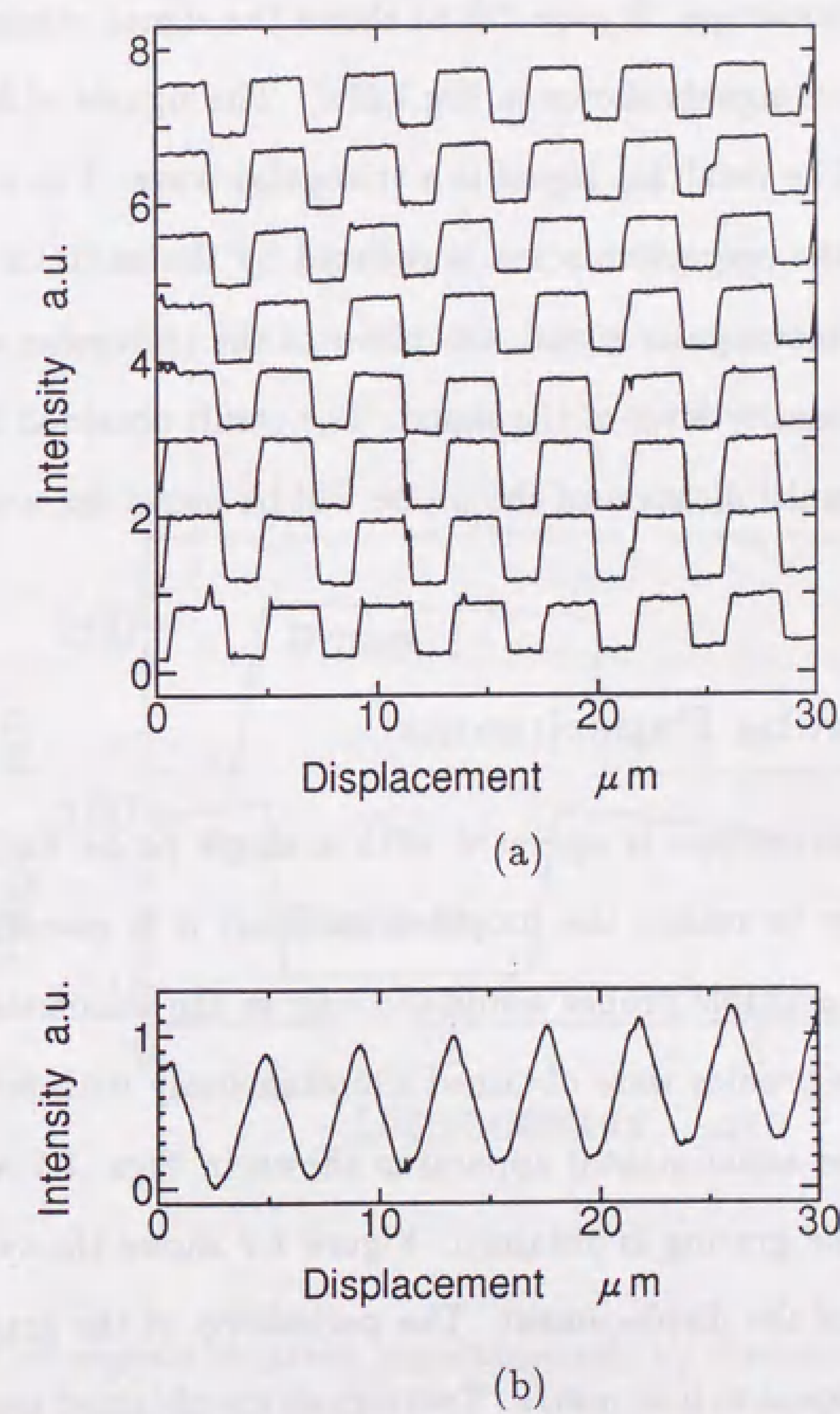

Figure 7.6: (a) Set of signals obtained by scanning the grating surface with the single probe force microscope; (b) Signal obtained after addition of the respective scans shown in (a).

60 nm. Rectangular signals delayed by the phase step of 5.5 degrees are obtained. The set of signals shown in Fig. 7.6(a) may correspond to the signals obtained by the multiple probe force microscope. Figure 7.6(b) shows the signal obtained after the addition of the respective signals shown in Fig.7.6(a). The signals of 30 scans were used for the addition. The resultant signal is a triangular wave. The irregularity of the signal observed in the respective scans is reduced by the addition as shown in Fig. 7.6(b). Unlike the rectangular signal, the phase of the triangular signal can be determined from the intensity level of the signal. The result obtained by the above simulation shows that multiplication of the probe will be useful for noise reduction and phase detection.

7.3.2 Double Probe Experiments

In general, the force microscope is operated with a single probe for imaging the surface profile. In order to realize the proposed encoder, it is essential to obtain the surface profile with multiple probes simultaneously in the nanometer region. In this experiment, surface profiles were obtained simultaneously with two probes for the first time. Using the experimental apparatus shown in Figs. 7.1 and 7.2, the surface topography of the grating is obtained. Figure 7.7 shows the typical signals obtained as a function of the displacement. The periodicity of the grating is 4 μm and the scan velocity is equal to 0.36 mm/s. Two signals are obtained simultaneously with the two probes of the multiple probe force microscope. The upper and lower curves show the signals obtained by probes 1 and 2, respectively. The two signals shown in Fig. 7.7 were obtained after subtracting the offset caused by the tilt of the stage. The tilt of the stage was equal to 1.4 degrees in the direction of stage

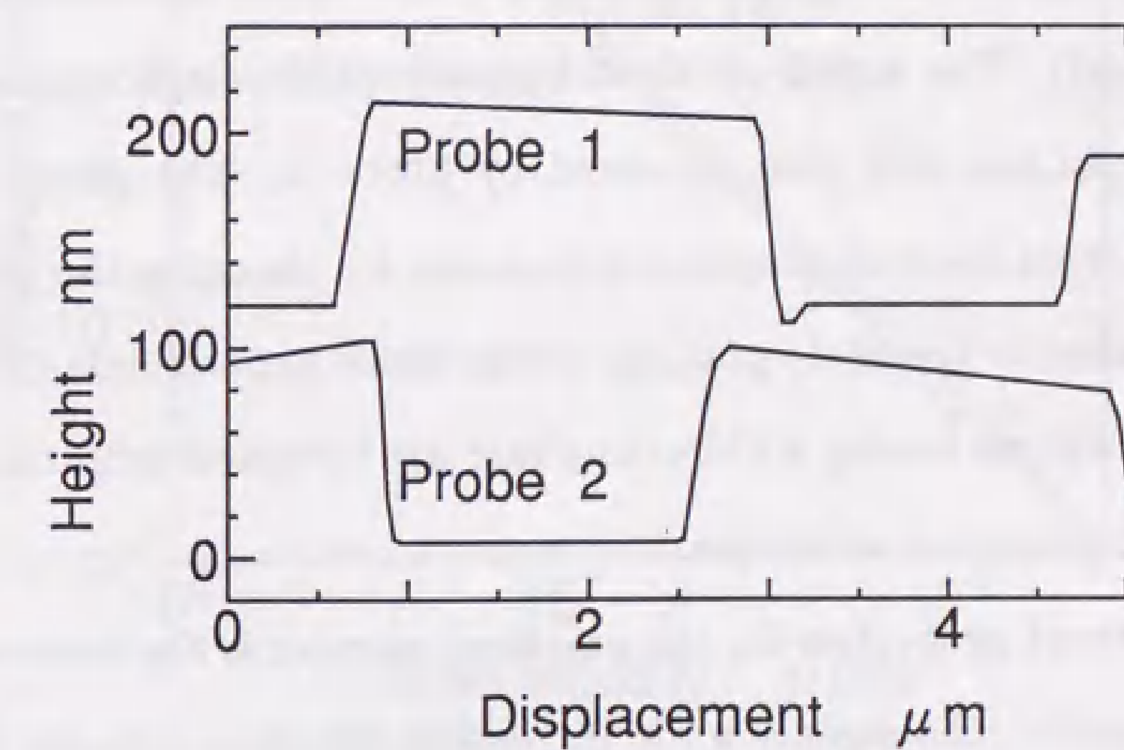

Figure 7.7: Two signals obtained simultaneously by the multiple probe force microscope.

movement. The forces applied to cantilever probes 1 and 2 were 120 nN and 60 nN, respectively. Rectangular profiles of the grating are obtained as shown in Fig. 7.7. The amplitudes of both rectangular waves are 20 mV. Therefore, the sensitivities for the vertical displacements of the cantilever probes are nearly equal to 0.24 mV/nm, since the thickness of the metal film consisting of the grating lines is 85 nm. The duty ratio of the rectangular wave signals shown in Fig. 7.7 is 0.558, which is larger than the ratio of 0.515 measured from the SEM photograph of the grating. The probe has a pyramidal tip with a base of 4 μm square. the duty ratio of 0.560 is obtained by considering the dimensions of the tip. The result agrees well with the measured value (0.558). The signal obtained by probe 2 is delayed approximately 135 degrees in comparison with that obtained by probe 1. The phase difference between the signals from the two probes is adjustable by changing the positions of the two probes relative to the scale grating. From those experiments, it has been shown that periodic signals having a different phase are obtained simultaneously by the force microscope detection technique.

One of the important properties for the practical encoder is the readout time of the displacement signals. the signals while increasing the scan velocity are investigated. When the rectangular grating is used as the sample, the microcantilever moves at maximum velocity at the positions at which step changes of the signal occur. Therefore, the signals in the step change region are obtained. The response times (the rise time and the fall time) in the step change region were measured as a function of scan velocity. The results are shown in Fig. 7.8. The solid circles and the open circles represent the rise time and the fall time, respectively. The measured response times decrease linearly with the increase of scan velocity in the region from

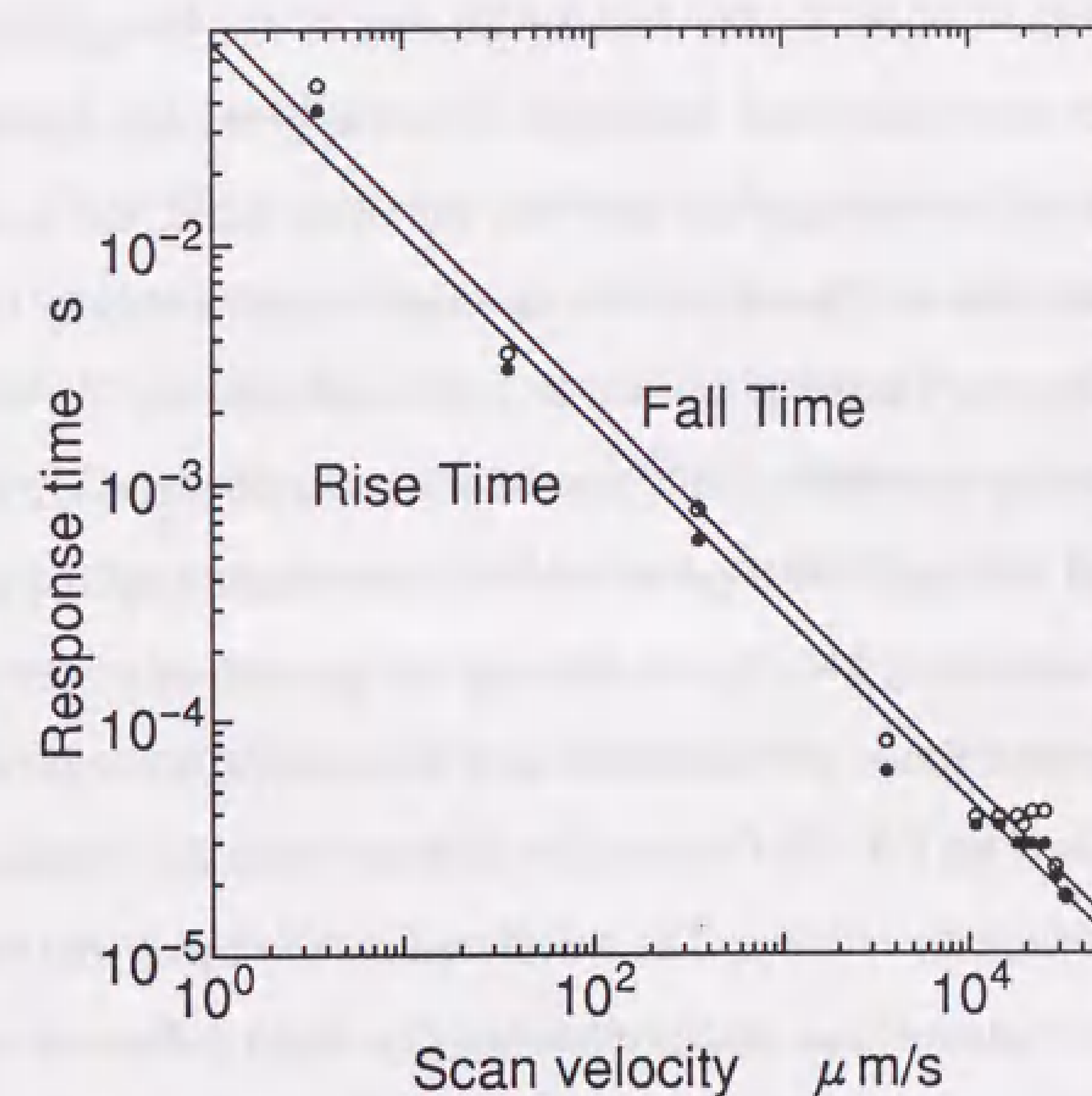

Figure 7.8: Response time as a function of moving speed of the grating sample. The force applied to the scale is about 180 nN.

1 μm/s to $10^4\mu$m/s. At velocities higher than $4 \times 10^4\mu$m/s, the rectangular periodic signal was not obtained because the signals were disturbed by mechanical vibration of the probes. In order to explain the variation of the signal response time, the geometrical shapes of the tip and the grating are considered. The grating has a rectangular surface profile caused by the etching process of the lithography. The edge of the grating line is so steep that the length of the step change region is less than the thickness (85 nm) of the grating line. On the other hand, the top radius of the probe is less than 40 nm. Therefore, the rise time is not caused by the radii of the tip. Although the top radius of the tip is very small, the tip has the elongated shape of a pyramidal structure. The base of the pyramid structure is 4 μm square and the angle of the tip is 55 degrees, which is determined by the angle of the $< 111 >$ planes of silicon crystal. By considering the geometries of the tip and grating, the signal response times are calculated as a function of the scan velocity. The results are shown in Fig. 7.8. The upper line and the lower line represent the fall time and the rise time, respectively. The calculated results agree well with the results measured in the region of less than $10^4\mu$m/s. The slight difference between the rise time and the fall time is caused by the tilt (1.4 degrees) of the tip to the tangent line of the grating plane. When the scan velocity was increased to higher than $3 \times 10^4\mu$m/s, the response times did not decrease linearly. Under those conditions, the sharp step of the signal gradually disappeared and it was difficult to obtain the periodic signal corresponding to the grating profile. Sinusoidal vibration at a frequency roughly equal to 65 kHz was observed in the distorted signals. The first resonant frequency of the free standing cantilever probe is equal to 17 kHz. The actual resonant frequency of the cantilever which is in contact with a surface is

generally higher than that of the free cantilever. The resonant frequency of the cantilever with contact was estimated with the equation used by Mamin et al.[48] to be less than 80 kHz under our experimental conditions. This value roughly explained the frequency of the distorted signal. Therefore, the distortion of the signal at the scan velocity higher than $3 \times 10^4\mu$m/s is considered to be caused by the mechanical resonance of the cantilever, and the signal does not show the surface profile of the grating. Since the mechanical motion of the microcantilever is in general slower than the response of the electronic circuit, the maximum readout velocity is limited to that of the mechanical response of the microcantilever. Under our experimental conditions, the maximum readout velocity is 32 mm/s.

Figure 7.9 shows the magnified portion of the signal as a function of displacement in the region where the probe falls from the metal film of the grating to the substrate. From the intensity change of the obtained signal, a very small displacement can be sensed. Since the gradient of the signal is 0.23 mV/nm and the fluctuation of the signal is approximately 1 mV as shown in Fig. 7.9, the resolution for the displacement sensing obtained by this experimental setup is as high as 5 nm. In this case, the probe touches the edge of the metal film grating with the side slope of the tip, not with the top of the tip. Therefore, this resolution is obtained only in the limited region of the scale grating.

In order to investigate the influence of the force acting on the cantilever, the signal by applying force to the cantilever are measured in the range from 60 nN to 200 nN. Increasing the force applied to the cantilever, the stability of the signal was somewhat improved at scan velocities higher than $10^4\mu$m/s. This was believed to be caused by the increase of the resonant frequency of the cantilever, since the contact

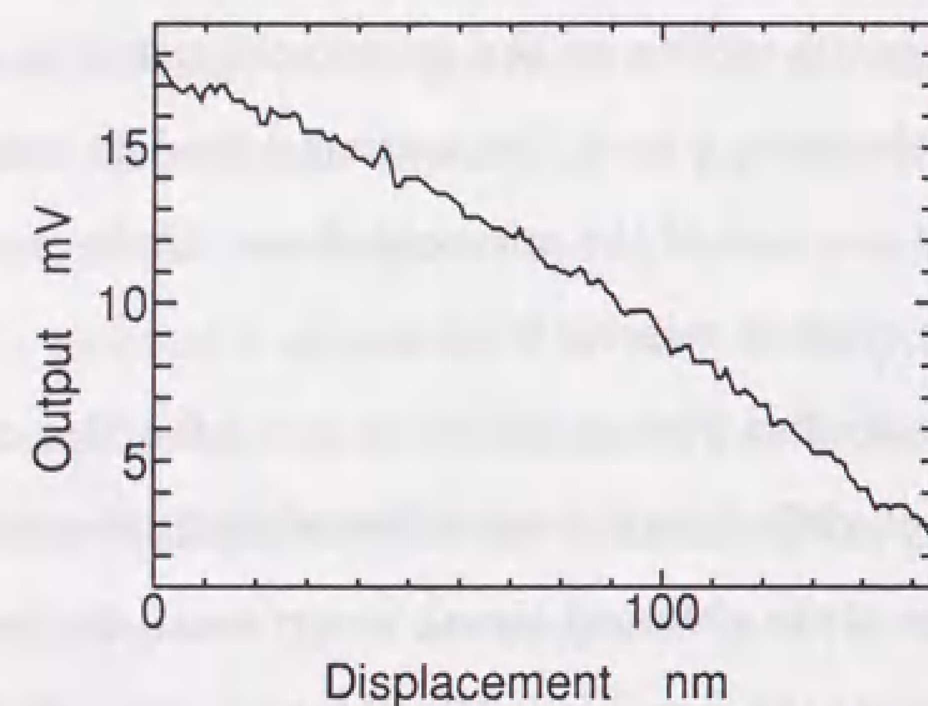

Figure 7.9: Magnified signal obtained from the optical grating. The force applied to the scale is about 180 nN.

force increased.

Finally, the durability of both the cantilever probe and the grating sample was investigated experimentally, since the wear resistance is important for long-term operation. Applying the force of about 180 nN between the probe and the grating surface, the grating surface was scanned by the probe repeatedly. After scanning for more than 4 hours with 100 Hz in the region of 16 μm, no change in the signal was found.

7.4 Conclusions

Position sensing technique using the AFM was studied in this chapter. A new type of a linear encoder using the principle of the force microscope was proposed and the characteristics of the force microscope in position sensing were investigated. Periodic structures of a fine grating fabricated by the lithographic process and of ordered latex particles were examined as a scale for displacement measurement. From the experimental results, it was shown that highly resolved displacement sensing was obtained by this method. However, the signal was sensitive to the irregularity of the surface of the scale. By multiplication of the probes of the force microscope, signals having the different phases were obtained simultaneously. The multiplication of the probe was useful for composing the conventional-type encoder and for reducing the noise due to surface irregularity. The force microscope having two probes was constructed using micromachined cantilevers and a multibeam optical detection system. The signal responses were investigated as a function of scan velocity. Under the experimental conditions, the maximum scan velocity was approximately $3 \times 10^4 \mu$m/s, which was explained in terms of the mechanical response of the microcantilevers.

The waveform of the signal was explained by considering the geometrical shapes of the tip and the grating surface.

The multiple probe can be fabricated precisely by the lithographic process. However, since the resolution of the lithographic mask is approximately 0.4 μm, the detailed shapes of the tips may be different from one another in fabrication tolerance. This systematic error due to the fabricating process should be calibrated by measuring a standard scale. Likewise, the spring constants of the probes fabricated by the lithographic process may be different from each other. However, in the experiment utilizing the two probes with different spring constants (0.064 N/m and 0.032 N/m) as described in section 7.3.2, no significant change in signal was observed in the force range from 60 nN to 200 nN and at the scan velocity of less than $3 \times 10^4 \mu$m/s. Therefore, the slight difference in the spring constant due to the fabrication process will not cause considerable error in the measurement.

The noise reduction effect exerted by the multiple probe was simulated by the single probe experiment. However, to realize the actual encoder system, more detailed study will be necessary. For the measurement using multiple probes, determination of the identity of the signal obtained from each probe is essential. The identity of the signal depends on the fabrication precision of the multiple probes and the signal detection technique. From the experience with the fabrication of a multiple cantilever array[25], the initial deflections of the cantilevers are scattered within 1 μm. This fabrication tolerance is acceptable in the proposed system, since the cantilever deflects about 3 μm in the measurements. Nine light beams having equal intensities have been obtained experimentally through multiplication with the diffraction grating[75], and the grating transmittance for obtaining 19 equal intensity beams

has been calculated using binary coding[76]. By these techniques, equal sensitivity for the detection by each probe will be obtained. Thus it is expected that the error caused by the intensity differences of laser beams is reduced.

Although the experiments carried out here are preliminary, the proposed encoding system will be a novel tool for precise position sensing in the nanometer region with improvement of the system to be suitable for an actual encoder. Future work will be necessary in order to construct a practical system.

Chapter 8

Summary

8.1 General Summary

Sacrificial layer etching technique awoke many researchers in the field of IC fabrication. Many kinds of surface micromachines were fabricated not only by using IC fabrication technique but also by conventional machining technique. Passive micromechanical parts, for example microcantilevers, were also fabricated by the IC fabrication process. They were often distorted by the adhesive force due to the capillary in a small gap. It was necessary to measure the adhesive force quantitatively. In addition, the investigation of the mechanical properties of the thin films is important for the design of the micromachines. In this thesis, the AFM was used to measure the elasticity and the adhesion of the microstructures. Knowledges on the elasticity and the adhesion force were helpful to design micromachines. The topography of the micromachined surface and the dimensions of the fabricated structures were measured by the AFM. Moreover, the multiple probe AFM was proposed for the precise measurement of the position. The results obtained in this thesis are summarized as follows:

8.1.1 Elastic Force Measurements in Microcantilever

For practical fabrication of the micromechanical systems, it is necessary to measure the mechanical properties of the materials used in micromechanical structures and to establish the method for designing the micromechanical structures. The evaluation of micromechanical properties by using the AFM was proposed. The AFM using the heterodyne interferometry was developed to measure the probe deflection with high accuracy. The small force was controlled in the range of nanonewton and applied to the micromechanical structure with the AFM probe.

The elastic force of microcantilevers was measured with the AFM. The force curves were obtained in the micrometer range. From the force curves, the elasticity of the self-sustained thin film was measured. The spring constant and the Young's modulus of the self-sustained thin films were derived by the proposed method. In addition, the Young's modulus of the thin films evaporated on the microcantilever was measured.

The proposed method is non-destructive and the force can be applied to a very small region in the nanonewton range. Therefore it is suitable for the evaluation of the elasticity and the strength of the mechanical structures.

8.1.2 Adhesive Force Measurements in Nanometer Region

The adhesive forces acting between the Si_3N_4 probe (top radius of 50 nm) and the four kinds of flat substrate (Si, SiO_2 , poly-Si, Si_3N_4) immersed into the etch and rinse solutions (H_2O , CH_3COCH_3 , C_2H_5OH , KOH , CCl_4) were investigated. The adhesive force was measured from the transition of the force curve. The adhesive force was independent of the pressing force in the range of smaller than 5 μN. The

measured adhesive forces were in the range from 10 nN to 1 μN. The adhesive forces generated by CH_3COCH_3 or C_2H_5OH were smaller than others. This was consistent with the result that the rinse with CH_3COCH_3 and C_2H_5OH reduced the pinning effect of the surface-micromachined structures.

The force in nanonewton range was measured with the AFM. The magnitude of the adhesive force was considered theoretically and the capillary force was shown to predominate in the experimental conditions. The micromachined cantilever pinned by solid bridging was pulled off by using a probe of the AFM. The magnitude of the pull-off force was approximately 3 μN. This value was larger than the capillary force.

8.1.3 Adhesive Force Distribution Measurements on Microstructures

The distribution of the adhesive force acting between an AFM probe (tip radius of 50 nm) and the sample surface was measured in air under atmospheric condition. The relation between the adhesive force and the surface topography was investigated. The samples used in the experiments were a flat glass, a grating (4 μm pitch) fabricated by the lithographic process and ordered latex particles (500 nm diameter).

In the case of the flat glass (roughness < 1 nm), the adhesive force distribution was uniform. The magnitude of the measured adhesive force was approximately 60 nN. In the case of the grating, the maximum adhesive force was 200 nN and the minimum adhesive force was 20 nN. The adhesive force decreased when the AFM tip approached the edge of the grating lines, which was explained by considering formation of a water meniscus. The adhesive force for the ordered latex particles

changed periodically with the topographic variation. The minimum adhesive force was 30 nN, which was obtained at the top of the latex particle. Therefore, the convex surface decreases the adhesive force. The relation between the adhesive force and the surface topography measured in this experiment will be useful to reduce the adhesive forces acting in the microelectromechanical system.

8.1.4 Position Measurements Using Multiple Probe AFM

Periodic structures of a fine grating and ordered latex particles were measured with the AFM. From the experimental results, it was shown that highly resolved displacement sensing was able to be performed by the AFM. However, the signal was sensitive to the irregularity of the sample surface. Based on the results, a new scheme of displacement measurement using the principle of the AFM was proposed. The characteristics of the proposed method were investigated.

The AFM having two probes was constructed. The micromachined cantilevers were used in the system. The multibeam optical detection technique was proposed to measure the deflections of the multiprobe. By the multiplication of the AFM probe, signals having the different phases were obtained simultaneously. The multiplication of the probe was useful for composing the conventional-type encoder and for reducing the noise due to surface irregularity. The noise reduction effect exerted by the multiple probe was simulated by the single probe AFM experiment.

8.2 Future Prospects

As summarized above, in this thesis, the applications of the AFM to the micromachines were studied. The force measurement and the position measurement by the

AFM were proposed and demonstrated to be useful for the development of micromachines. Nevertheless, in the proposed techniques, there are still some problems.

In this thesis, a normal force acting on the microcantilever was measured by the AFM. Although a small force acting between the AFM tip and the sample was detected, the measured direction of the force was vertical to the sample. However, the direction of the force generated by the MEMS is sometimes lateral to the surface. The lateral force generated by the MEMS is not detected by the conventional AFM. A specially designed AFM should be constructed to detect the forces in various directions.

In order to detect an absolute value of the force acting on the AFM tip, a correct spring constant of the AFM probe has to be known. In this thesis, the spring constant of the AFM probe was calibrated by attaching a small particle (weight) at an edge of the probe. Although this method is straightforward, more convenient measurement to calibrate the spring constant is required. In chapter 4, the spring constant of an SiO_2 cantilever was determined by using the AFM probe. Similarly, the cantilever magnified in centimeter dimensions can be used for the calibration of the spring constant. Several micromachines were actuated by electric power. The generated force and displacement were so small that the conventional measurement techniques could not be applied. It was important to measure forces generated by micromachines. The technique proposed in this thesis will be useful for the measurement of the force generated by micromachines.

In the multiple probe AFM, an incident beam was divided by an optical grating. The intensities of the divided beams were different from each other and the difference should be compensated by electric circuits. By using a coded optical grating and a

laser array, the beams of equal intensity can be obtained. And thus, the noise due to the differences of the beam intensities will be reduced.

Although the experiments carried out here are preliminary, the proposed encoding system will be a novel tool for precise displacement sensing in the nanometer region. From the experiences in the fabrication of the cantilever array, it is considered that the initial deflections of the cantilevers are scattered within $1\mu m$. This fabrication tolerance is acceptable in the proposed system, since the cantilever deflects by about $3\mu m$ in the measurements.

Bibliography

[1] M. A. Huff, A. D. Nikolich and M. A. Schmidt: "Design of sealed cavity microstructures formed by silicon wafer bonding", J. Microelectromec. Systems., 2, pp. 74–81 (1993).

[2] H. Behi, M. Mehregany and K. J. Gabriel: "A microfabricated three-degree-of-freedom parallel mechanism", Proceedings of IEEE Micro Electro Mechanical Systems, Napa Valley, USA, pp. 159–165 (1990).

[3] E. W. Becker, W. Ehrfeld, P. Hagmann, A. Maner and D. Münchmeyer: "Fabrication of microstructures with high aspect ratios and great structural heights by synchrotron radiation lithography, galvanoforming, and plastic moulding (LIGA process)", Microelectronic Eng., 4, pp. 35–56 (1986).

[4] M. Mehregany, K. J. Gabriel and W. S. N. Trimmer: "Integrated fabrication of polysilicon mechanisms", IEEE Trans. Electron Dev., ED35, pp. 719–723 (1988).

[5] L. C. Fan, Y. C. Tai and R. S. Muller: "Integrated movable micromechanical structures for sensors and actuators", IEEE Trans. Electron Devices, ED35, pp. 724–730 (1988).

[6] W. Riethmüller and W. Benecke: "Thermally excited silicon microactuators", IEEE Trans. Electron Devices, ED35, pp. 758–763 (1988).

[7] H. Fujita and A. Omodaka: "The fabrication of an electrostatic linear actuator by silicon micromachining", IEEE Trans. Electron Devices, ED35, pp. 731–734 (1988).

[8] L. Paratte, G. A. Racine, N. F. de Rooij and E. Bornand: "Design of an integrated electrostatic stepper motor with axial field", Sensors & Actuators, A27, pp. 597–603 (1991).

[9] R. L. Smith, R. W. Bower and S. D. Collins: "The design of a magnetically actuated micromachined flow valve", Sensors & Actuators, A27, p. 47 (1990).

[10] G. Fhur, R. Hagedorn, T. Müller, W. Benecke and B. Wagner: "Microfabricated electrohydrodynamic (ehd) pumps for liquids of higher conductivity", J. Microelectromec. Systems., 1, pp. 141–146 (1992).

[11] D. P. E. Smith and S. A. Elrod: "Magnetically driven micropositioners", Rev. Sci. Instrum., 56, p. 1970 (1985).

[12] R. T. Howe: "Surface micromachining for microsensors and microactuators", J. Vac. Sci. Technol., B6, pp. 1809–1813 (1988).

[13] C. L. Kuo, T. Matsuzawa and M. Fujino: "A micropipe fabrication process", Proc. IEEE MEMS Workshop, Nara, Japan, pp. 80–85 (1991).

[14] K. E. Bean: "Anisotropic etching of silicon", IEEE Trans. Electron Dev., ED25, p. 1185 (1978).

[15] D. F. Weirauch: "Correlation of the anisotropic etching of single crystal silicon spheres and wafers", J. Appl. Pys., 46, p. 1478 (1975).

[16] E. Bassous: "Fabrication of novel three-dimensional microstructures by the anisotropic etching of (100) and (110) silicon", IEEE Trans. Electron Dev., ED25, p. 1178 (1978).

[17] K. E. Petersen and C. R. Guarnieri: "Young's modulus measurements of thin films using micromechanics", J. Appl. Phys., 50, pp. 6761–6766 (1979).

[18] P. G. Borden: "A simple technique for determining the stress at the si/sio$_2$ interface", Appl. Phys. Lett.,36, pp. 829–831 (1980).

[19] E. I. Bromley, J. N. Randall, D. C. Flanders and W. Mountai: "A technique for the determination of stress in thin films", J. Vac. Sci. Technol., B1, pp. 1364–1366 (1983).

[20] R. T. Howe and R. S. Muller: "Stress in polycrystalline and amorphous silicon tin films", J. A. Phys., 54, pp. 4674–4675 (1983).

[21] T. R. H. Guckel and and D. W. Burns: "A simple technique for the determination of mechanical strain in thin films with applications to polysilicon", J. Appl. Phys., 57, pp. 1671–1675 (1985).

[22] M. G. Allen, M. Mehregany, R. T. Howe and S. D. Senturia: "Microfabricated structures for the in situ measurement of residual stress, young's modulus, and ultimate strain of thin films", Appl. Phys. Lett., 51, pp. 241–243 (1987).

[23] S. Sugiyama and O. Tabata: "Evaluation of thin film material for micromechanisms", J. of SICE, 28, p. 485 (1989). In Japanese.

[24] L. M. Zhang, D. Uttamchandani, B. Culshaw and P. Dobson: "Measurement of young's modulus and internal stress in silicon microresonators using a resonant frequency technique", Meas. Sci. Technol., 1, pp. 1343–1346 (1990).

[25] K. Hane, T. Naito and S. Hattori: "Phototermoelastic evaluation for small mechanical structures", Appl. Optics, 30, pp. 72–78 (1991).

[26] J. A. J. Griffin, F. R. Brotzen and C. F. Dunn: "Mechanical testing of thin metallic films", Thin Solid Films. 220, pp. 265–270 (1992).

[27] H. L. Chan and K. D. Wise: "An ultraminiature solid-state pressure sensor for a cardiovascular catheter", IEEE Trans. Electron Dev., ED35, pp. 2355–2362 (1988).

[28] S. J. O'Shea, M. E. Welland and T. Rayment: "Solvation forces near a graphite surface measured with an atomic force microscope", Appl. Phys. Lett., 60, pp. 2356–2358 (1992).

[29] G. Meyer and N. M. Amer: "Simultaneous measurement of lateral and normal forces with an optical-beam deflection atomic force microscope", Appl. Phys. Lett., 57, pp. 2089–2091 (1992).

[30] S. J. O'Shea, M. E. Welland and T. Rayment: "Atomic force microscope study of boundary layer lubrication.", Appl. Phys. Lett., 61, pp. 2240–2242 (1992).

[31] S. Ciraci: "Atomic-scale tip-sample interactions and contact phenomena", Ultramicroscopy, 42-44, pp. 16–21 (1992).

[32] S. R. Cohen: "An evaluation of the use of the atomic force microscope for studies in nanomechanics", Ultramicroscopy, 42-44, pp. 66–72 (1992).

[33] A. J. den Boef: "The influence of lateral forces in scanning force microscopy", Rev. Sci. Instrum., 62, pp. 88–92 (1991).

[34] D. R. Baselt and J. D. Baldeschwieler: "Lateral forces during atomic force microscopy of graphite in air", J. Vac. Sci. Technol., B10, pp. 2316–2322 (1992).

[35] C. Linder and N. F. de Rooij: "Investigations on free-standing polysilicon beams in view of their application as transducers", Sensors and Actuators, A21-A23, pp. 1053–1059 (1990).

[36] H. J. .Butt: "Measuring electrostatic, van der Waals, and hydration forces in electrolyte solutions with and atomic force microscope", Biophysical Journal, 60, pp. 1438–1444 (1991).

[37] U. Hartmann: "Intermolecular and surface forces in noncontact scanning force microscopy", Ultramicroscopy, 42-44, pp. 59–65 (1992).

[38] R. L. Alley, G. J. Cuan, R. T. Howe and K. Komvopoulos: "The effect of release-etch processing on surface microstructure stiction", IEEE Solid-State Sensor and Actuator Workshop, South Carolina, pp. 202–207 (1992).

[39] P. R. Scheeper, J. A. Voorthuyzen, W. Olthuis and P. Bergveld: "Investigation of attractive forces between pecvd silicon nitride microstructures and an oxidized silicon substrate", Sensors and Actuators, A30, pp. 231–239 (1992).

[40] J. Israelachvili: "Interfacial forces", J. Vac. Sci. Technol., A10, pp. 2961–2971 (1992).

[41] C. H. Mastrangelo and C. H. Hsu: "Mechanical stability and adhesion of microstructures under capillary forces - part i: basic theory", J. Microelectromechanical Systems, 2, pp. 33–43 (1993).

[42] C. H. Mastrangelo and C. H. Hsu: "Mechanical stability and adhesion of microstructures under capillary forces - part ii: experiments", J. Microelectromechanical Systems, 2, pp. 44–62 (1993).

[43] G. Binnig, H. Rohrer, C. Gerber and E. Weibel: "Surface studies by scanning tunneling microscopy", Phys. Rev. Lett., 49, pp. 57–61 (1982).

[44] G. Binnig, H. Rohrer, C. Gerber and E. Weibel: "Atomic force microscope", Phys. Rev. Lett., 56, pp. 930–933 (1986).

[45] N. A. Burnham and R. J. Colton: "Measuring the nanomechanical properties and surface forces of materials using an atomic force microscope", J. Vac. Sci. Technol., A7, pp. 2906–2913 (1989).

[46] H. Kawakatsu, Y. Hoshi and T. Higuchi: "Crystalline lattice for metrological applications and positioning control by a dual tunneling-unit scanning tunneling microscope", J. Vac. Sci. Technol., B9, pp. 651–654 (1991).

[47] Y. Li and S. M. Lindsay: "Polystyrene latex particles as a size calibration for the atomic force microscope", Rev. Sci. Instrum., 62, pp. 2630–2633 (1991).

[48] H. J. Mamin and D. Rugar: "Thermomechanical writing with an atomic force microscope tip", Appl. Phys. Lett., 61, pp. 1003–1995 (1992).

[49] J. Brugger, R. A. Buser and N. F. de Rooij: "Silicon cantilevers and tips for scanning force microscopy", Sensors and Actuators, A34, pp. 193–200 (1992).

[50] M. M. Farooqui, A. G. R. Evans, M. Stedman and J. Haycocks: "Micromachined silicon sensors for atomic force microscopy", Nanotechnology 3, pp. 91–97 (1993).

[51] D. W. Burns and H. Guckel: "Thin films for micromechanical sensors", J. Vac. Sci. Technol., A8, p. 3606 (1990).

[52] H. Fujita: "Micro mechatronics - potential, limit and problem-", IEE Japan C, 108, p. 830 (1989). In Japanese.

[53] Y. C. Tai and R. S. Muller: "Measurement of young's modulus on microfabricated structures using a surface profiler", Proceedings of IEEE Micro Electro Mechanical Systems, Napa Valley, California, p. 147 (1990).

[54] Y. C. Tai and R. S. Muller: "Integrated stylus-force gauge", Sensors and Actuators, A21-A23, pp. 410–413 (1990).

[55] G. Binnig and C. F. Quate: "Atomic force microscope", Phy. Rev. Lett., 56, pp. 930–933 (1986).

[56] E. Meyer, H. Heizelmann, D. Brodbeck, G. Overney, R. Overney, H. H. L. Howald, T. Jung, H. R. Hidber and H. J. Güntherodt: "Atomic resolution on the surface of lif(100) by atomic force microscopy", J. Vac. Sci. Techonol., B9, pp. 1329–1332 (1991).

[57] H. Yamada, T. Fujii and K. Nakayama: "Experimental study of forces between a tunnel tip and the graphite surface", J. Vac. Sci. Technol., A6, pp. 293–295 (1988).

[58] A. L. Weisenhorn, P. K. Hansma, T. R. Albrecht and C. F. Quate: "Forces in atomic force microscopy in air and water", Appl. Phys. Lett., 54, pp. 2651–2653 (1989).

[59] C. S. Tables: "Maruzen", p. 444 (1992). In Japanese.

[60] M. Laugier: "Determination of young's modulus in vacuum-evaporated thin films of aluminum and silver", Thin Solid Films, 75, p. L17 (1981).

[61] H. A. Mizes, K. G. Loh, R. J. D. Miller, S. K. Ahuja and E. F. Grabowski: "Submicron probe of polymer adhesion with atomic force microscopy: dependence on topography and material inhomogeneities", Appl. Phys. Lett., 59, pp. 2901–2903 (1991).

[62] U. Hartmann: "Theory of van der Waals microscopy", J. Vac. Sci. Technol., B9, pp. 465–469 (1992).

[63] H. W. Hao, A. M. Baro and J. J. Saenz: "Electrostatic and contact forces in force microscopy", J. Vac. Sci. Technol., B9, pp. 1323–1328 (1991).

[64] A. Torii, M. Sasaki, K. Hane and S. Okuma: "Adhesion of microstructures investigated by atomic force microscopy", Sensors & Actuators in printing.

[65] A. Torii, M. Sasaki, K. Hane and S. Okuma: "An elasticity evaluation method for micro mechanical structures by using load-deflection curve of force microscope", Trans. IEE of Japan, 112A, pp. 979–986 (1992). in Japanese.

[66] D. A. Grigg., P. E. Russell and J. E. Griffith: "Tip-sample forces in scanning probe microscopy in air and vacuum", J. Vac. Sci. Technol., A10, pp. 680–683 (1992).

[67] J. N. Israelachvili: "Intermolecular and surface forces", Academic press limited, London (1985).

[68] G. E. Poirier and J. M. White: "Diffraction grating calibration of scanning tunneling microscope piezoscanners", Rev. Sci. Instrum., 61, pp. 3917–3918 (1990).

[69] M. F. Bocko: "The scanning tunneling microscope as a high-gain, low-noise displacement sensor", Rev. Sci. Instrum., 61, pp. 3763–3768 (1990).

[70] S. Hattori, Y. Uchida and V. T. Chitnis: "An automatic super-accurate positioning technique using moiré interference", Bull. Japan Soc. of Prec. Eng., 20, pp. 73–78 (1986).

[71] H. Kinoshita, A. Une and M. Iki: "A dual grating alignment technique for x-ray lithography", J. Vac. Sci. Technol., B1, pp. 1276–1279 (1983).

[72] J. Guild: "Diffraction gratings as measuring scales", Oxford University Press, London, (1960).

[73] V. T. Chitnis, Y. Uchida, K. Hane and S. Hattori: "Moiré signals in reflection", Opt. Commun., 54, pp. 207-211 (1985).

[74] J. R. Leger, G. J. Swanson and W. B. Veldkamp: "Coherent beam addition of GaAlAs lasers by binary phase gratings", Appl. Phys. Lett., 48, pp. 888–890 (1986).

[75] W. Lee: "High efficiency multiple beam gratings", Appl. Opt., 18, pp. 2152–2158 (1979).

[76] H. Damman and K. Görtler: "High-efficiency in-line multiple imaging by means of multiple phase holograms", Opt. Commun., 3, pp. 312–315 (1971).

[77] G. Meyer and N. M. Amer: "Novel optical approach to atomic force microscopy ", Appl. Phys. Lett., 53, pp. 1045–1947 (1988).

[78] M. Sasaki, M. Hino, K. Fujita, Y. Bessho, K. Hane and S. Okuma: "Development of atomic force microscope using heterodyne interferometry", Int. J. Applied Electromagnetics in Materials Vol. 3 Suppl., pp. 437–440 (1992).

Acknowledgements

I wish to thank many people who contributed in various ways to this dissertation. I would like to express my thanks to Professor Shigeru Okuma, School of Engineering, Nagoya University, for his guidance during this study, and to Professor Yoshiki Uchikawa, School of Engineering, Nagoya University, for valuable suggestions. I am particularly indebted to Professor Kazuhiro Hane, School of Engineering, Nagoya University, for his continuous advice and discussions. I am thankful to Research Associate Tatsuya Suzuki, School of Engineering, Nagoya University, for his useful suggestions and comments on this dissertation. Special thanks are to Minoru Sasaki, Graduate Student, Nagoya University, for his development of the atomic force microscope and his useful discussions on various subjects.

I also thank Takahide Kanehara, Koji Yamada, Shin John Ho, Shinji Doki, Soichiro Hayakawa, Takashi Ogawa and Tsukasa Abe for their encouragement on my everyday life. It is also a pleasure to thank members of both Okuma laboratory and Uchikawa laboratory for all their beneficial comments.

Finally, I also thank my family for their support and encouragement, without which this dissertation could not have been brought to fruition.

論　文　目　録

氏　名　　鳥井　昭宏　　　　　　　　　　　　　（発表した論文）

論　文　題　目	公表の方法及び時期	著　者
I.　学会誌等		
1.フォース顕微鏡の荷重-たわみ曲線を用いたマイクロメカニカル構造の弾性評価法	電気学会論文誌A,112巻, pp.979-986 (1992)	鳥井　昭宏 佐々木　実 羽根　一博 大熊　繁
2.The Feasibility of a Precise Linear Displacement Encoder Using Multiple Probe Force Microscope	International Journal of the Japan Society for Precision Engineering, Vol.27, pp.367-372 (1993)	A.Torii M.Sasaki K.Hane S.Okuma
3.Adhesion of the Micro-structures Investigated by Atomic Force Microscopy	Sensors and Actuators A, Vol.40, pp.71-76 (1994) （印刷中）	A.Torii M.Sasaki K.Hane S.Okuma
4.Adhesive Force Distribution on Microstructures Investigated by an Atomic Force Microscope	Sensors and Actuators A （投稿中）	A.Torii M.Sasaki K.Hane S.Okuma
II.　国際会議		
1.Micro-Probe Encoder: Force Microscope Used in Displacement Sensing	Proceedings of the IEEE/SICE International Workshop on Emerging Technologies for Factory Automation, pp.72-80(1991)	A.Torii M.Sasaki K.Hane S.Okuma
2.Application of Scanning Force Microscopy to the Evaluation of Micro Mechanical Structure	Proceedings of International Symposium on Theory of Machines and Mechanisms, pp.298-306 (1992)	A.Torii M.Sasaki K.Hane S.Okuma

論 文 目 録

氏 名　鳥井 昭宏　　　　　　　　　　　　　　（発表した論文）

論 文 題 目	公表の方法及び時期	著 者
3. Adhesive Force of the Microstructures Measured by the Atomic Force Microscope	Proceedings of the IEEE Micro Electro Mechanical Systems Workshop, pp.111-116(1993)	A.Torii M.Sasaki K.Hane S.Okuma
4. Multi-Probe Force Microscopy for a Precise Linear Encoder	Proceedings of the 7th International Precision Engineering Seminar, pp.1003-1006(1993)	A.Torii K.Hane S.Okuma
5. Adhesive Force Mapping on Microstructures with an Atomic Force Microscope	Proceedings of Fourth International Symposium on Micro Machine and Human Science, pp.88-94 (1993)	A.Torii M.Sasaki K.Hane S.Okuma